Doctoral Dissertations and Master's Theses

Fall 11-18-2022

Biomass Characterization and Insulation Optimization Studies

Hussein Awad Kurdi Saad
Embry-Riddle Aeronautical University, saadh@my.erau.edu

BIOMASS CHARACTERIZATION AND INSULATION OPTIMIZATION STUDIES

by

Hussein Awad Kurdi Saad

A Dissertation Submitted to the College of Engineering Department of Mechanical
Engineering in Partial Fulfillment of the Requirements for the Degree of
Doctor of Philosophy in Mechanical Engineering

Embry-Riddle Aeronautical University
Daytona Beach, Florida
November 2022

BIOMASS CHARACTERIZATION AND INSULATION OPTIMIZATION STUDIES

by

Hussein Awad Kurdi Saad

This dissertation was prepared under the direction of the candidate's Dissertation Committee Chair, Dr. Birce Dikici, Associate Professor, Daytona Beach Campus, and Dissertation Committee Members Dr. Eduardo A. Divo, Professor, Daytona Beach Campus, and Dr. Rafael M. Rodriguez, Associate Professor, Daytona Beach Campus, Dr. Marc Compere, Associate Professor, Daytona Beach Campus, and Dr. Jeff R. Brown, Professor, Daytona Beach Campus and has been approved by the Dissertation Committee. It was submitted to the Department of Mechanical Engineering in partial fulfillment of the requirements for the degree of Doctor of Philosophy in Mechanical Engineering
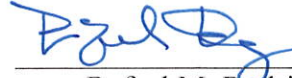
Dissertation Review Committee:
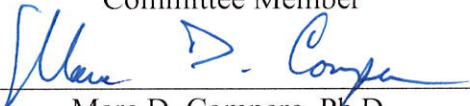
_____
Birce Dikici, Ph.D.
Committee Chair

_____
Eduardo A. Divo, Ph.D.
Committee Member

_____
Rafael M. Rodriguez, Ph.D.
Committee Member

_____
Marc D. Compere, Ph.D.
Committee Member

_____
Jeff R.Brown, Ph.D.
Committee Member

_____
Eric Coyle, Ph.D.
Ph.D. Program Chair,
Mechanical Engineering

_____
Patrick Currier, Ph.D.
Department Chair,
Mechanical Engineering

_____
James Gregory, Ph.D.
Dean, College of Engineering

_____
Lon Moeller, J.D.
Senior Vice President for Academic
Affairs and Provost

i

Acknowledgements

Abstract

Researcher: Hussein Awad Kurdi Saad

Title: Biomass Characterization and Insulation Optimization Studies

Institution: Embry-Riddle Aeronautical University

Degree: Doctor of Philosophy in Mechanical Engineering

Year: 2022

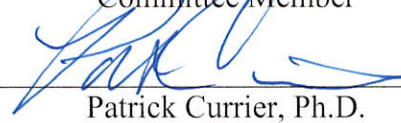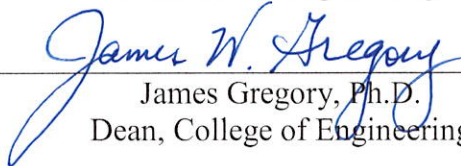This study indicates how biomass materials can be effectively used as naturally sustainable alternatives to insulation materials. Barley grains and oak leaves, straw, and jute are collected, and crushed into powders/ chopped pieces. The physical characteristics are measured to characterize each powder. The biomass powder reinforced composites are manufactured in varying weight ratios. The density and thermal conductivity of composite materials are measured. The properties of composites compared to those of commercial insulation materials are found to be close to them. Furthermore, genetic algorithms (GA) can be used to achieve multi-objective optimization entailing maximizing insulation (minimizing heat transfer) and simultaneously maximizing sustainability (minimizing carbon footprint) of a designed insulation structure. The two resulting nonlinear competing objective functions will be maximized by means of evolutionary optimization techniques within a defined design space. The multi-objective optimization is achieved by building a Pareto front and determining the points of best compromise between the two objectives.

Table of Contents

List of Tables

List of Figures

xiv

1. Section One: Biomass Characteristics

1 Introduction

Increased concentration has been placed on the need to decrease global climate change, ecological harm, and pollution. The scientific community attempts have focused on developing eco-friendly materials that can be used instead of the non-renewable materials [1][2]. Usage of nonrenewable materials and the ensuing waste production have driven ecological pollution. New materials, techniques, machines have been developed using excessively available waste materials to protect the environment. Such waste materials as coco peat powder, jute, and silk can be transformed into sources of renewable energy [3]. Natural/ biomass fibers are not synthetic. These fibers can be found from two sources, plants or animals. In recent decades, such natural fibers as sisal, oil palm, flax, and jute have attracted significant interest because they arise from renewable and nonrenewable resources and can be used to create composite materials. The plants can be categorized into bast fibers (flax, jute, ramie, kenaf, and hemp), seed fibers (coir, cotton, and kapok), grass and reed fibers (wheat, rice, and corn), and leaf fibers (pineapple, sisal, and abaca), as well as all other types like wood, and roots [4]. Biomass fibers are the most significant components in different manufacturing applications, including textile, paper manufacturing, packaging, and building materials. Since biomass fibers are renewable and eco-friendly, these fibers lead to eco-friendly materials [5]. Table 1 shows some biomass and waste products.

Table 1: Biomass and waste products

Biomass products	Waste products

Wheat	Rice straw
Barley grains	Rice husk
Corn	Palm kernel shell
Rice	Corn straw
pumpkin seeds	Oil palm fiber
coffee seeds	Wheat straw
lentil seeds	Switchgrass
white lupin seeds	Corn stover
sunflower seeds	Sawdust
Bambara groundnuts	Oat straw
groundnut kernel	Barley straw
fennel seed	Wood pellets
	Torrefied pellets
	Alfalfa grind
	Kenaf
	Hemp
	Flax
	Sisal
	Date palm fiber
	Coir
	Bermuda grass seeds
	Conifer cones
	Pinecones
	Coconut husk
	Palm kernel husk
	Soybean husk
	Coconut shell
	Oak leaves
	Banana pseudo-stem
	Sugarcane bagasse

Sugarcane tops
Sugarcane coir
Pecan husk
Corn husk

In addition, industry is trying to identify materials that possess better characteristics like hardness, strength, density, and less cost along with enhanced sustainability. The composite materials have these properties. For the last few decades, polymers have been used in numerous applications because the polymers provide benefits when combined with conventional materials. The most significant advantages are the ease of treatment, lighter weight, better productivity, and low cost. Fillers and fibers are added to modify the properties of polymers to fit the high-strength modulus needs. The polymer matrix composites (PMC) consist of different kinds of organic polymers consisting of short or continuous fibers with the type of reinforcing parameters that enhance the characteristics of high strength, stiffness, and fracture. The PMC is manufactured in a way that enhances the mechanical loads, which are supported by fibers. The purpose of the matrix is to make the fibers cohere to generate an effective load transfer between them. A great resistance and the interfacial bonding between a polymer matrix reinforced with biomass fibers help the resulting materials maintain their chemical and mechanical properties [6]. In manufacturing applications, biomass-reinforced composites are performed widely from consumer products to automobile components due to biodegradable, less weight, and better strength compared to glass fiber–reinforced composites [7]. While natural fibers are considered insulation materials, these fibers can also be manufactured to form new composite materials. Therefore, biomass products can be effectively and efficiently used

as naturally sustainable alternatives to insulation materials. The properties of natural fiber-reinforced composites (NFRC) can be compared to those of commercial insulation materials such as bakelite, plaster board, fluoroelastomer, and neoprene rubber. Sustainable materials such as barley grains, oak leaves, barley straw, and jute have been studied, and used as biomass materials due to their high availability and affordability.

1.1. Barley

Barley, *Hordeum vulgare L.*, is a yearly grass in the family *Poacease* and serves as a significant grain crops. It is grown usually in winter on an annual basis. It is a tall grass with a hairy stem. Barley grass stands up straight and creates spikelets at the top. The height of barley is between 60 and 120 cm. The heads of barley grain are cylindrical spikes consisting of strings. Each one has three spikelets. The plant produces 20-60 seeds. The kernel of barley is a seed or grain which is wrapped in a husk [8]. They have light tan to yellowish color and are spindle shaped [9]. Seed heads are harvested after the spikes have been dried and turn from green to brown. The spikes are removed from the plant. These spikes should be dried on a plate in a cool, dry place for a few days. The seeds are extracted by hands. Split seeds should be dried for several days [10]. There are different regions of producing barley in the world, including Russia, Ukraine, France, Germany, Spain, Australia, Canada…. etc. [11]. The barley seeds are ground into flour with a white color. The barley grain is approximately a spindle body in shape, decreasing at each end, with a shoaly groove passing along the ventral direction as shown in Figure 1. The husk (at the top and base of the seed) is ordinarily broken when the "apical appendage" -- the awn -- and basal attachment have been damaged in threshing. It is a little patterned with wrinkles, and its color is pale yellow. The dorsal, the rounded part of the seed, is taken by the lemma

which protect the grain. This dorsal transfers five longitudinal surface pinnacles, or "nerves" under that pass vascular packs [12]. Figure 2 presents barley grains after harvesting.
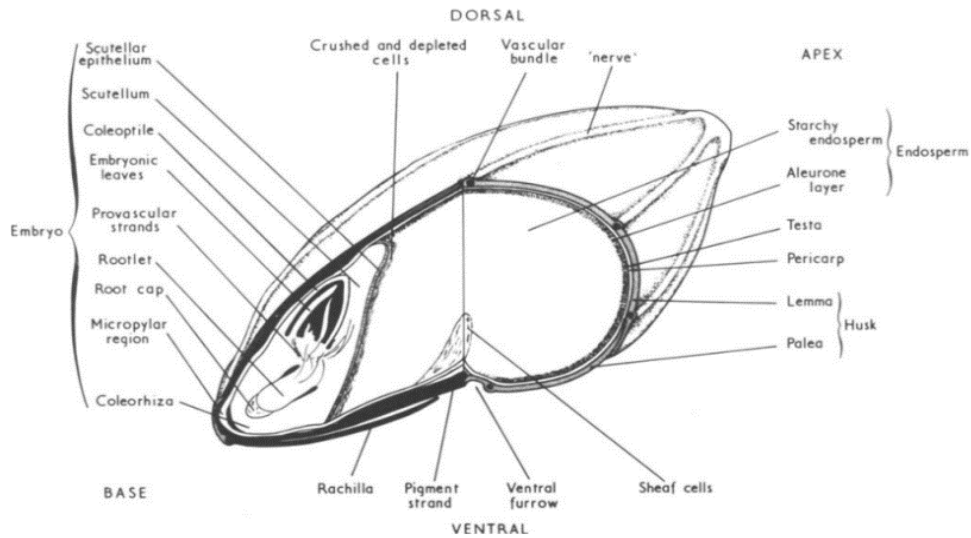
Figure1: Morphological cross-section view of barley grain [12].

Figure 2: Barley grains

Table 2 shows the top 20 countries by the quantity of barley produced are given below (tonnes).

Table 2: The top 20 countries produced barley [11].

Rank	Country	Production Quantity (in Tonnes)
1	Russian Federation	16,938,000
2	Ukraine	9,097,700
3	France	8,775,000
4	Germany	8,733,800
5	Spain	8,287,073
6	Australia	7,994,720
7	Canada	7,755,700
8	Turkey	7,600,000
9	United Kingdom	5,494,000
10	Argentina	4,076,940
11	United States of America	3,391,710
12	Poland	3,325,900
13	Denmark	3,264,100
14	Kazakhstan	2,593,100
15	Morocco	2,317,611
16	Belarus	1,978,794
17	Czech Republic	1,813,679
18	Ethiopia	1,703,347
19	India	1,662,900
20	China, mainland	1,636,900

The other crops can produce waste products utilized in many applications. For example, the main crops such as wheat, rice, and corn are grown in metric tonnes per year as shown in Table 3.

Table 3: Top 10 producing countries 2020

No.	Wheat [13]		Rice [14]		Corn [15]	
	Country	Production (Tonnes/year)	Country	Production (Tonnes/year)	Country	Production (Tonnes/year)
1	China	134,254,710	China	211,400,000	U.S. A	347,047,570
2	India	107,590,000	India	177,600,000	China	260,957,662
3	Russia	85,896,326	Indonesia	54,600,000	Brazil	101,138,617
4	U.S. A	49,690,680	Bangladesh	54,600,000	Argentina	56,860,704
5	Canada	35,183,000	Vietnam	43,400,000	Ukraine	35,880,050
6	France	30,144,110	Thailand	28,300,000	Indonesia	30,693,355
7	Pakistan	25,247,511	Myanmar	26,300,000	India	27,715,100
8	Ukraine	24,912,350	Philippines	18,800,000	Mexico	27,228,242
9	Germany	22,172,100	Pakistan	11,100,000	Romania	17,432,220
10	Turkey	20,500,000	Brazil	10.4M	Russian Federation	14,282,352

1.2. Oak

Oak leaves are another selected biomass material. The leaves are the products of huge shade trees that are crucial to forest ecologies. There are several species of oak trees, including white oak, red oak, black oak, pin oak, live oak…etc. These types of plants are cultivated based on the region, various growth habits, and the shape of the leaves [16]. In this research, live oak tree leaves are chosen as shown in Figure 3 because they are widespread in Florida. Live oak trees, *Quercus virginiana*, are located around the lower

coastlines between Virginia and southern Florida. They also are common in Texas. The leaves have a denser layer of trichome and possess highly packed particle tissues, which improve carbon dioxide absorption and chlorophyll content. The trichome layer serves as mechanical barrier against biotic attack. Moreover, this layer provides added resistance to the water vapor diffusion between inside of leaf and environment, and it functions as a reflector by decreasing the radiance absorbed by the leaf [17].

Figure 3: Live oak tree

The leaves remain green throughout the year. The length of the leaves extends usually between 5 cm to 10 cm. The leaves might stay on the oak tree during winter season until the new leaves start to prosper in the spring season. The leaves are describe as strong, and their shapes are narrow to a tall oval. The upper side of the leaves is shiny, and the downside is usually a light green [18]. After leaves fall through the winter, they stay as agricultural waste products, and their colors turn brown (Figure 4). They are collected and dried before

being fed into a mechanical grind grinder. Then, these leaves are converted to dark brown powder.

Figure 4: Oak leaves

1.3. Barley Straw

Another material is barley straw (*Hordeum vulgare L.*). As mentioned before, the globally growing regions of barley are Russia, Ukraine, France, Germany... etc. [11]. After harvesting barley, the dry stalky barley residues are called straw as presented in Figure 5 – and are crushed using a mechanical grind grinder. The straw particles were strained to eliminate coarse elements. The color of barley straw is dried yellow. In last two decades, barley straw has become widespread in U.S. This straw is used to avoid cyanobacteria, which has lignin-containing cell walls that decompose [11]. Barley straw has high amount of holocellulose with a comparatively tiny portions of lignin compared to the other biomass fibers sources [19]. Two kinds of residues are produced by lignin decomposition to restrict the growth of cyanobacterial. This kind of biomass materials (straw) is wealthy in

holocellulose with a comparatively small section of lignin compared with other natural fibers [20].
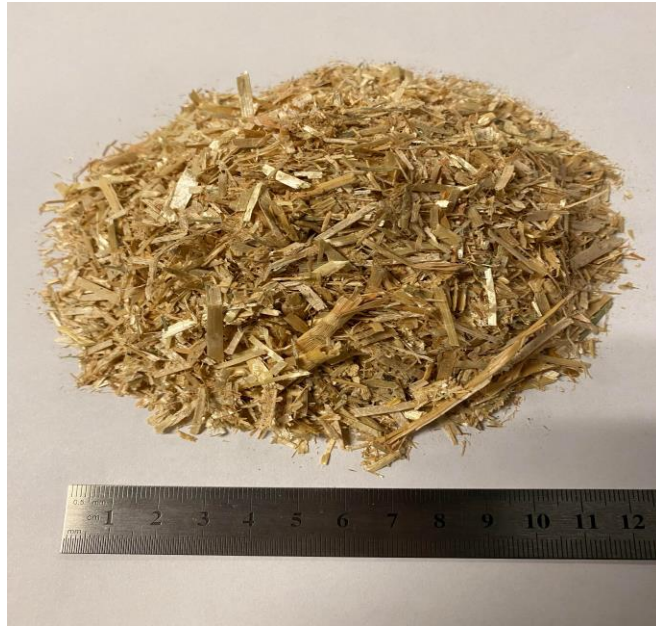
Figure 5: Straw

1.4. Jute

The other biomass material is jute, *Corchorus*. It is one of the tallest natural fibers and the most utilized fibers in different textile applications. Jute is derived from the bark of the white jute plant, *Corchorus capsularis*, and extracted with a lesser range from *tossa* jute, *Corchorus olitorius*. It is called the Golden Fiber due to its silky and golden shine. This crop takes 120 days to grow with a growing season usually from April to August. The length of jute ranges from 1 to 4 m; its diameter is between 17 to 20 microns. Figure 6 shows the long rope of jute fibers. The fibers are formed from plant materials called cellulose and lignin. These fibers are extracted by a chemical or biological process called retting, during which pectic material that bonds the fibers are broken down. Jute is considered as eco-friendly because the plant is totally recyclable and biodegradable. Jute's

most impressive feature is its capability to be utilized independently or mixed with other materials. Jute has benefits that include good insulating and antistatic characteristics, low thermal conductivity, and middle moisture content. Also, jute does not create harmful gases while burnt [21]. The color of jute ranges from off-white to brown [22]. Although jute is used in many applications, it is not usually utilized for clothing production because of its tough texture [23]. Jute agriculture requires a warm and moist weather with adequate rainfall and muddy soils and is planted in different countries like India, Bangladesh, China, Uzbekistan, and Nepal [24]. Jute is chopped using scissor into tiny pieces between 1.5 and 2.5 mm.

Figure 6: Jute rope

Although natural fiber composites have many advantages, there are also some drawbacks that limit usage in aerospace and automobile industries, including moisture absorption, lower fire resistance, and low temperature limitations [25]. There are some chemical treatments that could enhance the properties of the composites. The combinations between

natural fiber and polymer are considered a challenge because the chemical structures of fibers and matrix vary. The fiber structures are modified to change composition. The chemical treatments are essential to improve interface parameters. Then, fiber modifications cause a reduction in moisture absorption of the natural fibers, leading to an excellent enhancement of compatibility between the fiber and polymer matrix [4]. In this study, characterization techniques of biomass materials have been examined in an effort to manufacture sustainable biomass-reinforced composites (BRC) for use in several applications.

Definitions of Terms

α	Static angle of repose in (degrees).
H	Height (mm).
R	Radius (mm).
D	Diameter (mm).
V	Volume in (mm^3)
μ	Static angle of friction.
θ	Inclined angle in (degrees).
ρ	Density (g/cm^3).
W_d	Dry weight in air (g)
W_w	Wet weight in air (g)
ρ_w	Water density (g/cm^3).
m	Mass in (g)
k	Thermal conductivity in (W/mK).
Q	Heat flux in (W).

A	Cross-sectional area in (m^2).
Δ x	Thickness difference of the sample in (m).
ΔT	Temperature difference in (K)
R_{th}	Thermal resistance in (K/W)

List of Acronyms

DA	Torbal Density Analyzer
TPS	Transient Plane Source
PSD	Particle size distribution
RH	Relative humidity
NEAT	Neat epoxy composite
OAK	Oak leaves reinforced composite
BRY	Barley grains reinforced composite
STR	Straw reinforced composite
JUT	Jute reinforced composite
GA	Genetic Algorithms

2. Review of the Relevant Literature

Biomass materials play a vital role in engineering design to generate effective sustainable results. Due to environmental concerns, the materials have been explored, studied, and used as alternative sources. Engineering characteristics of biomass materials are essential for design and process control for handling, storage, transportation, and transformation to heat, power, and fuels. These properties can be classified into structural, thermal, compositional, and electromagnetic parameters. Structural properties might demonstrate themselves in the shape of mechanical and physical characteristics [26]. The utilize of natural fibers diminishes both waste disposal issues and ecological contamination [27]. Not only is a biomass material important for mechanical properties but the physical properties of products are considered as significant factors in the manufacturing processes to satisfy the ecological concerns of customers [28].

In recent years, physical characteristics have been investigated for numerous agriculture crops consisting of grains, leaves, and straws. Lam et al (2014) studied the physical properties of three biomass materials: switchgrass, corn stover, and wheat straw. Bulk density, particle density, particle size, moisture content, and flowability were examined for each sample of these biomass materials. Researchers found that standard parameters steps and statistical samples improvement are needed by the heterogeneous nature of biomass materials to incorporate their physical characteristics into both engineering design and operation. They also mentioned that conventional sieve tests cannot provide the measurements of the particles' three dimensions. Thus, it could link well with both packing and flowability information [26]. Stasiak et al (2015) examined the physical properties of sawdust and wood chips at five levels of moisture content. The scientists measured

moisture content, density, flowability, and coefficient of friction against construction surfaces on black, stainless steel, galvanized, and aluminum surfaces. They found that the average value of internal friction angle was 27 degrees for sawdust while it was about 33 degrees for wood chips. The effective angle of internal friction was between 34 degrees for sawdust and 42 degrees for wood chips. The moisture content was measured at 50 percent. The flow property of sawdust was cohesive/easy flow while wood chips provided a cohesive flow. Sawdust has a robust negative relationship between angle of internal friction and moisture content. They discovered that there were inefficient relationships between cohesion and moisture content for both examined materials whereas cohesion was found lower than strong impact by consolidation stress. Moisture content was increased by 30 percent for sawdust and reduced by 20 percent for wood chips in friction coefficient [29]. Zhang et al (2012) also experimentally studied the physical properties of wheat straw varieties under different climatic and soil conditions in three continents (Africa, North America, and South America). The moisture content, particle size, bulk density, and porosity were determined. Wheat straw was chosen as energy source in gasification and combustion systems due to its availability and sustainability. The physical properties measured were different from one country to another due to variations in climatic conditions, soil type, and fertilizer [30]. Wu, M.R. et al (2011) analyzed the physical properties of three kinds of solid biomass fuels. The physical parameters of wood pellets, wood chips, and torrefied pellets were tested while these materials interacted with both the storage and handling equipment [31]. Torrefied pellets, which are called black pellets, are considered a densified biofuel created from solid biomass treated thermally with additives or without them. They commonly have a cylindrical shape [32]. Particle density, bulk

density, particle size, moisture content, angle of repose, and angle of internal friction were measured. They found that wood pellets possess the best flow properties among the examined biomass materials, followed by torrefied pellets and wood chips. Wood chips have the maximum percentage of the moisture content because they are partly manufactured with more brittle materials due to their behaviors related to flowability [31]. Bouasker et al (2014) explored the physical characterizations of four types of straw fibers, one barley straw and three wheat straws, to find new alternative materials that met sustainable development criteria for use in construction applications [33]. Moreover, many researchers have studied the physical characteristics on various agricultural products, such as pumpkin seeds [34], coffee seeds and powder [35], lentil seeds [36], white lupin seeds [37], sunflower seeds [38], alfalfa grind [39], Bambara groundnuts [40], groundnut kernel [41], fennel seed [42], wheat and barley straws, corn stover and switchgrass [43]. However, no detailed study of such properties that has been conducted on barley seeds, oak leaves, barley straw, and jute. In this study, the biomass materials (barley seeds, oak leaves, barley straw, and jute) are employed as reinforced composites for polymer-based matrices. Recently, the biomass reinforced composites have become extremely valuable materials due their application benefits. Khan et al (2018) presented manufacturing fibers from natural resources that rely on biomass fiber-reinforced composites composed of kenaf and jute. In the aeronautics field, airplane interiors and several structures are made from aluminum or synthetic composite materials. Carbon fiber composites are utilized for reducing the mass of airplane. High strength can be provided by composites to mass ratio, enhanced aerodynamic efficiencies, and minimum manufacturing costs. The glass fiber composites' used in the airplane industry are very attractive because they are lower

industrial expenses. Toxins during the industrial steps are released by carbon filler and glass fiber, leading to harmful environmental impact. Biomass composites' materials are sustainable, and appropriate, when bast fibers like hemp, kenaf, flax, jute, sisal, and other biomass materials are implemented as reinforced composites [25]. Al-Oqla et al (2014) used the date palm to investigate natural fibers in natural fiber-reinforced polymer composites for automobile industry. Their study categorized the considerable parameters and criteria influencing the selection procedure of natural fiber composites' materials for various uses. It classified the abilities of the date palm fibers compared to alternatives such as hemp, coir, and sisal, all of which are applied in automobile industry among specific selective criteria [28]. The physical properties are affected by the orientation of the composites. Rangasamy et al (2021) manufactured jute fiber composites with an epoxy matrix and studied the effects of the mechanical, thermal, and physical properties with various fiber orientations (0º, 15º, 30º, 45º, 60º and 75º). They found the maximum value of mechanical properties of the jute resin composites came with 30º orientation when compared to the other orientations of composites [44].

The literature reviews pointed that there is an inadequate information concerning of choosing the appropriate biomass reinforced composites. The reason of that lack is due to the large probabilities of manufacturing new composites with new parameters [45]. Therefore, there is still a need for comparisons of the natural fiber composites among widespread of preferred criteria which impact the choose of the specified implementations.

2.1. The Adhesion Between the Matrix and Natural Fibers

The adhesion between the matrix and natural fibers is considered as a challenge because of the chemical structures of both fibers and matrix. This adhesion through chemical reactions

is developed by chemical fibers. Comprehensive investigations have been conducted to study the influence of chemical treatment on natural fibers. The nature of natural fibers can be classified into two various phases: the hydrophobic nature of natural fibers; and the hydrophobic nature of matrices. Then, a weak bonding is caused at the natural fiber composites interfaces [46]. The inherent hydrophilic behavior is reduced, and the adhesion characteristics of the matrix and fiber are developed by the chemical treatment of natural fibers [47]. For example, the interfacial adhesion between two materials is important for the mechanical performance of composites. The weakness of mechanical parameters for a composite is caused by poor bonding at the phase boundary. The weak compatibility of natural fibers between fibers and the matrix results from high moisture absorption [46]. Although natural fibers are influenced by moisture absorption, some of resins absorb a huge percentage of moisture [47]. Therefore, chemical modification for both the surface of fiber and the matrix is necessary to improve the adhesion of natural fibers to the matrix, enhancing the strength and stiffness of the natural fiber composite [46].

The reasons behind the use of natural fibers consist of availability, sustainability, low cost, good properties of thermal and acoustical insulation, energy enhancement, decreased respiratory and dermal irritation, and decreased tool fatigue in machining processes [45-51].

2.2. Thermal Decomposition

Although the natural fibers have many advantages, there are some drawbacks, including moisture, mold, fire risk, decomposition, degradation, and low temperature limits. About 60 percent of the thermal decomposition for natural fibers occurs within a temperature rate from 215 to 310º C. While several investigations have studied the thermal decomposition

of natural fibers, a prediction technique for thermal decomposition under the usual processing temperatures of composites has not been found [52].

2.3. Moisture Absorption

The moisture absorption of the natural fibers is reduced by using alkali treatment or acetylation. Alkali treatment called mercerization is one of the most popular treatments for natural fibers. The procedure uses potassium hydroxide (KOH), lithium hydroxide (LiOH), or sodium hydroxide (NaOH) to reduce the hydrogen content of the cellulose, and the crystalline cellulose is added to raise the amorphous cellulose amount at the expense of crystalline cellulose. The alkali treatment modifies the noncellulosic parts of the fiber like the lignin, hemi-cellulose, and pectin. Mercerization also modifies one of the most moist-absorbing components of the natural fiber, hemicellulose. The acetylation technique of the natural fibers is also called the esterification procedure. The aim of this process is to decrease the chemical, hygroscopic nature of the fibers, while increasing the stability of the composite. The acetylation is usually applied in the surface treatment of fibers. The morphology of surface and the moisture resistance of the flax fiber is enhanced because of modifications utilized by the acetylation method. Some of the fiber's characteristics rise with increasing acetylation degree between 15 percent and 18 percent and are reduced based on increase in the acetylation degree. Drawbacks of alkali treatment include the higher levels of pH, mechanical and chemical degradation of cellulose fibers, and high surface content polluted wastewater. These natural fibers are extremely enhanced by chemical modifications [25].

2.4. Mold

The other drawback is mold. One of the natural, effective, and non-toxic mold cleaners is distilled white vinegar, which is derived from diluted alcohol outcomes. White vinegar is moderate acidic, and it has been demonstrated to be efficient in treating more than 80 percent of mold types. This type of vinegar is safe, available, and affordable [53].

2.5. Fire Resistance

The fire resistance of the biomass reinforced composites can be enhanced by reducing the cellulose content of natural fiber, raising the crystallinity, and reducing the polymerization of the composites. The flammability of composites is not consistent among various kinds of natural fibers because they possess various microstructures and chemical compositions [54]. Improving fire resistance of these composites could be done by using the coatings and additives like ceramic, silicone, intumescent, ablative, phenolic, and glass mats [55]. Moreover, the treating temperature is another crucial parameter. The maximum temperature, which can be achieved in the treating period to prevent degradation of the natural fibers, is 200º C within 20 minutes [56][57].

2.6. Degradation

Degradation, low performance, shrinkage of the natural fiber composites can be caused if the temperature exceeds this limit (200º C) because the mechanical, physical, and chemical properties of the natural fibers are varied by oxidation, dehydration, depolymerization, decarboxylation, hydrolysis, and recrystallization [58].

2.7. Application of Biomass Reinforced Composites

Several researchers have studied the abilities, competitiveness, and appropriateness of biomass fibers as polymeric matrices with reinforced fillers. Most of the investigators have concentrated on the mechanical parameters, the chemical properties needed to modify

fiber/ polymer compatibility, and manufacturing operations. Some of the researchers have compared various natural fibers composites to achieve their suitability for specific aims and uses. Polypropylene composites, which are reinforced with hemp fibers, have been widely explored by Pickering et al. (2007) through the injection of molding procedure [50]. Natural fibers modifications, treatments, and enhancing the hemp fiber quality have been studied. Previous studies had been conducted the characteristics of jute/ plastic composites. Several parameters were examined, including fiber modification, crystallinity, thermal stability, climate resistance, hardness and strength, and their suitability in certain applications [48][49][51]. Also, the usage of date palm fibers was investigated by Al-Khanbashi et al. (2005) as a reinforced polymeric matrix along with the characteristics of composites [59].

Biomass-reinforced composites have been applied in aerospace and automotive manufacturing because the temperatures of the circumferential conditions could be suitable in fluctuating climates. For instance, an eco-plastic manufactured from sugar cane has been developed by Toyota company and can be utilized to line a car's interior [60]. The other application of using the natural fibers composites in fluctuated weather conditions was developed by Mazda, which uses polylactic acid in the interior console of the Mazda 5 with kenaf (also called Java jute) in seat covers [61].

There are some studies that compare thermal conductivity with the other properties like moisture, density, porosity, and orientation of the biomass materials. These studies will be mentioned in Results and Discussions section. Thermal conductivity of barley is mostly impacted by moisture content and temperature [62-64]. The thermal conductivity of bulk barley has been studied by Alagusundaram et al (1991). The researchers determined

thermal conductivities from 0.169 to 0.232 W/(m.K) using five moisture contents between 9 and 23 percent with five temperatures measurements from -28 to +29 ℃ [65]. Zach et al (2013) measured the thermal conductivity of hemp implemented in building uses combined with polyester fiber and fire retardants. The thermal conductivity measured was from 0.038 and 0.060 W/mK while the density ranged from 20 and 90 kg/m^3, and the specific heat was from 1.6 to 1.7 kJ/kg. K [66]. Thermal conductivity of kenaf fibers measured between 0.034 and 0.043 W/m.K with the density from 30 to 180 kg/m^3 and the specific heat between 1.6 and 1.7 kJ/kg K [67]. The thermal conductivity of the renewable materials likejute, flax, and hemp to manufacture insulation materials was measured by Korjenic et al (2011) and calculated between 0.039 and 0.046 W/m.K, while the density ranged from 26 to 82 kg/m^3 [68]. The properties of the thermal conductivity and acoustic absorption of manufactured kenaf panel binderless particleboard was tested by Xu et al (2004). The thermal conductivity depends on the density. The thermal conductivity of the panels ranged from 0.040 W/m.K to 0.065 W/m.K, and the density was between 100 kg/m^3 and 250 kg/m^3 [69]. Dikici et al (2020) investigated the thermal conductivity of natural fiber-reinforced polymer composites (NFRP) as potential structural materials. The natural fibers chosen were Bermuda grass seeds, conifer cones, and pinecones. The matrix consists of vinyl ester resin, and the thermal conductivity was measured using transient plane source technique performed in the TPS 2500S Thermal Constants Analyzer. They found that the increase of 9 percent Bermuda fibers resulted a reduce of 19.3 percent in thermal conductivity compared to the neat epoxy. The increase of 9 percent nanocellulose fibers yielded a reduction of 40.7 percent in the thermal conductivity in the nanocellulose/ vinyl ester resin composite compared to the neat vinyl ester materials [70]. Collet et al (2014) studied the

influence of formulation, density, and moisture content on the thermal conductivity of hemp concretes. The examinations were performed on practical measurements by modeling a self-symmetric scheme. The values of the thermal conductivity were between 90 and 160 mW/(m·K) at (23 º C temperature, 50 percent relative humidity). They found also that the effect of density on thermal conductivity is more significant than the effect of water content. The thermal conductivity enhanced about 54 percent when the density increased about 66 percent while it increased from 15 percent to 20 percent between dry state and 90 percent RH [71]. Ogedengbe et al (2013) evaluated thermal conductivity of biomass composites like sawdust, rice husk, coconut husk and palm kernel husk and their composites using Lees' Conductivity Apparatus. The thermal conductivity values of these biomass composites were calculated at temperatures from 35 to 50 ºC. They found the thermal conductivity ranged from 0.073 W/m.ºC to 0.303 W/m.ºC. The thermal conductivity values of biomass composites measured were compared and found lower than the thermal conductivity values of the industrial insulation materials. Hence, using biomass composites materials as alternative source for commercial insulators will be good insulation materials because they provide decreased insulation cost in addition to helping maintain a sustainable environment [72]. According to the previous scientific literature, much attention has been taken to the field of biomass materials that is sustainable, available, and affordable as insulation materials, and the reason that oak, barley, straw, and jute are picked because they are not available in the literature now.

Also, there are some studies related to thermal analysis and its applications. Thermal analysis techniques are applied to analyze polymers, particularly to investigate the performance of thermoplastics, thermosets, and elastomers. In addition, there are four main

techniques, Differential Scanning Calorimetry (DSC), Thermomechanical Analysis (TMA), Thermogravimetric Analysis (TGA), and Dynamic Mechanical Analysis (DMA), and there is a combination of these techniques. Various perspectives are provided by these different techniques used to characterize the processes such as the glass transition, melting, and crystallization, relying on the data required [73].

Blanco et al (2021) reported the usage of thermal techniques in the characterization of bio-sourced polymers. The thermal characteristics include glass transition temperature, crystallization temperature, melting temperature, the temperature at maximum mass loss rate, and initial decomposition temperature. They mentioned these properties play a vital role in progressing with a profitable biopolymers design, polymers recycling, recyclable polymer preparation, and potential tools for biopolymer design in additive manufacturing. Then, it provides a good grasp of the parameters of the studied materials and the correct path to the optimal design and preparation [74].

There are many applications for using natural fiber-reinforced composites. Gotmare et al (2017) mentioned some studies on concrete reinforcement utilizing non-textile estimates and recycled fibers derived from biomass, carpet waste, plastic bottles, and other manufactured and domestic wastes. They reported that a large amount of energy in the construction actions that used such as cement, steel, synthetic polymers, and metal alloys, is consumed, and environmental impacts can be caused during the whole life cycle. There are many natural and recycled resources, and it is so essential to study these resources. The natural and recycled fiber composites have been grown to begin currently. For example, fiber-reinforced concrete is used as a sustainable design with a low effect on the

environment. In addition, using sustainable and recycled materials provides inexpensive energy costs. They concluded that biomass and recycled materials can be used in industrial applications such as panels, roof tiles, prefabricated structures, precast elements, and curtain walls. The fiber-reinforced concrete composites are used in these applications because they have several benefits such as renewable, available, low cost, and non-harmful replacement of asbestos [75].

Vázquez-Núñez et al (2021) indicated some studies based on green polymer-based composites and natural reinforcements of renewable sources. Attractive properties have been observed by using the natural-fiber-reinforced bio-composites based on a bio-based polymer. One of the most significant features of the new green materials, hemp, flax, and kenaf, is biodegradability which permits them to contribute to an environmental solution in the global market. Significant developments have been revealed by the industrial steps for producing new green materials due to the characteristics of each raw material. Furthermore, their environmental impact has facilitated its integration into various fields like construction, packaging, automotive, and medicine. Their segment drives society toward enhancing the creation of green economies by using raw materials as alternatives to rural areas where these materials are available [76].

Therefore, these four biomass materials have been implemented to manufacture biomass-reinforced composite materials as alternative source for commercial industrial insulations through the assessment of their thermal conductivity and density and comparing those values against the traditional thermal insulators. After manufacturing biomass reinforced composites in varying weight ratios of biomass materials, the properties like density and

thermal conductivity of these composites will be measured and compared with commercial insulation materials.

3. Methodology

3.1. Physical Properties of Biomass Materials

In this study, various experiments are implemented in order to acquire the crucial physical properties of biomass materials. There are different biomass materials and measuring devices used. Biomass materials include barley grains, oak leaves, straw, and jute. Measuring devices were manual grind grinder, Geotech Sand Shaker, microscope (B 120 Model), relative humidity meter PCE-MA 110, a 50 ml aluminum density cup (pycnometer), flowability test, angle of internal friction measurement, Torbal Density Analyzer (DA) kits, and TPS 2500S Thermal Constants Analyzer. The physical properties of biomass materials like moisture, particle size distribution, microscopy, bulk density, flowability, and static coefficients of frictions were measured in order to manufacture the biomass reinforced composites materials. Figure 7 shows the four types of biomass materials. This figure presents barley grains collected after harvesting, oak leaves gathered after their fall-down from live oak trees, barley straw assembled after harvesting, and jute fibers rope.

| Barley grains | Oak leaves | Straw | Jute |

Figure 7: Biomass materials, barley grains, oak leaves, straw, and jute rope

3.1.1. Sample Preparation

Barley grains, oak leaves, and straw are collected and grinded by using manual grain grinder made from cast iron as shown in Figure 8. For the other sample preparation, jute fiber roll was chopped by a scissor into short pieces with length about 1.5 mm to 2.5 mm. These three powders (barley grains, oak leaves, and straw), and the chopped jute were kept for the storage. For the storage conditions, ambient conditions of (ME-131) Clean Energy Laboratory were between 56 percent and 67 percent relative humidity (RH), and the environmental temperatures were between 16° C and 21° C.

Figure 8: Manual low hopper grain grinder.

After doing the milling process of the three biomass materials, an unstrained powder was sieved with mesh equal to sieve designation of 26 OPN (660.4 μm) to keep the particles in consistent size. Figure 9 shows sieve designation of 26 OPN.

Figure 9**:** Sieve designation of 26 OPN (660.4 μm)

Then, the three powders (barley grains, oak leaves, and straw), and the chopped jute are prepared. Figure 10 illustrates the biomass materials prepared for studying the physical properties.

| Barley grains powder | Oak leaves powder | Straw powder | Chopped jute |
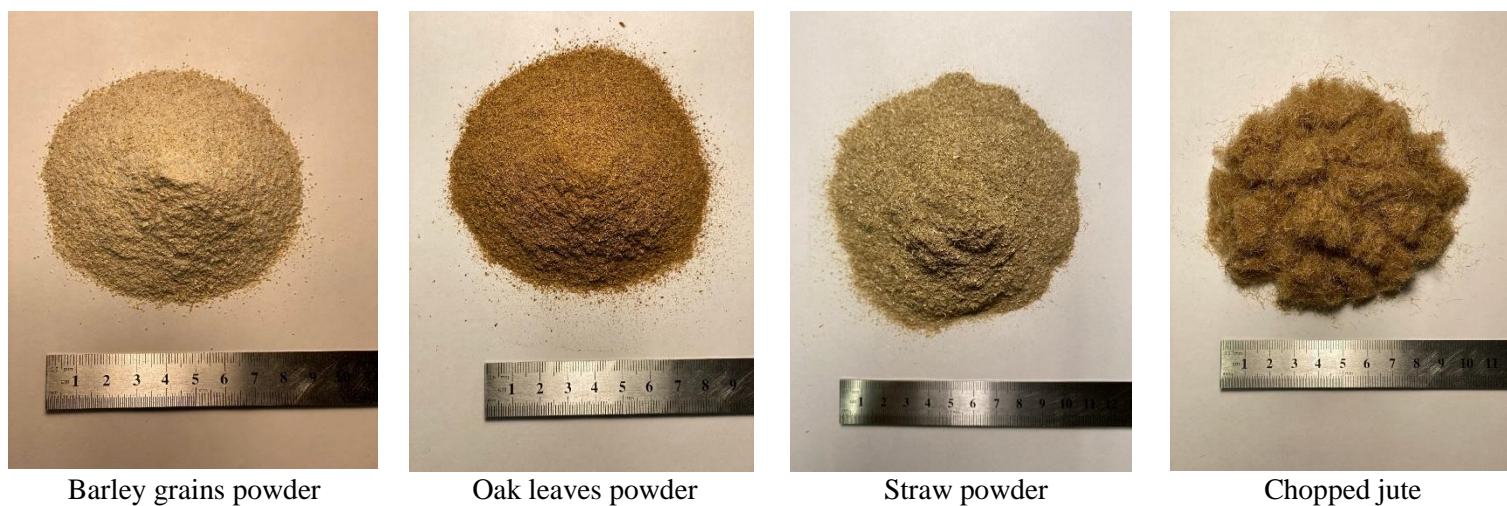
Figure 10: Ground/ chopped biomass powders

3.1.2. Moisture Measurement

Moisture content is one of the most crucial physical characteristics for the procedure of a drying biomass material. Each sample can be tested separately to measure the moisture content. In order to measure many samples at the same time, these samples have to be placed into enclosed containers to ensure their features do not vary during storage. The sample on the pan is distributed equally in a thin layer between 2 mm and 5 mm to obtain duplicatable results. Unequal application of sample produces inhomogeneous heat distribution in the sample that is required to be dried. That means that the sample is not completely dried or the drying time has been increased. Because the material lies in a pile, the top layers will heat more roughly, generating combustion or incrustation. The sample thickness of an exceedingly high layer or likely incrustations blocks the moisture from leaving the sample. Moreover, there are tools provided for sample preparation. These instruments possess a huge influence on the precision and reliability of the measurements. The tools with heat-conducting properties are avoided, because they can transfer heat easily to the sample. Inappropriate handling and preparation of the sample will cause an inaccurate measurement. To overcome that possibility, an aluminum pan is utilized once. If the pan is used again, the result of the measurement would be falsified due to the sticking residues. The temperature probe should be set in the cover of the moisture balance. Also, the sample should not be touched because the results will be affected. Solids, powdery and grained samples should be distributed equally on the sample pan. Coarse-grained samples should be crushed in a mortar device. Then, any heat supply should be avoided while crushing the sample, because that will cause moisture loss [77].

Figure 11: Relative humidity meter PCE-MA 110

Figure 11 shows relative humidity meter PCE-MA 110. The samples weights chosen varied

from 1 g to 5.41 g based on the powder particles distributed on the test pan of moisture

analyzer. For example, the highest values of sample weights of barley seeds powder were

between 3.13 g and 5.41 g during the three tests because this powder is too fine. So, more

powder was needed to distribute in the pan. The weight values of oak leaves were 1.53,

1.70, and 2 g for the three tests, and the average weight of oak leaves powder distributed

on the sample pan was 1.74 g. The weights of barley straw were 2.03, 2.30, and 2.03 g, and

the average weight was 2.12 g. Finally, the weight for chopped jute was 1 gram for each

test of the three experiments because of the nature of this material, which is not the same

as the milled powders. For the ambient conditions, the values of relative humidity were

between 56 percent – 67 percent (RH), and the environmental temperatures were from 16° C to 21° C during the implementation of these experiments.

Experimental Test Setup

Prior to begin the measurement, the sample, and the glass fiber filter on the pan retainer should be placed inside the relative humidity meter device. Then, the device should be tared to make sure that only the weight of sample is estimated. If different sequential measurements are carried out, the temperature from the former measurement still warm in the measuring chamber, and the evaporation previously occurs while the cover is closed. It is important to wait either to let some of time for the drying chamber to cool down or accept the deviations and begin the following measurement as soon as possible [77]. The moisture content is measured. Then, each biomass material should be dried as possible as to reduce mold formation by handling and storage that biomass material [26]. Figures 12, 13, 14, and 15 show the biomass materials like barley seeds, oak leaves, barley straw, and jute, respectively, were tested in humidity meter. This test was repeated three times for each sample of biomass materials.

(a)   (b)

Figure 12: Measuring moisture percentage of barley grain powder.

(a)   (b)

Figure 13: Measuring moisture percentage of oak leaves powder

<table>
<tr><td>(a)</td><td>(b)</td></tr>
</table>

Figure 14: Measuring moisture percentage of straw powder

(a)	(b)

Figure 15: Measuring moisture percentage of chopped jute.

3.1.3. Particle Size Distribution

Biomass materials must be reduced in size after being harvested. Particle size distribution (PSD) is the procedure in which a powder of biomass material is examined to distinguish the average size of the particles. The particle size distribution is an important physical parameter of biomass materials because it affects flowability and particles contact [35]. The three powders, barley grains, oak leaves, and straw, are placed in Geotech Sand Shaker, which contains five clear acrylic cylinders. The shaker is a mechanical sieve kit manufactured to supply reliable grain size analysis. There are 20 stainless steel screens ranging in size from United States sieve number (US Sieve No.) 4 to 270 using industrial standard units of OPN representing mesh size. Table 4 shows standard sieve screen sizes [78]. The weight of each sample was 25 g. Each powder was placed in the upper stage of the cylinders and vibrated to spread their particles using different screen sizes of the sieves square holes opening based on the particles of the strained powder. Due to light weight and string shape, jute cannot go through a Geotech Shank Shaker to determine particle size distribution. However, it could be examined for the other physical properties. Figure 16 presents Geotech Sand Shaker and its components.

Table 4: Standard sieve screen sizes [78]

Sieve Designation	Mesh Opening (inches)	Mesh Opening (mm)	US Standard Sieve No.
187 OPN	0.1870	4.7498	4
132 OPN	0.1320	3.3528	6
90 OPN	0.0900	2.2860	5
72 OPN	0.0720	1.8288	10

60 OPN	0.0600	1.5240	12
51 OPN	0.0510	1.2954	14
46 OPN	0.0460	1.1684	16
40 OPN	0.0400	1.0160	18
30 OPN	0.0300	0.7620	20
26 OPN	0.026	0.6604	25
23 OPN	0.023	0.5842	30
20 OPN	0.0200	0.5080	35
15 OPN	0.0150	0.3810	40
09 OPN	0.0090	0.2286	60
055 OPN	0.0055	0.1397	100
046 OPN	0.0046	0.1168	120
041 OPN	0.0041	0.1041	140
029 OPN	0.0029	0.0737	200
024 OPN	0.0024	0.0610	230
021 OPN	0.0021	0.0533	270
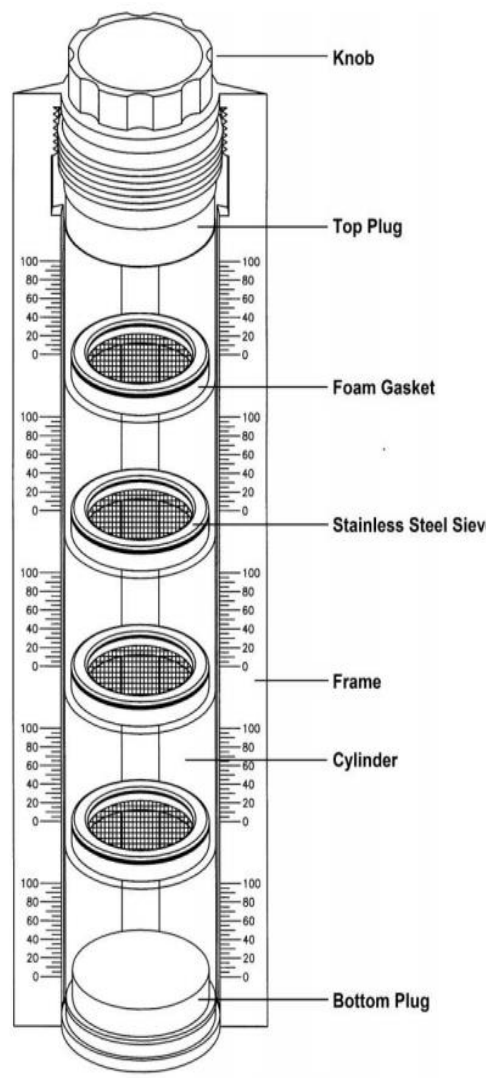
(a): Geotech Sand Shaker.   (b): Shaker Components.

Figure 16: Geotech Sand Shaker with standard sieve screen sizes [78]

Before this test, the moisture content of each powder was recorded. The sample of barley grain powder was taken with 25 g weight. The average moisture percentage of barley grains was 7 percent. The low moisture percentage helps the powder be ground easily. The shaker is divided into five stages, and the four upper stages have different standard values of sieves, and the fifth stage (bottom) is the pan. The sieves placed in the shaker by applying

the highest value of sieve until reaching the lowest value before the pan. These standard sieves were chosen according to the nature of the particles of the barley grain powder. The sieves samples applied were 26 OPN (d_p> 660.4 µm), 23 OPN (584.2 µm< d_p <660.4 µm), 20 OPN (508 µm< d_p < 584.2 µm), and 15 OPN (381 µm< d_p <508 µm) (Where d_p is the particle diameter) as indicated in Figure 17. The 25 g of the sample were placed on the top sieve in upper stage of the shaker. Then, the shaker was vibrated from 15 to 20 minutes. The barley grain powder gathered at each size stage was weighed. The weight percentage of each size stage was calculated by subtracting the original measured weight (25 g) of the powder from each size stage.
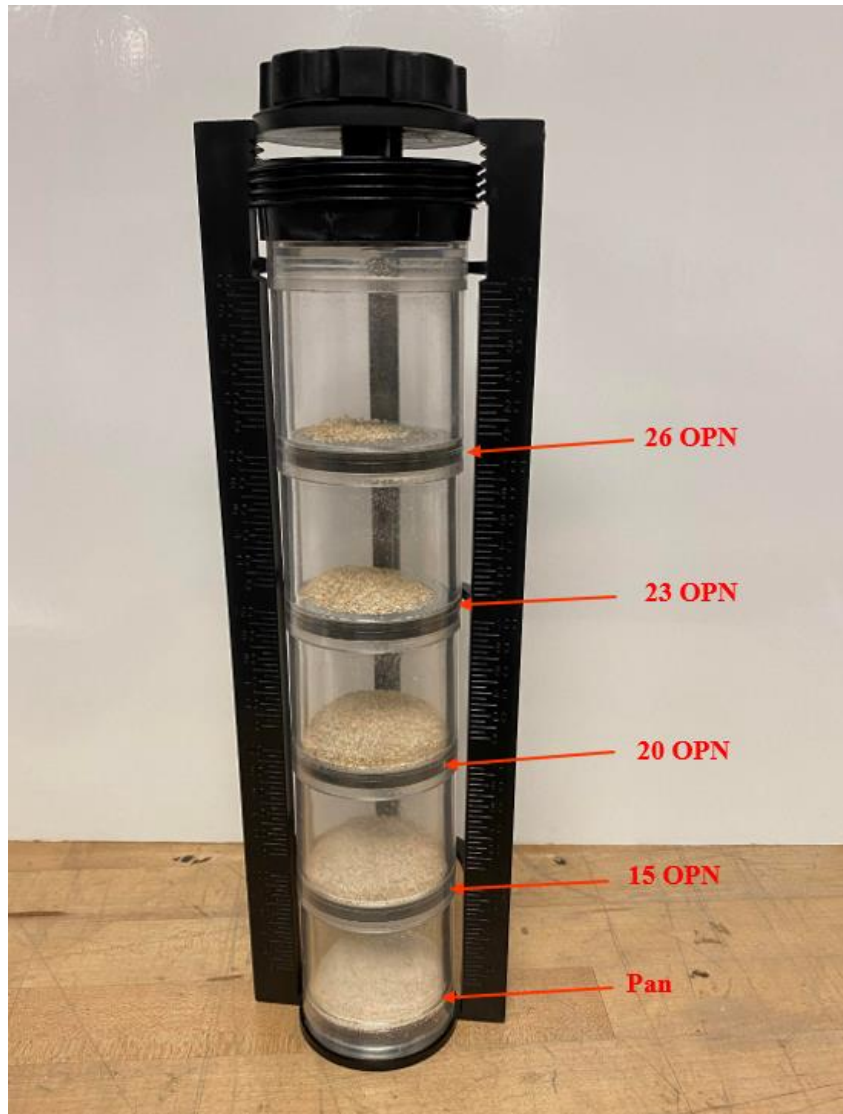
Figure 17: Barley grain powder on Sand Shaker with standard sieve screen sizes of 26, 23, 20, 15 OPN, and pan.

The sieves used for oak leaf powder were 46 OPN (d_p >1168.4 µm), 40 OPN (16 µm< d_p <1168.4 µm), 30 OPN (762 µm< d_p < 16 µm), and 26 OPN (660.4 µm< d_p <762 µm) as shown in Figure 18, and the same procedure was done with running five times of experiments.
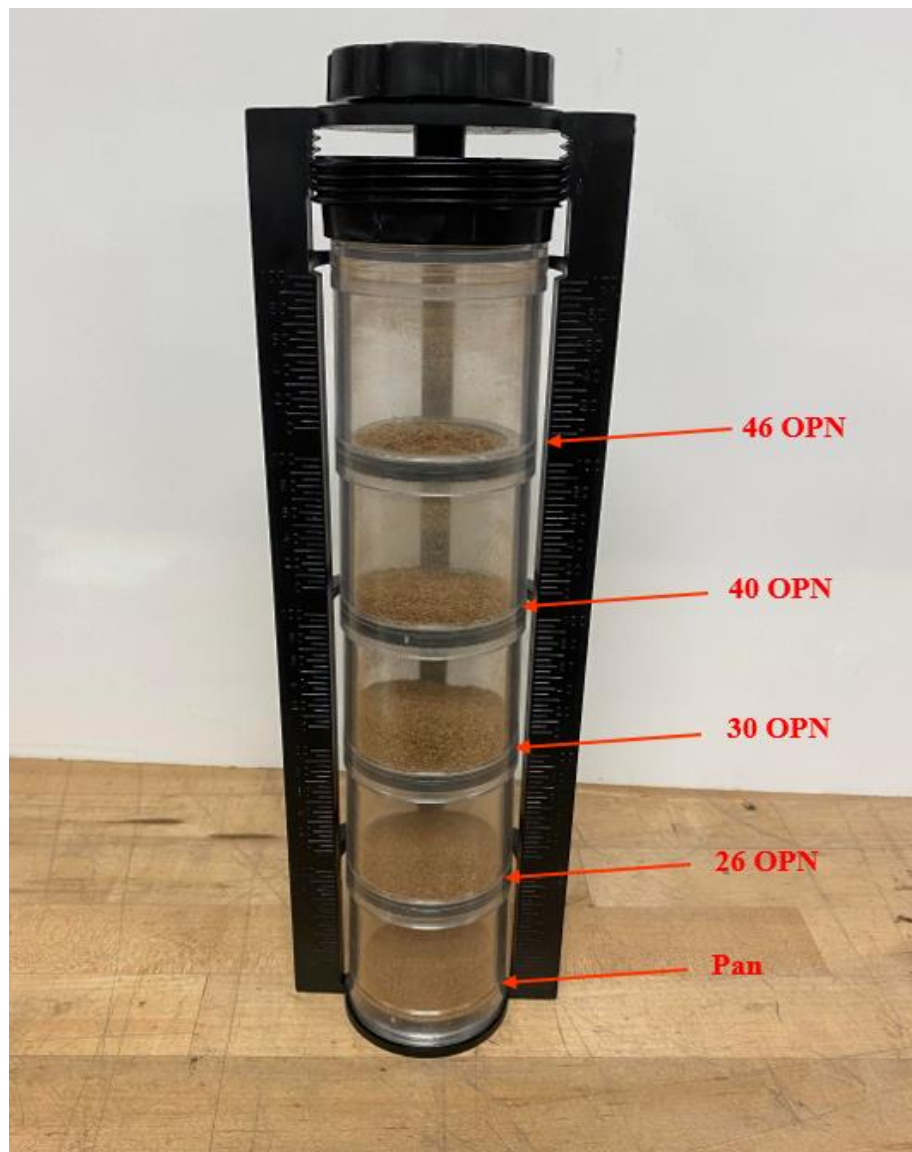
Figure 18: Oak leaf powder on Geotech Sand Shaker with standard sieve screen sizes of 46, 40, 30, 26 OPN, and pan.

The sieves used for straw powder were 60 OPN (d_p >1524 µm), 51 OPN (1295.4 µm< d_p <1524 µm), 46 OPN (1168.4 µm< d_p < 1295.4 µm), and 40 OPN (16 µm< d_p <1168.4 µm) as shown in Figure 19.
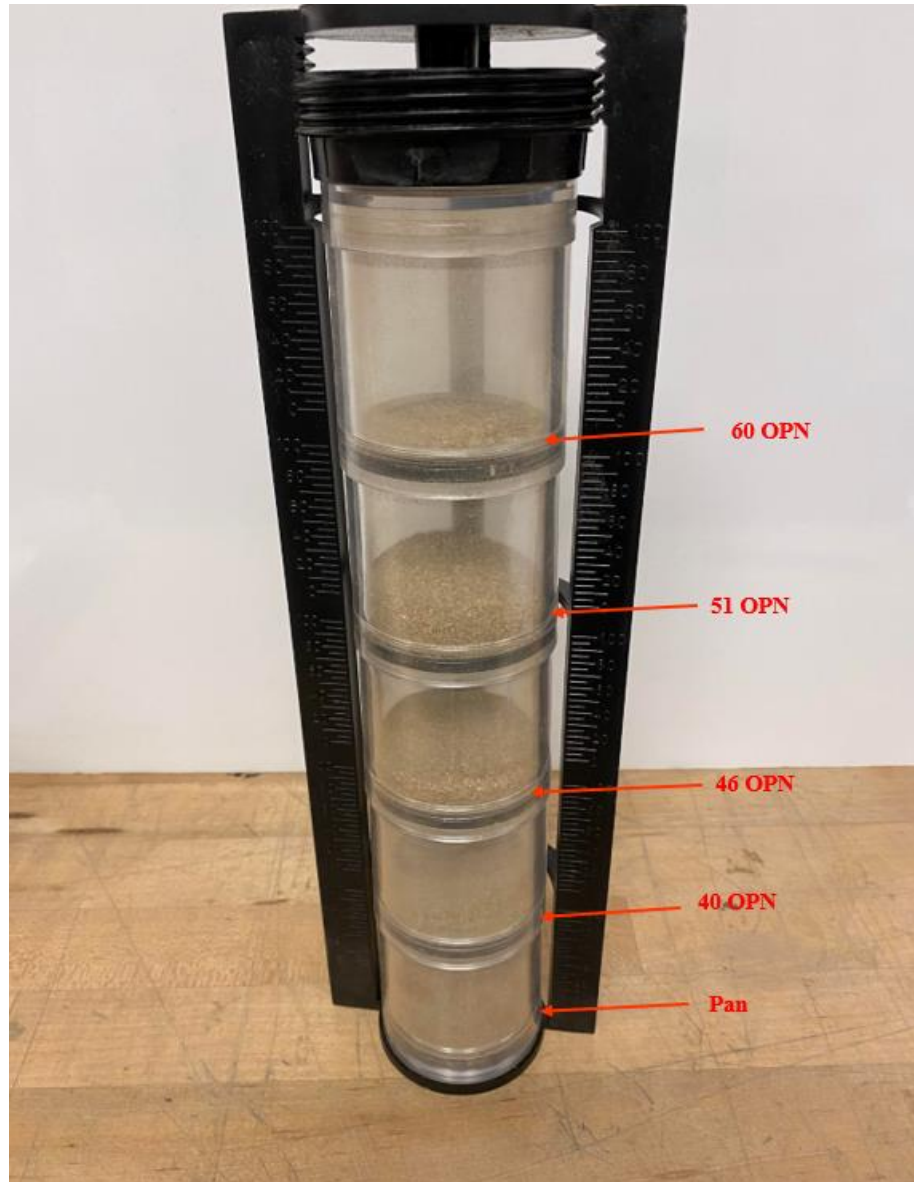
Figure 19: Straw powder on Geotech Sand Shaker with standard sieve screen sizes of 60, 51, 46, 40 OPN and pan.

This test was performed five times for each sample. For the environmental conditions, the measurements of relative humidity were between 56 percent to 67 percent (RH), and the ambient temperatures were from 16° C to 21° C during performing these experiments.

3.1.4. Microscope

One part of AmScope (B120) consist of a Base Lens, which guides the light source towards the slide. The other component is Coarse Focusing Knob, which is used to take the slide into the sight and focus. The quantity of light which concentrates on the slide is controlled by Condenser & Iris Diaphragm. The condenser is fastened by a condenser screw, which is set it to the mechanical stage. The quantity of light that flows from the base lens is controlled by a dimmer. Diopter lets the concentration to be ideal for both eyes separated from each other. Enhancing concentration to get a clear image is done by a fine focusing knob. The upward movement of the mechanical stage is controlled by a limit stop screw to prevent any damage to the slide. The slide is moved mechanically along an X and Y axis for best position by the mechanical stage. The objective lenses are positioned by a nosepiece. The rotating Siedentopf head adjusts the distance between the user's eyes for added comfort. The tension of the focusing knobs is set by a tension knob. Figure 20 and Figure 21 show the microscope (B 120 Model) with all parts. The microscope container is opened precisely to prevent the sample from falling and damaging the optical items. The packing list is examined to ensure that all parts are received such as one Siedentopf microscope head (binocular or trinocular), a microscope base, Four DIN Standard Objectives (4x, 10x, 40x, 100x), 20x Widefield eyepieces, blue color filters, a bottle of immersion oil, a spare fuse, and a dust cover. The unit consists of the base, the stage, the

arm, the nosepiece, and the head. In addition, the eyetube caps should be removed, and the desired eyepieces should be dropped into the eyepiece ocular tubes. The lens should be prevented from touching to make sure there are no relics (remains of fingerprints due to touch) that could appear in an image which is being tested. Also, the objectives should be screwed into the microscope nosepiece from the lowest magnification to the highest to prevent touching the lenses. Finally, the microscope is plugged in and turned it on [79]. Figure 22 demonstrates the microscope in Clean Energy Laboratory.
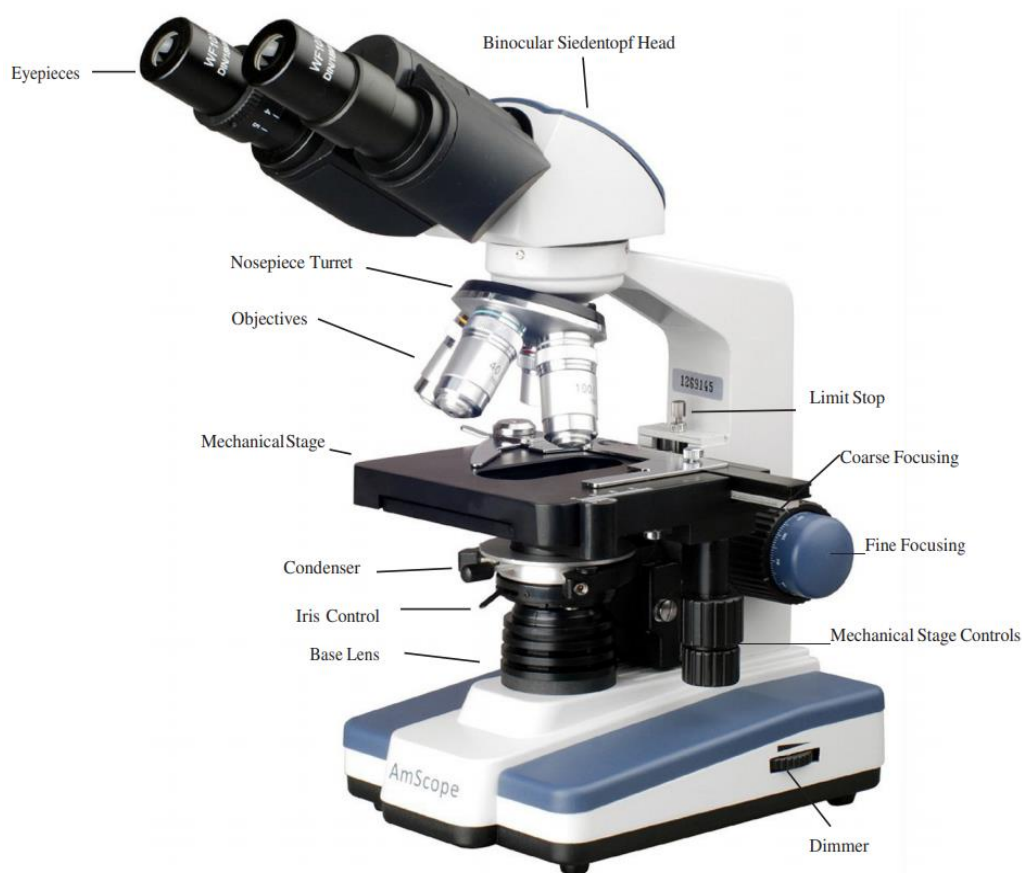
Figure 20: Microscope (B 120 Model) [79]

Figure 21: Base and condenser (B 120 Model) [79]

Figure 22: Microscope

This type of microscope is set up by the following steps. The microscope head is placed in the proper position to get a suitable situation for observation. Also, the researcher should examine into the eyepieces by opening both eyes. The interpupillary distance is set by controlling the eye tubes and rotating the eyepiece tubes in both directions either toward or away from each other since only one circle of illumination is observed by both eyes. In

addition, the specimen to be studied on a glass slide is placed in the microscope stage, and it should be put it on the stage by holding it with metal slide of the mechanical stage. The vertical pillar with dual knobs under the right side of the stage is controlled by using the mechanical stage. The specimen over the stage opening should be centered with matching it with the light and the objective lens. Finally, the dimmer on the right side of the base is gradually turned to modify the light until the desired intensity of illumination is obtained.

The process of focusing is done by the followings. The nosepiece is turned to select an objective. The easiest way to do that is to select the lowest magnification with 4x objective in order concentrate on the specimen. Sometimes, the mechanical stage is moved up or down to refocus the image. Furthermore, the sample concentration is examined with one eye through eyepiece without the diopter, while the other eye is closed. The coarse focusing knob is used to set the height of the stage until the sample appears clearly. Finally, while the image in view field is clear, the fine focusing knob is slightly adjusted to get perfect results [79]. The condenser and diaphragm are adjusted by using these steps. The distance between the light condenser and the stage can be changed by utilizing the condenser-adjustment knob. Then, the concentration of the light which is hitting the slide can be controlled. The environmental temperatures of Clean Energy Laboratory (ME-131) were from 16 °C to 21 °C and the values of relative humidity (RH) were 56 to 67 percent during experiment measurements.

3.1.5. Bulk Density

Bulk density is defined as the measurement of biomass mass per unit volume (g/cm^3). Bulk density measurements of barley grains, oak leaves, straw, and jute were calculated

according to ISO 2811, DIN 53217, ASTM D 1475 [80]. It was measured by using a density cup called pycnometer. The volume of pycnometer is 50ml (50 cm3) made from aluminum as displayed in Figure 23, and the mass of pycnometer is 50.16 g while it is empty. A scale with capacity to weigh the sample of the pycnometer to within 100 g is required. The sample magnitude should be big enough to be represented. The bulk density is determined by using this equation [81]:

$$Bulk\ density \left(\frac{g}{cm^3}\right)$$
$$= \frac{(Pycnometer\ and\ sample\ weight) - (Pycnometer\ weight)}{(Pycnometer\ volume)} \quad (1)$$

The amount of bulk density differs with how the biomass in the container is packed. Biomass with high bulk density is appropriate for transport while needing less volume for storage. The 50ml aluminum density cup (pycnometer) is completely filled with each of the biomass materials. The powder is tapped five times in the density cup in a vertical direction so all the voids were filled with powder or tiny chopped materials of jute to reach a fully enclosed system as shown in Figure 24. The mass of the biomass powder is obtained from a Torbal AD Series Precision Balances device as indicated in Figure 24. Each measurement is repeated for five refills, utilizing the same biomass particles and obtained the average of bulk density for each sample. The bulk density should be determined with the moisture percentage and size and shape of particles because a powder bulk density affects with its particle size and water content [26]. The bulk density was measured in regard to the surrounding conditions (Clean Energy Lab (ME-131). The ambient

temperatures were from 16 °C to 21 °C and the values of relative humidity (RH) were 56 to 67 percent.

Figure 23: Aluminum Density Cup (pycnometer)

(a) Barley grains   (b) Oak leaves   (c) Straw   (d) Jute

Figure 24: Biomass materials filled in pycnometer

Figure 25: Torbal AD Series Precision Balances device.

3.1.6. Flowability Technique (Static Angle of Repose)

Biomass materials are considered sustainable and renewable sources of energy. To illustrate, lignocellulosic materials are transformed to beneficial energy sorts in many methods like thermochemical or biochemical ways [82][83]. Engineering challenges anticipated in providing biomass for these transformations in a biorefinery consist of harvesting, handling, storage, transportation, and processing [84-86]. A numerical technique was done by Jenike, which determined minimum hopper angle, opening size, and the bulk flow of particular materials utilizing from direct shear technologies [87]. A flowability method of a material is referred as static angle of repose. It is considered as a function of particle shape, friction, and cohesiveness. It could be clarified as the angle at which a material will stay on a constant powder pile. Designing the height and the heap

dimensions of the biomass particles is supported by flowability technique [31] [88-91]. The angle of repose examination could determine flowability of biomass grinds utilizing a Mark 4 version tester enhanced by Geldart (Powder Research Ltd., UK). The model of flowability can be classified in three categories: free flowing, fair flowing, and cohesive [92]. A flowability method had been investigated for ground particles of wheat straw, switchgrass, and corn stover by using the Mark 4 version examiner. The weight of experimental study of the flowability was collected 25 g for each material ground on each mesh after sieving. In addition, it was gradually poured onto the upper stage with the vibrating chute [93]. Figure 26 shows Mark 4 version tester [94].

Figure 26: Mark 4 version tester [94]

The angle of repose is one major element to distinguish the flow attitude of granular materials. The repose angle is concerned with different significant phenomena, such as stratification, avalanching, and segregation [95-100]. Moreover, this angle has been used in numerous applications like the transportation and commodity storage, formations of

aeolian, stability of slope, barchan dune formation, concrete slump examination, bulk cargo, deterioration of mass, trench of oceanic, retaining walls, sand volcanos, scree, kiln of rotary, mountaineering, calibration of simulation model, physics, pharmacology, geology, mining engineering, agricultural engineering, and geotechnical engineering. The angle of repose belongs to a comparatively modern field of study, and additional studies are required to increase the lack in data obtainable in this field [101]. The repose angle is an important parameter usually applied for the valuation of interparticle forces. The easiest way to calculate the repose angle is the flowability technique. The relationship has been found between properties of flows and the repose angle. Enhancing the flow properties had been studied by Raj et al (2016) on a spherical crystallization of Meloxicam crystals by calculating the angle of repose in order to determine the flowability. For example, the flow is an excellent if the angle of repose is less than 25 degrees. The flow is good while the repose angle is ranged between 25 to 30 degrees. The flowability is moderate when the repose angle is between 30 to 40 degrees. Finally, the flow is poor when the angle of repose is larger than 40 degrees [102]. The flow property of the biomass powders is affected by the size and shape of particles. The classification of the biomass powder types is relied on the repose angle measurement [26].

 After getting reliable grain size analysis from the mechanical sieve kit, the weight of each powder applied in this test is 25 g. The powders are ready to be used in flowability technique to calculate the angle of repose for barley grains, oak leaves, and straw. Also, the device is installed by using a funnel placed on a steel stand with dimensions as indicated in Figure 27. The distance between the end of the funnel, which the powder is poured, and

the test surface is 7.5 cm as indicated in Figure 27. Furthermore, this figure shows that the distance between the funnel holder and the test surface is 26 cm.
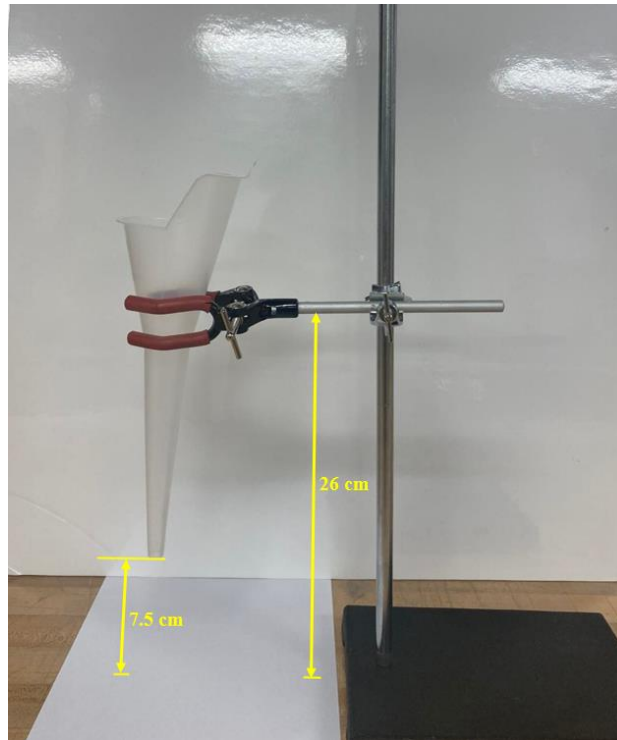
Figure 27: Flowability test set-up with it dimensions

The funnel is made from plastic, and its dimensions are drawn in Figure 28. The funnel dimensions include the total length of 230 mm, the upper diameter (70 mm), the middle diameter (30 mm), and the lower diameter (9 mm). Also, the funnel thickness is 1 mm.
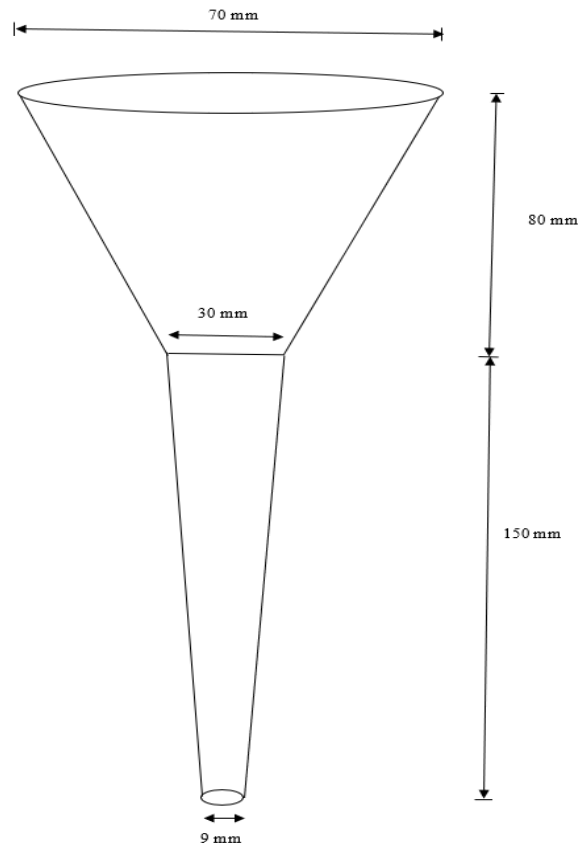
Figure 28: Funnel dimensions.

The funnel volume is 0.214 Liter calculated from the general formula [103]:

$$V = \frac{\pi}{3}(R_1^2 + R_1.R_2 + R_2^2).H \qquad\qquad (2)$$

The total volume is divided in two sections: the volume of upper section is

$$V_1 = \frac{\pi}{3}((35)^2 + 35 * 15 + (15)^2) * 80$$

$$V_1 = 165,373.33 \ mm^3$$

While the volume of the lower section of the funnel is calculated by

$$V_2 = \frac{\pi}{3}((15)^2 + 15 * 4.5 + (4.5)^2) * 150$$

$$V_2 = 49101.75 \; mm^3$$

Therefore, the total volume is the total of the volumes of the upper and lower sections.

$$V = V_1 + V_2 = 165{,}373.33 + 49101.75 = 214{,}475.08 \; mm^3 = 0.214 \; Liter$$

Figure (4) demonstrates the installation of flowability apparatus.

Figure 29: Flowability test set-up

The sample is poured continuously and easily into the funnel. The sample of biomass powder is flowed through the funnel so as to create a plie with a conical form. The height (*H*) and radius (*R*) of the rest heap are measured five times to calculate the average of angle of repose [26]. Figure 30 displays the right-angled triangle to exhibit the angle of repose with the heap height and radius.
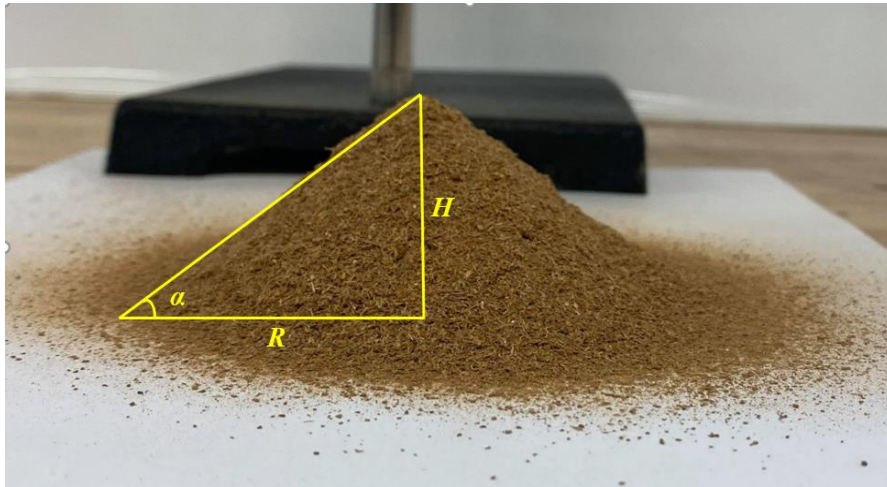
Figure 30: Angle of repose (α).

The height and radius of the semi-cone are measured. Then, the angle of repose is calculated by applying the following equation [96].

$$\alpha = \tan^{-1}(\frac{H}{R}) \qquad\qquad (3)$$

where α is the static angle of repose in (degrees), H is the height (mm), and R is the radius (mm).

The funnel is placed at a distance of 7.5 cm above the bench, where a piece of paper is put directly under the funnel. Each powder is poured continuously and smoothly through the upper stage of the funnel, distributing the powder equally to make a homogeneous

distribution and to create a heap with a conical shape as presented in Figure 32. Then, the pile height and the diameter are measured by using Vernier caliper. However, the circle is drawn manually on the paper as the example shown in Figure 31, and measured the diameters (D_1, and D_2).

| a: D_1 measurement | b: D_2 measurement |

Figure 31: D_1, and D_2 measurements

After that, the mean diameter of the cone is taken, and divided by 2 to get the mean radius of the heap. After getting the height and radius, the angle of repose is calculated by applying the equation (3). This process is represented for one time, and the completed process should be repeated five times for each biomass powder.
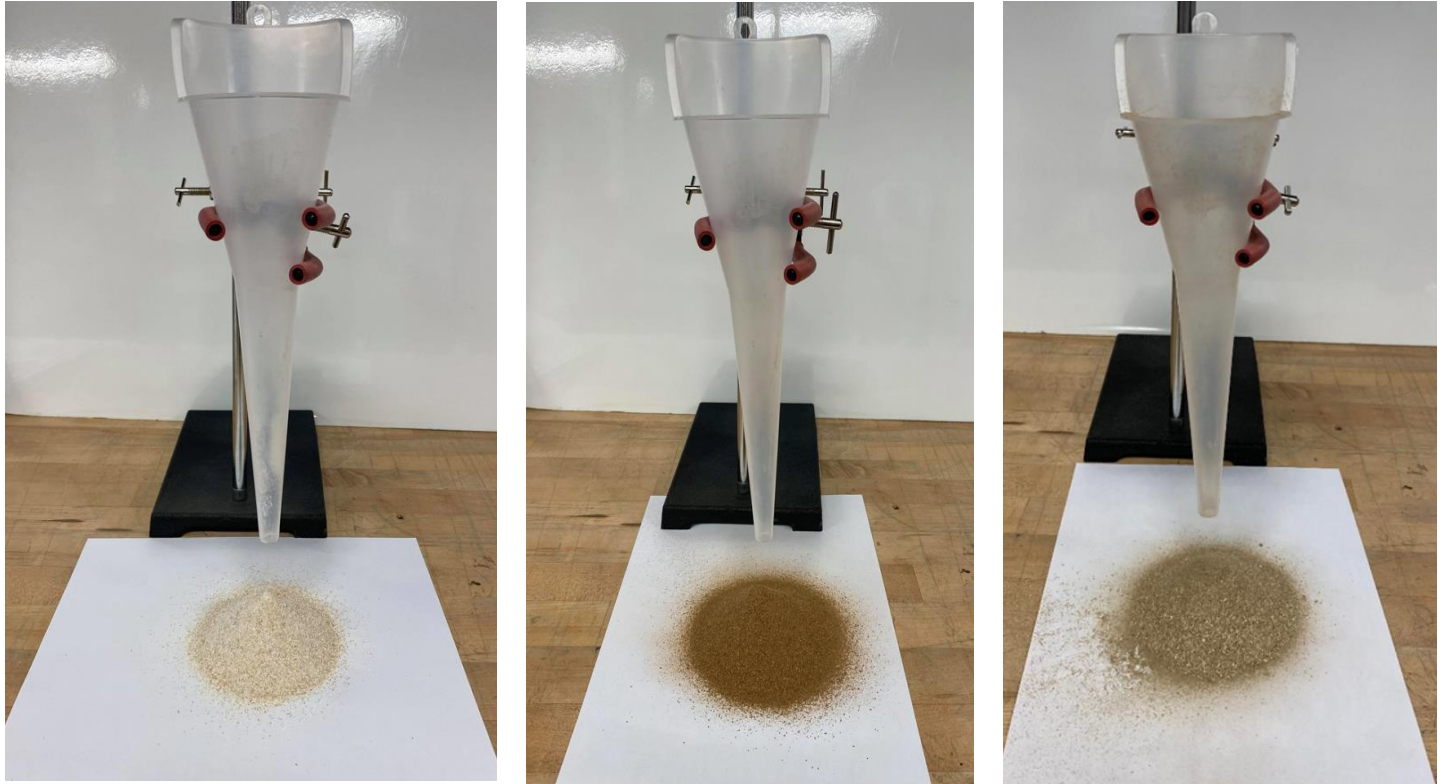
(a) Barley grains   (b) Oak leaves   (c) Straw

Figure 32: Flowability method with the three biomass powders.

The experiments were implemented with respecting the ambient conditions of (ME-131) Clean Energy Laboratory. The relative humidity for the five runs for each powder was between 56 percent and 67 percent and the environmental temperatures were from 16 ℃ to 21 ℃.

3.1.7.   Static Coefficient of Friction

Static coefficient of friction (μ) is defined as the measurement of the value of friction indicating between two surfaces. It is a dimensionless number. A low amount of coefficient of friction represents that the force needed for sliding to happen is less than the force needed while the coefficient of friction is high [104]. Sometimes, it is indicated that the coefficient of friction is always less than 1, but this is not correct. While μ is less than 1 in many applications, a value larger than one means the force needed to slide a material along the surface is larger than the normal force of the surface on the material. For instance, acrylic rubber-coated and silicone rubber surfaces possess a coefficient of friction that could be greater than 1 [105]. Zhang et al described the static coefficient of friction of red lentil via four various basic materials like concrete, wood, rubber, and stainless steel. A wooden box with dimensions of 150 mm length, 100 mm width, and 40 mm height was used. Red lentils filled the box and put on a convertible tilting table. The table surface was adjusted with the chosen material. The tilting table with the box carrying it was tilted slightly with a screw device until the red lentil in the box began to slide down, and the tilted angle was observed from a graduated scale [106]. Mattsson studied the angle of static friction of wood fuels. The angle of static friction was between 10 degrees to 40 degrees. It was influenced more by the type of surface than the fuel, and it was followed the descending order: rubber belt conveyor, concrete, stainless steel, particle board, urethane rubber, and coated plywood [107]. Wu et al presented different physical material characteristics of three kinds of solid biomass fuels such as wood pellets, wood chips and torrefied pellets. The researchers explored which angle of internal friction in the physical material properties reacted with both storage and handling equipment. There were four wall material samples utilized

together with seven exam materials for the wall friction examinations like: concrete, mild steel, stainless steel, and Ultra-High Molecular Weight Polyethylene (UHMW-PE) (Tivar 88) [31]. Stasiak et al studied mechanical properties for design and procedure control, which were found for sawdust and woodchips at five levels of moisture content. The strength characteristics such as the flowability, and coefficient of friction against common structure materials were calculated by applying direct shear tester possessing 210 mm in a diameter shear box [29].

The static coefficient of friction of ground/ chopped biomass powders was tested against four different surfaces: aluminum (6061-T6), plywood, rubber, and paper. The plate dimensions of 3.20 mm thickness, 22 cm length, and 21 cm width were applied for the four various structural materials. Also, each powder was weighed 25 g. For instance, the heap powder of straw was placed on an adjustable inclined plate with 14 cm from the fixed end of the plate as shown in Figure 33, and then the plate was raised slightly and smoothly from the free end of the plate until the powder heap started to slide down to the fixed end of the plate. After the powder fell on the surface, the free end was fixed with a stand to read the inclined angle from the protractor as shown in Figure 34. However, each material was measured five times to get the static angles of friction. Then, the static coefficient of friction was calculated by applying the following formula [95]:

$$\mu = \tan\theta \qquad (4)$$

Where μ is the static angle of friction and

θ: the inclined angle in degrees.
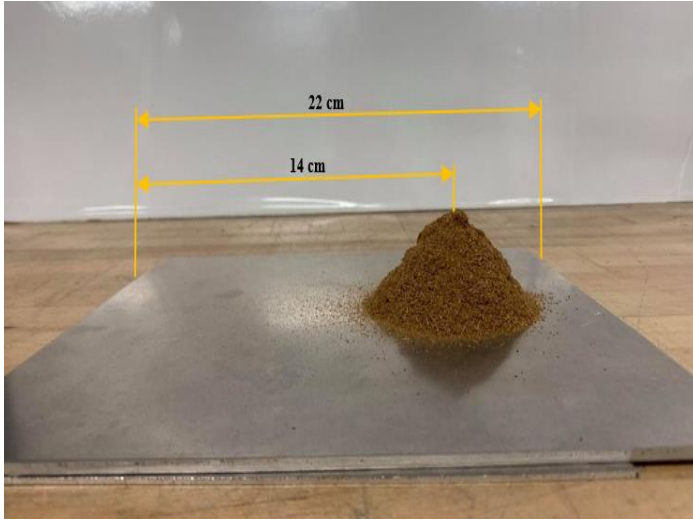
Figure 33: Oak leaves were placed on the plate
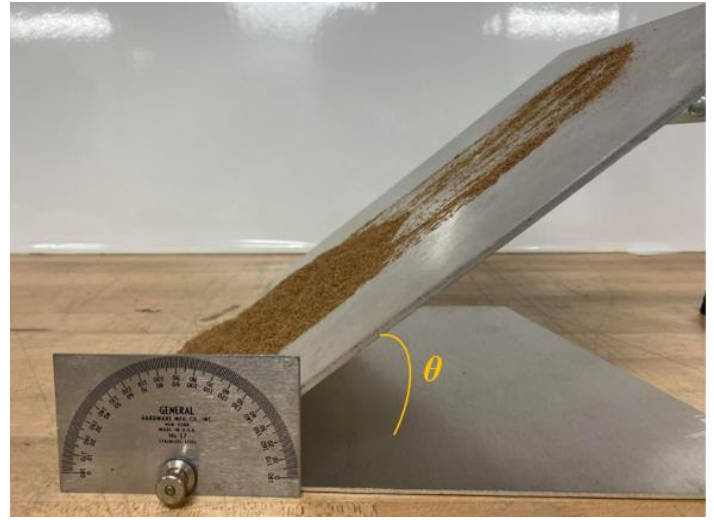
Figure 34: Angle of friction measurement

Each sample was tested five times on each surface to measure the internal angle of friction. Then, the results were applied in equation (4) to measure a static coefficient of friction of the four biomass materials on the four different surfaces. The tests were performed with respecting the ambient conditions of (ME-131) Clean Energy Laboratory. The relative humidity for the five runs for each powder was between 56 percent and 67 percent, and the environmental temperatures were from 16 ℃ to 21 ℃.

3.2. Biomass Reinforced Composites Preparation

Before measuring the physical properties of biomass powders, barley grains, oak leaves, straw, and jute, should be dried by using oven. The device used is Lab Oven from Quincy Lab. The model is 10GC as shown in Figure 35. This device is used for drying, curing, baking, sterilizing, heat treating, evaporating, annealing, and testing. Table 5 shows some general specifications of Model 10GC Oven [108].

Figure 35: Model 10 GC Lab Oven from Quincy Lab.

Table 5: Oven specifications of Model 10GC

Specifications	Values
Interior dimensions	30.5 cm (width)
	25.4 cm (height)
	25.4 cm (depth)
Exterior dimensions	35.6 cm (width)
	44.5 cm (height)

	31.2 cm (depth)
Capacity	19.8 Liters
Temperature Maximum	232 ºC
Electrical	115/5.2 (Volts/AMPS)
	600 (Watts)
	5-15P (Plug/NEMA)

Each biomass material is kept for four hours with retaining oven temperature about 100 ºC during this process. Then, the materials are ready for making the reinforced composites materials.

Biomass reinforced composite materials are produced materials from two or more constituent materials. The biomass materials have notably various chemical, or physical characteristics, and they are merged to produce materials with characteristics unlike the individual materials. The chemical materials are used to make biomass reinforced composites materials are EPON Resin 828, EPIKURE Curing Agent 3140, and Dry Film Mold Release as shown in Figure 36.

| E408 Dry Film Mold Release | EPON Resin 828 | EPIKURE Curing Agent 3140 |

Figure 36: Chemicals used for composite makes.

3.2.1. E408 Dry Film Mold Release

E408 dry film mold release is derived from halogenated hydrocarbon/ Ether blend mixture with dimethyl carbinol. The physical and chemical properties are presented in Table 6. Its vapor density is 2.01 g/cm^3. Its appearance is cloudy white, and evaporator rate is between 0.5-2 (N-Butyl acetate=1) [109].

Table 6: Physical and chemical properties [109]

Property	details
Physical state	Aerosol can
Vapor density	2.01 g/cm^3
Evaporator rate	0.5-2 (N-Butyl acetate=1)

Appearance	cloudy white
Solubility in water	0-1% (negligible)
Odor	Slight Ethereal
Specific gravity	0.77 (H_2O=1)
Vapor pressure	68 PSIG @ 70 F

3.2.2. EPON Resin 828

EPON Resin 828 is defined as an unmixed, clear, difunctional bisphenol A/epichlorohydrin originated from liquid epoxy resin. While cross-linked or strengthened with suitable curing agents, it could obtain very good mechanical, and chemical characteristics. EPON Resin 828 is considered as a standard epoxy resin utilized in formulation, fusion and fabrication techniques due to that variety of its properties. EPON Resin 828 has several advantages and be used for fiber reinforced composites, pipes, and tanks, electrical, construction, and aerospace adhesives, electrical laminates and encapsulations, casting and molding compounds, high solids, and marine coatings, base resin for epoxy fusion technical, and chemical resistant tank linings, flooring and grouts. EPON Resin 828 can be treated or cross-linked with a type of curing agents based on parameters desired in the completed product and the processing conditions used. High-performance, high-strength materials are obtained when this resin is cured with a variety of curing agents. The density of EPON Resin 828 is 1.16 g/cm^3 according to ASTM D1475. Using the resin cured with a different of curing agents gives high effectiveness, and strength materials. One of the most distinguished characteristics of cured EPON Resin 828 is strong adhesion to a broad range of substrates. Furthermore, EPON Resin 828 has a very good electrical insulating

properties and dielectric characteristics. It also possesses great resistance to a broad range of chemicals like acids, caustic, fuels, and solvents. Structures that are resistant, such as reinforced chemically and linings or coatings over material, can be manufactured with EPON Resin 828. For the formulation techniques, the initial components of a resin formula are the epoxy resin and the hardener or EPIKURE Curing Agent 3140 [110].

3.2.3. EPIKURE™ Curing Agent 3140

EPIKURE™ Curing Agent 3140 is a mild, molecular-weight epoxy curing agent that relies on polyamines and dimerized fatty acid, and it has a fewer amount of viscosity reactive polyamide, high imidazoline. Compatibility of epoxy resin and thin film curves are very good. EPIKURE Curing Agent 3140 is used in many applications like the adhesives between metal and plastic, deck rehabilitation of highway and bridge, systems of synthetic flooring systems, coating of maintenance, casting, and encapsulation, and tank and pipe linings. EPIKURE Curing Agent 3140 is used because it has a good chemical and corrosion resistance, water resistance, pigment and substrate wetting, and adhesion. The density of EPIKURE Curing Agent is 67.6 g/cm^3 [111]. Table 7 shows the properties of EPON Resin 828 cured with EPIKURE Curing Agent 3140.

Table 4 demonstrates the properties of EPON Resin 828 cured with EPIKURE Curing Agent 3140. These properties are determined at 25 °C on 1/8-inch-thick test specimens. There are four systems such as A, B, C, and D. The systems like A, and B were cured for 16 hours at 25 °C followed by two hours at 100 °C. Systems C and D were cured for two weeks at room temperature.

Table 7: Properties of EPON Resin 828 cured with EPIKURE Curing Agent 3140 [111]

		A	B	C	D
EPON™ Resin 828		100	100	100	100
EPIKURE Curing Agent 3140		45	90	45	90
Blend properties at 25 °C					
Viscosity, Original	cp	11,300	9,900	11,300	9,900
Gel Time, 100 gram mass	hours	2.5	2	2.5	2
Cured State Properties*					
Heat Deflection Temperature	°C	97	72	66	64
Tensile Strength, Ultimate	psi	8,500	7,300	7,400	7,500
Tensile Elongation	%	4.5	11.8	3.0	7.2
Tensile Modulus, Initial	ksi	420	320	340	290
Flexural Strength, Ultimate	psi	14,000	12,000	12,500	11,000

Flexural Deflection	in.	0.44	>0.60	>0.60	>0.60
Flexural Modulus, initial	ksi	310	340	400	340
Compression Strength, Ultimate	Psi	33,000	34,000	12,600	17,200
Compression Strength, Yield	psi	-	9,100	11,500	9,600
Hardness		84	82	84	82
Water Absorption (Percent weight gain after immersion for 24 hours)		0.18	0.33	0.16	0.25
Weight Loss (percent weight loss after 24 hours at 150 °C)		0.02	0.05	0.02	0

After measuring physical properties of the four biomass powders, the next step is manufacturing the composites materials. The first step is to prepare the materials that will be mixed with the natural fiber materials. The Hexion Epon, 828 Epoxy resin was used for making the biomass reinforced composites. For the matrix, Epon Epoxy is mixed with

Epikure 3140 using 33 parts per hundreds of resins (PHR). The PHR calculation is the amount of an additive to be added per hundred parts of base polymer in the compounding mixture. Figure 37 illustrates some images of making composites in (ME-131) Clean Energy Laboratory.

Figure 37: Preparing and making biomass reinforced composites

PHR is the amount of an additive to be added per hundred parts of base polymer in the compounding mixture. For instance, biomass fibers were added at 20 percent by weight for oak leaves reinforced composites as shown in Table 8.

Table 8: PHR calculation of 20%

Fiber	Fiber Glast		Mixture
	Resin	Hardener	
20 g	100 X	17.5 X	100 g
20 g	68 g	11.9 g	100 g

Biomass fibers are added at 10 percent and 20 percent by weight for oak leaf-reinforced composites, 10 percent, 20 percent, and 30 percent by weight for barley grains reinforced resin, 10percent and 20 percent by weight for straw-reinforced composites, and 2.25 percent, and 4.5 percent by weight for jute-reinforced resin. The reason for using these specific weight percentages of fibers in composites -- 20 percent of OAK, 30 percent of BRY, 20 percent of STR, and 4.5 percent of JUT – was because if these percentages are increased, the mixture will be more viscous and more powder could not be added. Cylindrical composite elements with 60 mm diameter and 20 mm height were prepared. Neat epoxy is denoted as NEAT, oak is denoted as OAK, and barley is denoted as BRY, Straw is denoted as STR, and jute is denoted as JUT. Therefore, 10 percent to 30 percent biomass added epoxy samples are denoted as OAK 10 percent, OAK 20 percent, BRY 10 percent, BRY 20 percent, BRY 30 percent, STR 10 percent, STR 20 percent, JUT 2.25 percent, and JUT 4.5 percent.

The process of making 10 percent weight barley fiber-infused composites. Condiment cups were sprayed with Stoner Mold release after waiting at least five minutes before pouring the mixture. The powder should be strained about 15-20 g to break up agglomerations by using the big stain and tin. The weight of barley powder was 11.8 g, Hexion Epon resin 828 was 81.2 g, and Hexion Epikure Curing Agent 3140 was 26.8 g. A whisk is used to blend the mixture. Epon resin was added into big cup, and biomass powder was added and carefully mixed with blender. When it is mixed well, curing agent is added. Then, after the hardener is added to the mixture, it hardened quickly. The mixture is poured into condiment cups. Figure 38 displays reinforced composites materials of six samples, NEAT, OAK10

percent, OAK20 percent, BRY 10 percent, BRY 20 percent, BRY 30 percent, STR 10
percent, STR 20 percent, JUT2.25 percent, and JUT 4.5 percent, respectively.

| NEAT | OAK10% | OAK20% | BRY10% | BRY20% | BRY30% |

| STR10% | STR20% | JUT2.25% | JUT4.5% |
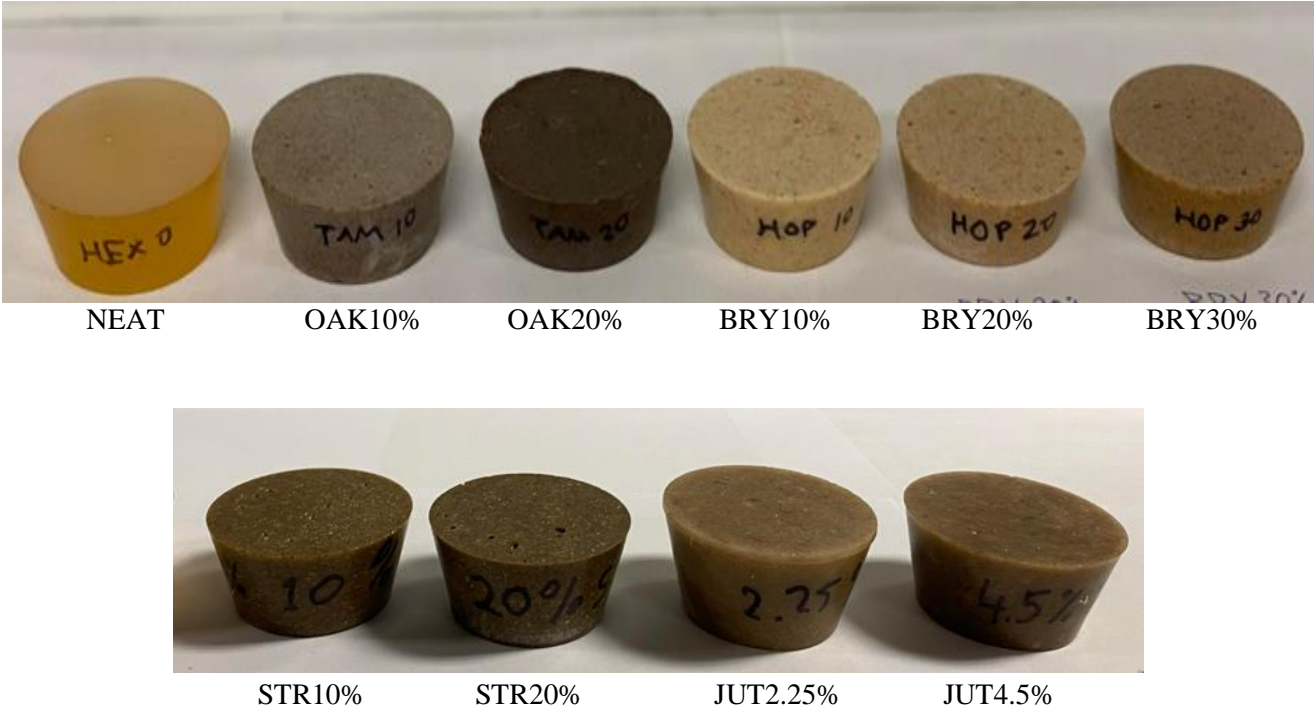
Figure 38: Biomass powder reinforced composites, NEAT, OAK10%, OAK20%, BRY10%,
BRY20%, BRY30%, STR10%, STR20%, JUT2.25%, and JUT4.5%

The tests were achieved with respecting the surrounding conditions of (ME-131) Clean
Energy Laboratory. The relative humidity for the five times of running for each material
was between 56% and 67%, and the environmental temperatures were from 16 ℃ to 21 ℃
recorded by using Hydrofarm APCEM2 Autopilot Desktop CO_2 Monitor & Data Logger,
Data device as shown in Figure 39.
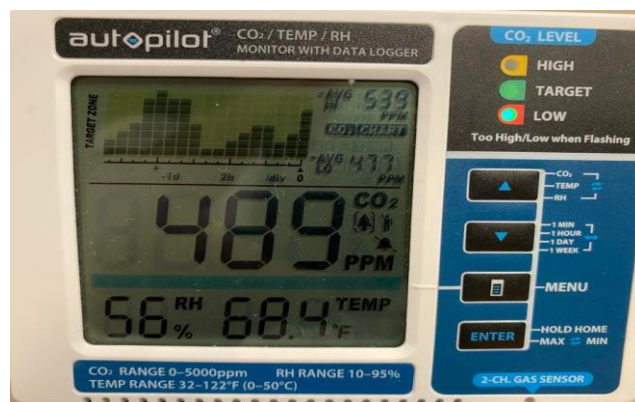
Figure 39: Hydrofarm APCEM2 Autopilot Desktop CO_2 Monitor & Data Logger, Data device.

The weight rates of all biomass materials mixed with the chemical materials rates are

demonstrated in Table 9.

Table 9: Weight percentages of biomass powders/ chopped material with chemicals used for composite manufactures.

Sample	Mass (g)	Hexion Epon resin 828 (g)	Hexion Epikure Curing Agent 3140 (g)	Total mass (g)
OAK10%	12	81.2	26.8	120
OAK20%	19.4	58.3	19.2	96.9
BRY10%	12	81.2	26.8	120
BRY20%	19.4	58.3	19.2	96.9
BRY30%	29.1	51.02	16.8	96.92
STR10%	12	81.2	26.8	120
STR20%	25	75.207	24.8	125
JUT4.5%	14.79	235.14	77.48	327.41
JUT2.25%	3.825	124	40.92	168.745

After pouring the mixture into the molds, the biomass reinforced composites should be left to dry for approximately five days. Then, the containers should be removed from the core softly using scissor or any sharp tools to avoid any scratch for these composites

3.3. Density Measurement of Biomass Reinforced Composites

3.3.1. Measuring Density Using Torbal Analytical Balance

The technique used to determine the solid density requires Torbal Density Analyzer (DA) kits. This process relies on an Archimedes principle used extensively to determine density with accurate balances. The Archimedes principle explains that the force of buoyancy faced by a submerged object is equal to the liquid weight displaced by the object. Therefore, the object volume is figured out if the apparent change in weight according to immersion is measured, and the fluid density which is used due to immersion is recognized. There are two properties such as the dry weight and the volume of the object. So, if these properties are known, the density is calculated. A Torbal Density Analyzer (DA) kit lets the researcher to precise measure the apparent change in weight due to immersion. The (DA) kits contain an accurately weighted pan holder which substitutes the weigh pan and adapter, and there is a frame that supports the beaker weight. A platform is created to place the pan holder, and the weight of the beaker with all contents such fluid, thermometer hanger, and thermometer. A 400 ml beaker includes the fluid, and a bracket is placed to hold the thermometer for fluid temperature measurement in the beaker [112]. An excel spreadsheet is provided which includes table of water density with temperature between 15 °C and 28 °C in 0.1 increments [113]. Figure 40 shows all components of Torbal Balance [112].

1. Beaker pan
2. Pan with frame
3. Pan fulcrum
4. Sleeve
5. Kit Frame
6. Upper pan
7. Lower pan
8. Lower pan hanger
9. Pan hanger
10. Balance sleeve
11. Ballast
12. Plunger
13. Plunger hanger
14. Plunger wire
15. Beaker
16. Thermometer
17. Thermometer hanger
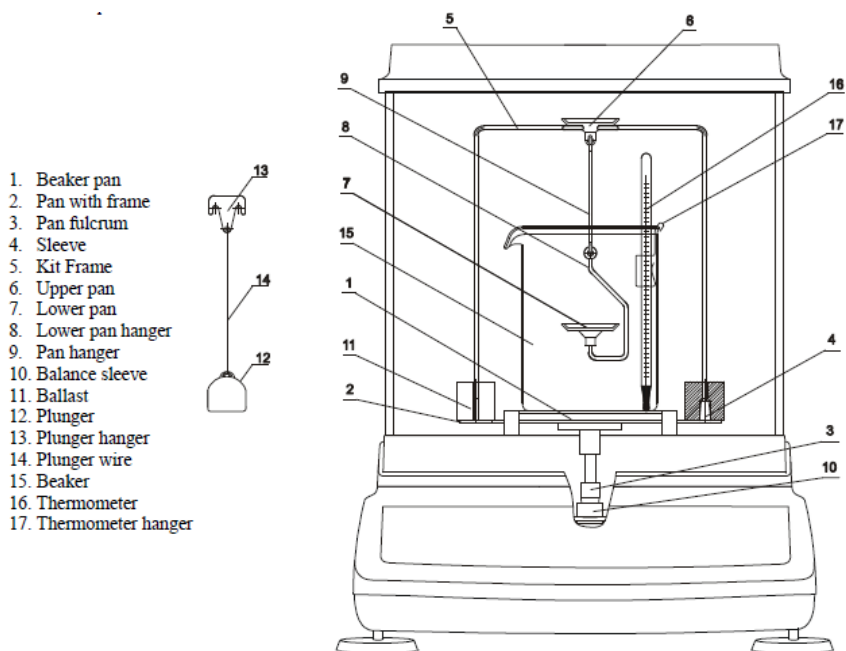
Figure 40: Torbal Balance components [112].

The procedure of this study begins with the following steps. First, a spreadsheet is built in the table while the fluid temperature is recorded to the closest 0.1 °C as measured by the thermometer through the experimental measurement. The same effect could be found by calculating the ratio of the suspension wire diameters and the beaker. The utilization of a beaker with a large inner diameter helps decrease this effect. A factor used by the spreadsheet is determined by the 400 ml beaker and the supplied suspension wire. If any of these vary in diameter, the density calculation will be different. The air density at sea level with 50 percent humidity and 20 °C temperature is nearly 0.0012 g/cm^3. A third error can result in measurements of the density, and this should be substituted in the calculation process. This 0.0012 g/cm^3 is utilized by the spreadsheet in its calculations with a view to rectify for air buoyancy. Furthermore, this effect is considered as mostly self-canceling while the sinker is submerged for both measurements such as dry weight and wet weight,

and the balance at the starting of each experimental measurements is <u>tared</u>. (unclear) Moreover, adding a drop or two of ordinary non-staining dishwasher detergent to the fluid decreases the meniscus effect and minimizes this concern. Then, the effect is eliminated by the spreadsheet. Finally, a considerable effect on measurements could be possessed by air bubbles. These bubbles can be brushed off. On the other hand, the sample can be pre-soaked to remove these bubbles. There is no way the spreadsheet can rectify this issue, and the user must work hard to overcome it. The density equation as implemented in the simplest way is:

$$\rho = \left[\frac{W_d}{W_d - W_w}\right] \times \rho_w \qquad (5)$$

Where W_d: dry weight in air (g)

W_w: wet weight in water (g)

ρ_w: water density (g/cm^3)

Also, it could be represented in its final spreadsheet form as:

$$\rho = \frac{[W_d \times (\rho_w - \rho_{air})]}{[Kimmersion \times (W_d - W_w)]} + \rho_{air} \qquad (6)$$

There are some general rules to determine the denisty of solids. For instance, both the sinker and suspension wire should have been cleaned at the beginning. In addition, distilled water is used as the fluid in this measurement. Decreasing meniscus effects for optimal results may be done with adding two drops of dishwasher detergent. The 400 ml breaker on the beaker supply frame should be in the center, under the suspension wire for the sinker. The thermometer could be attached to the retaining bracket and placed in the breaker. Then, the beaker will be filled to the 400 ml level. The technique of calculating the density demonstrates by the following steps. The researcher should <u>tare</u> (this word apppears

repeatedly but cannopt be correct) the balance, and the pattern is put on the upper frame pan after recording the results(W_d). Also, the same process should be done by placing the pattern on the wet sample holder "sinker." The temperature is determined by reading it from the thermometer to the closest 0.1 °C. The last steps of calculating the density are represented by entering the 2 or 3 values which are recorded above into the suitable cells in Torbal Density Calculator spreadsheet operating in Excel on a standard PC, or utilizing the spreadsheet formula provided above where the table gives D_w value, Kimmersion = 0.99989 for the 400 ml beaker, and D_{air} could be at 0.0012 g/cm^3 [123]. Figure 41 shows Torbal balance device. The tests were applied with respecting the ambient conditions of (ME-131) Clean Energy Laboratory. The relative humidity for the five runs for each powder was between 56 percent and 67 percent, and the environmental temperatures ranged from 16 ℃ to 21 ℃.
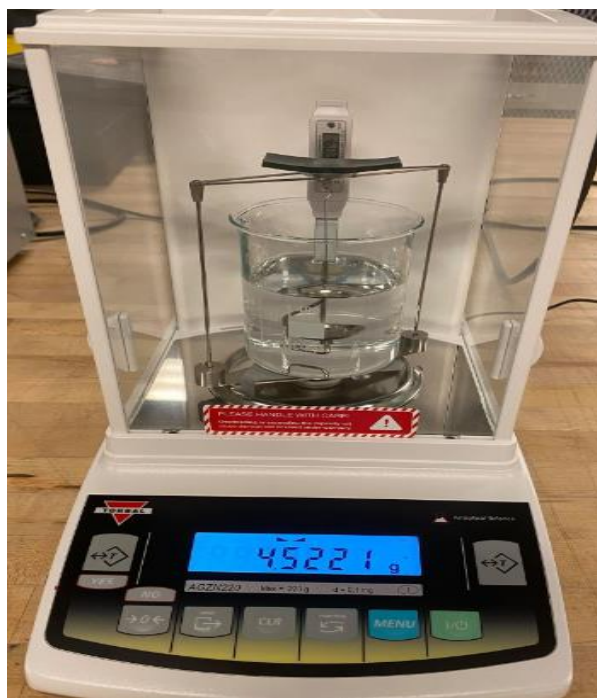
Figure 41: Torbal Balance.

3.3.2. Measuring Theoretical Density

The other way of measuring solid density of composites materials was done by theoretically calculations of a truncated cone using a Vernier caliper with the following:

The dimensions of BRY 30 percent were the following and Figure 42 illustrates the dimensions and mass of BRY 30 percent:

m= 33.4741 g

D_1= diameter of small circle = 43.15 mm $\longrightarrow$ R_1=21.575 mm

D_2= diameter of large circle = 52.74 mm $\longrightarrow$ R_2= 26.37 mm

H= height of the disc = 20.53 mm

$$V = \frac{\pi}{3}(R_1^2 + R_1.R_2 + R_2^2).H \qquad (7)$$

Applying equation (1) [102], the volume of the truncated cone is

V= 37169.8 mm^3 = 37.1698 cm^3

$$\rho = \frac{m}{V} = \frac{33.4741}{37.1698} = 0.90058 \text{ g/cm}^3$$
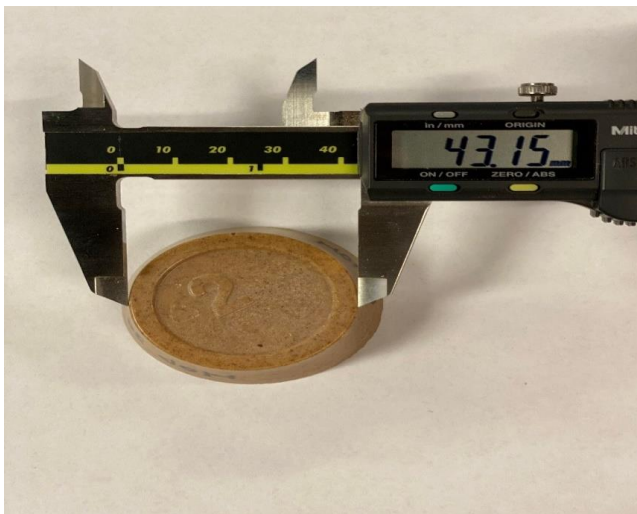
Figure 42: Mass and dimensions of BRY30%.

Also, the same calculations for the other samples were applied, and this process was tested three times for each sample.

3.4. Thermal Conductivity of Biomass Reinforced Composites

Thermal conductivity is defined as, "*The rate of heat transfer through a unit thickness of the material per unit area per unit temperature difference.*" Thermal conductivity is used to measure a material's ability to conduct heat. If a material has lower thermal conductivity, it will be a good heat insulator, and vice versa. For one-dimensional heat conduction, the equation (Fourier's law of heat conduction) can be given as [114]:

$$Q = -kA\frac{\Delta T}{\Delta x} \qquad (8)$$

Where Q is the heat flux in (W), k is amount of the thermal conductivity (W/mK), ΔT is the temperature difference in (K), A is the cross-sectional area in (m^2), and Δx is the thickness difference of the sample in (m).

The thermal resistance of a composite can be derived from equation (8)

$$R_{th} = \frac{(T_1 - T_2)}{Q} \qquad (9)$$

Where R_{th} is the thermal resistance in (K/W)

The thermal conductivity of the samples was measured using the transient plane source technique implemented in the TPS 2500S Thermal Constants Analyzer as presented in Figure 43. TPS 2500 S device is designed for an accurate analysis of thermal transport characteristics of materials such as solids, liquids, pastes, and powders. This device deals with millimeter-thick samples, and the thermal conductivity of this device range from 0.005 to 1800 W/mK. The temperatures are accommodated from cold to 1000 ℃. The anisotropy of thermal transport parameters of uniaxial materials can be analyzed by TPS 2500 S, which uses ISO Standard 22007-2. When performing a measurement, a plane Hot

Disk sensor is placed between two pieces of the cylindrically-shaped sample. Measurements on standard materials show that the accuracy over the entire range of thermal conductivities is within +/- 5 percent and the reproducibility is within +/- 2 percent [115]. The sensor element is manufactured from a 10 mm thick nickel-metal double spiral. The sensor of TPS represents as a heat source to raise the temperature of the material which is measured and a resistance thermometer for reporting the temperature increase with respect to time.

Figure 43: TPS 2500S Thermal Constants Analyzer [116].

Tekce et al (2007) used Hot-Disk method to measure thermal conductivity of copper-reinforced polymer composites. They used the transient plane source (TPS) as an accurate and suitable method to cope with thermal transport parameters [116].

3.5. Porosity

Porosity is defined as the percent of the cavities or air bubbles in the bulk grain that is not occupied by the material. It was calculated by applying the following equation [106]:

$$P = \left(1 - \frac{\rho_{Torbal}}{\rho_{TheoreticalSolidDensity}}\right) x\ 100 \qquad (10)$$

Where P is the porosity (%)

ρ_{Torbal}: density measured by Torbal Analytical balance (g/cm^3)

$\rho_{therotical}$: theoretical solid density calculation (g/cm^3)

Theoretical solid density calculations are the following:

Oak 10% (added oak 10% by weight for oak leaves reinforced composites)

$$\rho_{TheoreticalSolidDensity} = \left(\frac{10}{100} * \rho_{particle(OAK)}\right) + \left(\frac{90}{100} * \rho_{particle(NEAT)}\right)$$

Oak 20% (added oak 10% by weight for oak leaves reinforced composites)

$$\rho_{TheoreticalSolidDensity} = \left(\frac{20}{100} * \rho_{particle(OAK)}\right) + \left(\frac{80}{100} * \rho_{particle(NEAT)}\right)$$

BRY 10% (added BRY 10% by weight for barley grains reinforced composites)

$$\rho_{TheoreticalSolidDensity} = \left(\frac{10}{100} * \rho_{particle(BRY)}\right) + \left(\frac{90}{100} * \rho_{particle(NEAT)}\right)$$

BRY 20% (added BRY 10% by weight for barley grains reinforced composites)

$$\rho_{TheoreticalSolidDensity} = \left(\frac{20}{100} * \rho_{particle(BRY)}\right) + \left(\frac{80}{100} * \rho_{particle(NEAT)}\right)$$

BRY 30% (added BRY 30% by weight for barley grains reinforced composites)

$$\rho_{TheoreticalSolidDensity} = \left(\frac{30}{100} * \rho_{particle(BRY)}\right) + \left(\frac{70}{100} * \rho_{particle(NEAT)}\right)$$

STR 10% (added STR 10% by weight for straw reinforced composites)

$$\rho_{TheoreticalSolidDensity} = \left(\frac{10}{100} * \rho_{particle(STR)}\right) + \left(\frac{90}{100} * \rho_{particle(NEAT)}\right)$$

STR 20% (added STR 20% by weight for straw reinforced composites)

$$\rho_{TheoreticalSolidDensity} = \left(\frac{20}{100} * \rho_{particle(STR)}\right) + \left(\frac{80}{100} * \rho_{particle(NEAT)}\right)$$

JUT 2.25% (added JUT 2.25% by weight for jute reinforced composites)

$$\rho_{TheoreticalSolidDensity} = \left(\frac{2.25}{100} * \rho_{particle(JUT)}\right) + \left(\frac{97.75}{100} * \rho_{particle(NEAT)}\right)$$

JUT 4.5% (added JUT 10% by weight for jute reinforced composites)

$$\rho_{TheoreticalSolidDensity} = \left(\frac{4.5}{100} * \rho_{particle(JUT)}\right) + \left(\frac{95.5}{100} * \rho_{particle(NEAT)}\right)$$

Where Oak particle density = 0.593 g/cm^3 [117], Barley particle density = 1.2 g/cm^3 [118], straw particle density is 1.323 g/cm^3 [119], jute particle density is 1.46 g/cm^3 [120], and Neat Epon particle density = 1.16 g/cm^3 [121].

4. Results

4.1. Physical Properties Results

4.1.1. Moisture Content

The results are provided in Table 10, which includes moisture percentages of barley grains, oak leaves, jute and straw with three times of running. Table 11 consists of the overall results of moisture percentages with three tests and the standard deviations of each biomass material.

Table 10: Moisture percentages of barley grains, oak leaves, jute and straw with three tests of running.

Biomass materials	Runs	Sample weight in device (g)	Device Temperature (T)	Time (t)(sec)	Moisture percentage (%)	Measurements dates	Relative humidity (%)	Environm-ental temperatu-re (ºC)
Barley grains	Run#1	3.88	60 ºC	190	7.7	4/19/2021	56 %	18.5 ºC
	Run#2	5.41	60 ºC	170	4.1	5/26/2022	56 %	18.6 ºC
	Run#3	3.13	60 ºC	165	9.6	5/31/2022	56 %	18.8 ºC
	Number of runs (n)				3			
	Average				7.133			
	Standard deviation				2.7934			
Oak leaves	Run#1	1.53	60 ºC	201	10.5	4/19/2021	56 %	18.5 ºC
	Run#2	1.70	60 ºC	130	10.6	5/26/2022	56 %	18.6 ºC

	Run#3	2	60 ℃	165	10	5/31/2022	56 %	18.4 ℃
	Number of runs (n)				3			
	Average				10.366			
	Standard deviation				0.3214			
Straw	Run#1	2.03 g	60 ℃	150	10.8	6/10/2022	67 %	18.8 ℃
	Run#2	2.03 g	60 ℃	130	9.9	6/14/2022	56 %	20.7 ℃
	Run#3	2.30 g	60 ℃	135	9.1	6/16/2022	56 %	19.7 ℃
	Number of runs (n)				3			
	Average				9.933			
	Standard deviation				0.8504			
Jute	Run#1	1 g	60 ℃	110	12	6/10/2022	67 %	18.8 ℃
	Run#2	1 g	60 ℃	105	11.8	6/14/2022	56 %	20.7 ℃
	Run#3	1 g	60 ℃	105	11.7	6/16/2022	56 %	19.7 ℃
	Number of runs (n)				3			
	Average				11.833			
	Standard deviation				0.1527			

Table 11: Moisture percentages and standard deviations of barley grains, oak leaves, straw, and jute

	Run#1	Run#2	Run#3	Number of runs (n)	Average moisture percentage (%)	Standard deviation
Barley grains	7.7	4.1	9.6	3	7.13	2.793
Oak leaves	10.5	10.6	10	3	10.36	0.321
Straw	10.8	9.9	9.1	3	9.93	0.850
Jute	12	11.8	11.7	3	11.83	0.152

The lowest average of moisture content was 7.13% on barley grain powder while the highest average of moisture content was 11.83% on jute. For the ambient conditions, the values of relative humidity were ranged between 56% and 67% (RH), and the environmental temperatures were ranged from 16 °C to 20 °C during implementing these experiments.
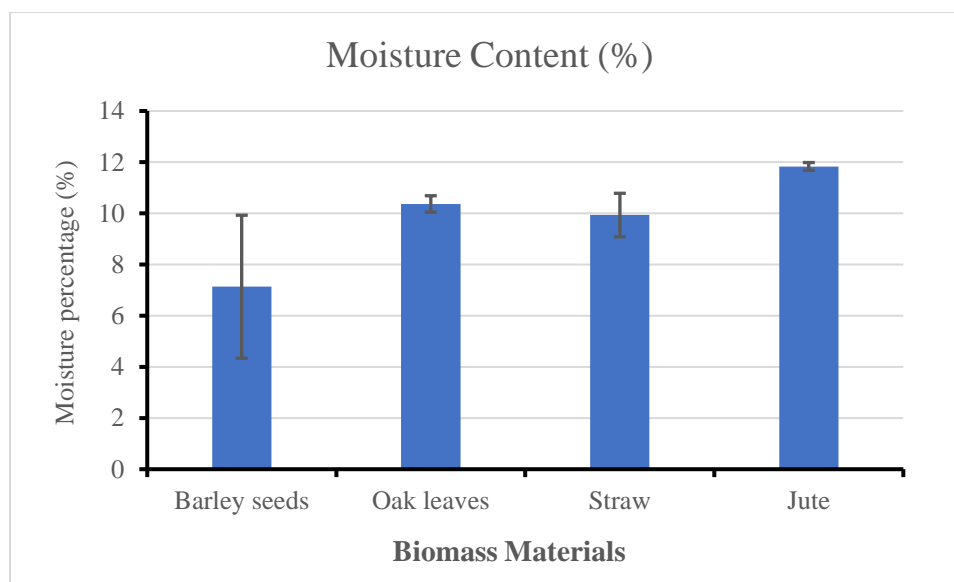
Figure 44: Moisture contents of the biomass materials with standard deviations.

The moisture percentages of the biomass materials should be decreased as much as possible during the manufacture of reinforced composite materials. The higher drying time, the lower the moisture content and milling energy consumption. While the final water content decreased more, the result became brittle and provided greater resistance through milling [122]. Figure 44 presents the moisture percentages of the four biomass materials: barley grains, oak leaves, straw, and jute.

4.1.2. Particle Size Distribution

4.1.2.1. Barley Grain Powder

The sieves were selected based on the nature of the particles of the barley grain powder. These samples of sieves applied were 26 OPN (d_p> 660.4 μm), 23 OPN (584.2 μm< d_p <660.4 μm), 20 OPN (508 μm< d_p < 584.2 μm), and 15 OPN (381 μm< d_p <508 μm) and barley powder collected as shown in Figure 45.
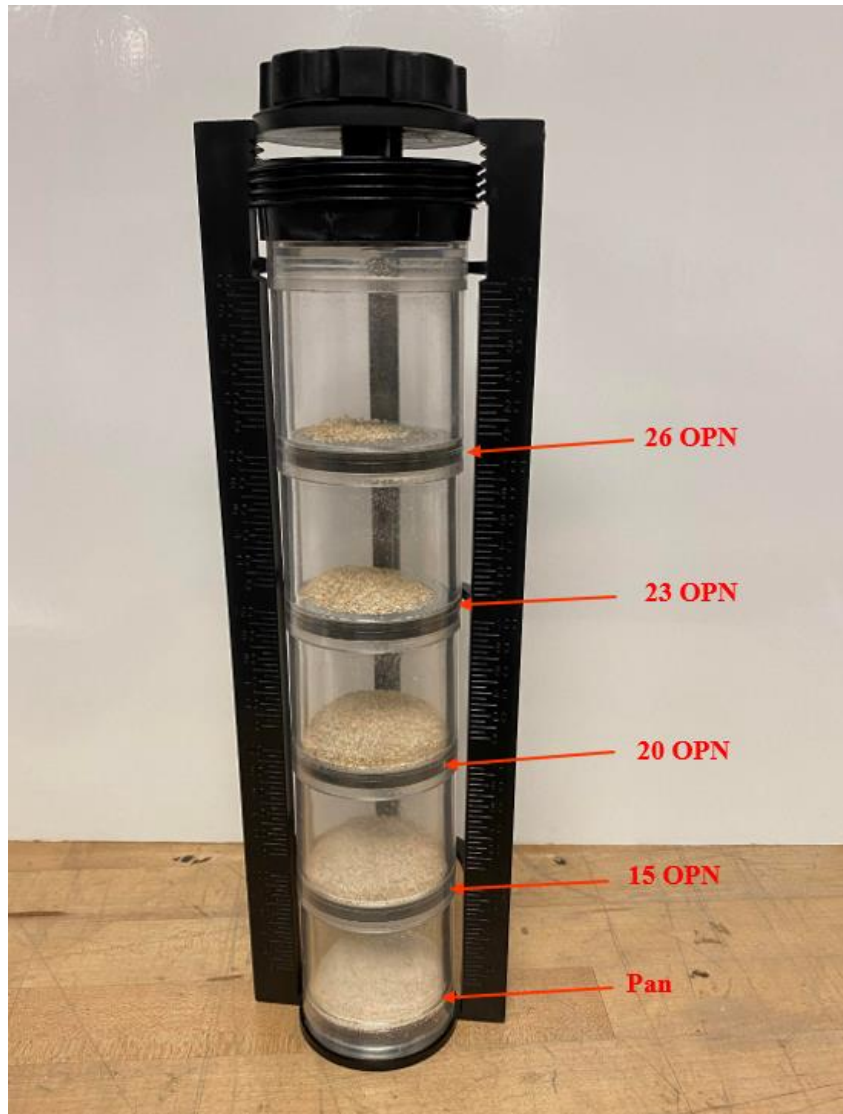
Figure 45: Barley grain powder on Sand Shaker with standard sieve screen sizes of 26, 23, 20, 15 OPN, and pan.

After running this sample in this test five times, the average value of the particle size distribution of barley grains was 1.72%, 6.1%, 31.94%, 34.48% and 25.76% on the sieves' designations 26 OPN, 23 OPN, 20 OPN, 15 OPN, and pan respectively as displayed in Table 12. The average value of the particle size distribution of barley grains was 1.72%,

6.1%, 31.94%, 34.48% and 25.76% on the sieves' designations 26 OPN, 23 OPN, 20 OPN,

15 OPN, and pan respectively.

Table 12: Percentages determination of particle size distribution of barley grain powder

Barley grains	(Pan) d_p <381 µm (%)	(15 OPN) 381 µm < d_p <508 µm (%)	(20 OPN) 508 µm < d_p <584.2 µm (%)	(23 OPN) 584.2 µm < d_p <660.4 µm (%)	(26 OPN) d_p >660.4 µm (%)
Run#1	22	37.2	31.8	6.8	2.2
Run#2	30.9	34.5	27.6	5.8	1.2
Run#3	31.6	27.6	31.6	7.6	1.6
Run#4	23.3	34.5	34.7	5.5	2
Run#5	21	38.6	34	4.8	1.6
Average	25.76	34.48	31.94	6.1	1.72
Standard deviation	5.083	4.234	2.776	1.104	0.389

Figure 46 demonstrates particle size distribution percentages and the standard deviation

of barley grain powder.
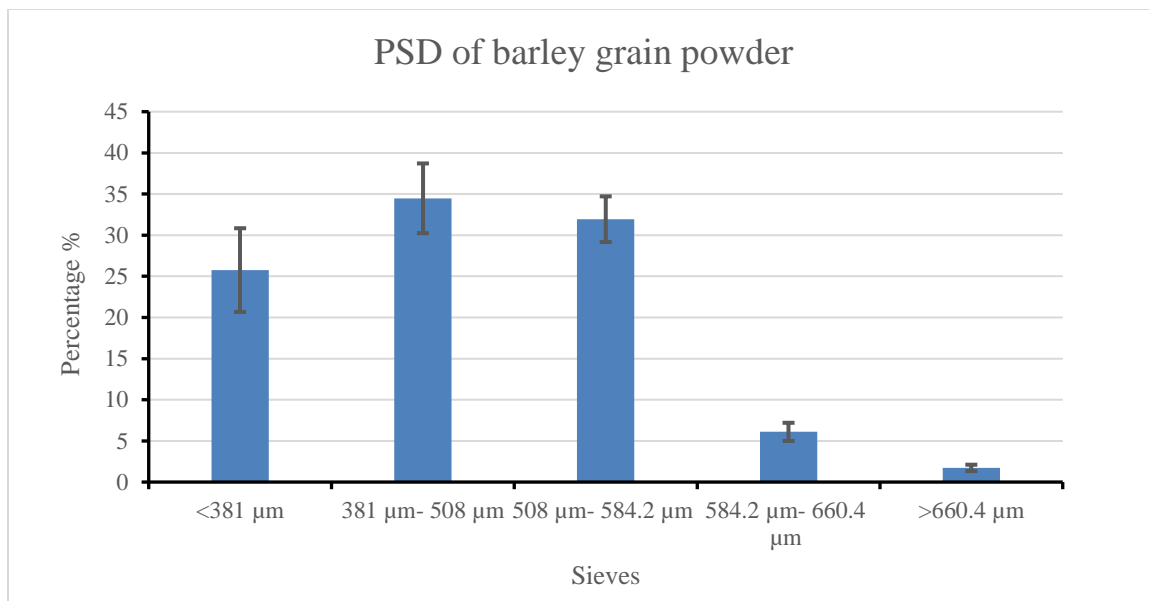
Figure 46: Particle size distribution percentages of barley grain powder.

4.1.2.2. Oak Leaf Powder

The sieves applied for oak leaf powder were 46 OPN (d_p >1168.4 µm), 40 OPN (1016 µm< d_p <1168.4 µm), 30 OPN (762 µm< d_p < 1016 µm), and 26 OPN (660.4 µm< d_p <762 µm) and powder is collected as illustrated in Figure 47.
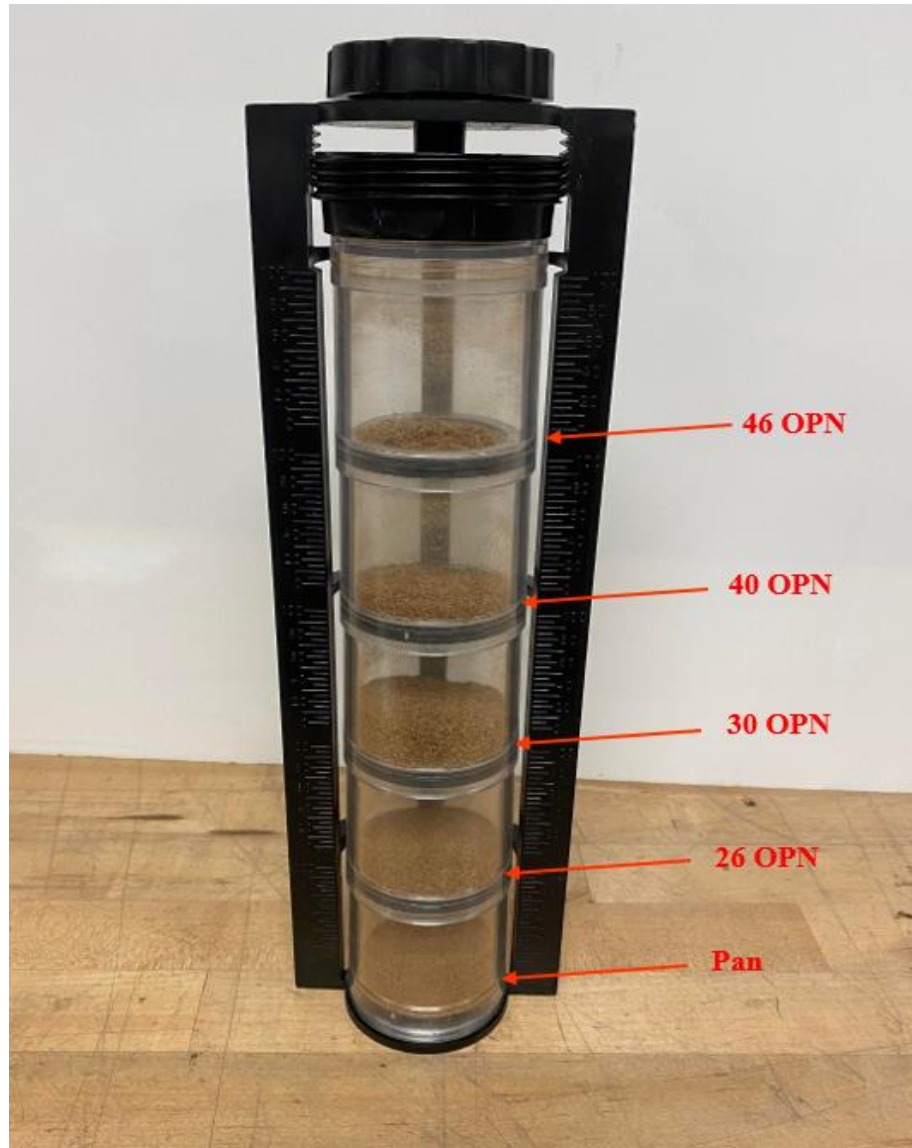
Figure 47: Oak leaves powder on Geotech Sand Shaker with standard sieve screen sizes of 46, 40, 30, 26 OPN, and pan.

Milling oak leaf powder resulted in fibrous particles that made the powder relatively coarse. Based on the coarse particles, the bigger mesh opening was used for oak leaf powder. Table 13 shows the average value of the particle size distribution of oak leaf

powder which was 0.72%, 6.32%, 31.04%, 18.56% and 43.36% on the sieves' designations

46 OPN, 40 OPN, 30 OPN, 26 OPN, and pan respectively.

Table 13: Percentages' determination of particle size distribution of oak leaves powder

Oak leaves	(Pan)	(26 OPN)	(30 OPN)	(40 OPN)	(46 OPN)
	d_p <660.4 µm	660.4 µm < d_p <762 µm	762 µm < d_p <1016 µm	1016 µm < d_p <1168.4 µm	d_p >1168.4 µm
	(%)	(%)	(%)	(%)	(%)
Run#1	38	18.8	35.2	6.8	1.2
Run#2	47.2	18	28.4	6	0.4
Run#3	42.4	18.8	31.2	7.2	0.4
Run#4	46	19.6	27.6	6	0.8
Run#5	43.2	17.6	32.8	5.6	0.8
Average	43.36	18.56	31.04	6.32	0.72
Standard deviation	3.584	0.779	3.131	0.657	0.334

Particle size distribution percentages and the standard deviation of oak leaf powder are

indicated in Figure 48.
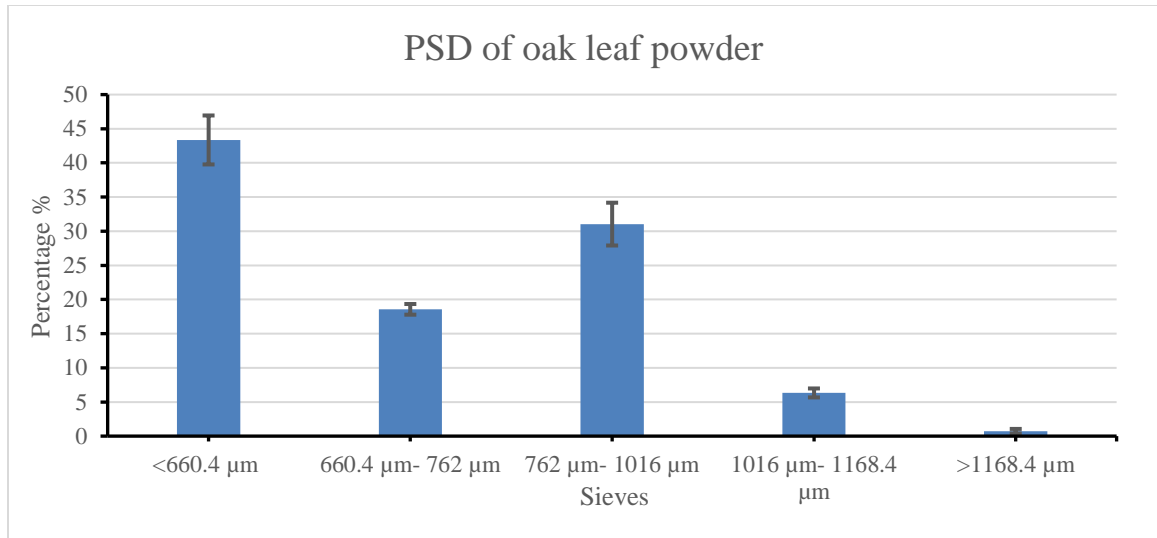
Figure 48: Particle size distribution percentages of oak leaf powder

4.1.2.3. Straw Powder

The sieves applied for straw powder were 60 OPN (d_p >1524 µm), 51 OPN (1295.4 µm< d_p <1524 µm), 46 OPN (1168.4 µm< d_p < 1295.4 µm), and 40 OPN (1016 µm< d_p <1168.4 µm) and straw powder is collected as shown in Figure 49.
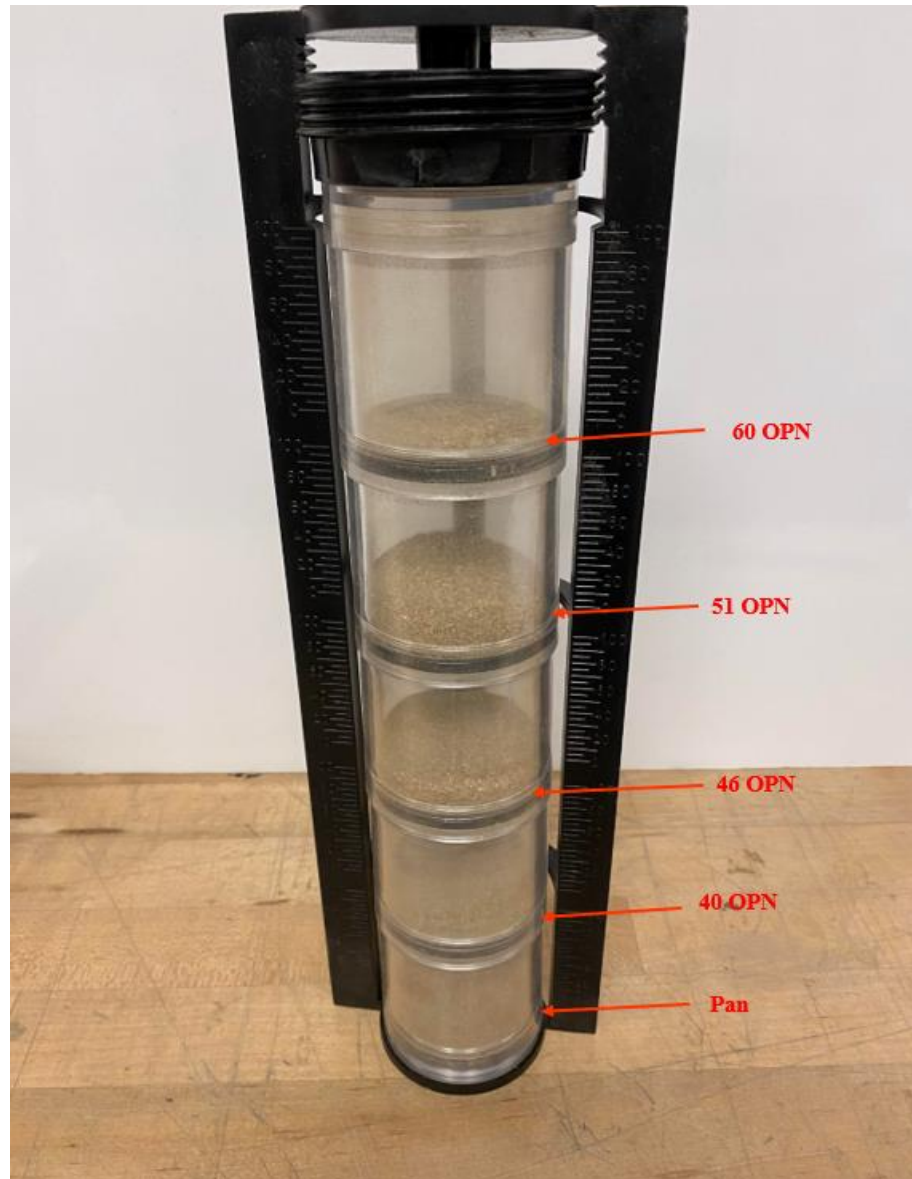
Figure 49: Straw powder on Geotech Sand Shaker with standard sieve screen sizes of 60, 51, 46, 40 OPN and pan.

Table 14 indicates the average value of the particle size distribution of straw powder: 2.08%, 31.28%, 24.08%, 21.6% and 20.96% on the sieves' designations 60 OPN, 51 OPN, 46 OPN, 40 OPN, and pan respectively.

Table 14: Percentages' determination of particle size distribution of straw powder

Straw	Pan	40 OPN	46 OPN	51 OPN	60 OPN
	d_p <1016 μm	1016 μm < d_p <1168.4 μm	1168.4 μm < d_p <1295.4 μm	1295.4 μm < d_p <1524 μm	d_p >1524 μm
	(%)	(%)	(%)	(%)	(%)
Run#1	21.6	20.4	25.2	27.2	5.6
Run#2	25.2	19.6	25.2	28.4	1.6
Run#3	17.2	18	23.2	40.8	0.8
Run#4	21.2	19.6	23.6	34	1.6
Run#5	19.6	30.4	23.2	26	0.8
Average	20.96	21.6	24.08	31.28	2.08
Standard deviation	2.933	4.995	1.035	6.141	2.007

Figure 50 presents particle size distribution percentages and the standard deviation of straw powder.
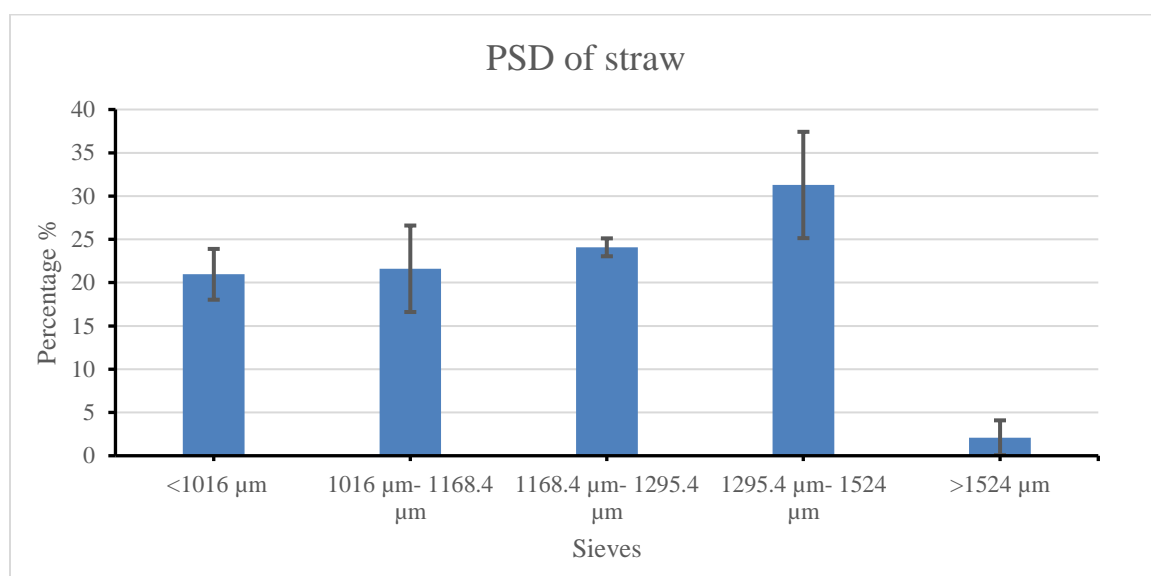
Figure 50: Particle size distribution percentages of straw powder

4.1.2.4. Jute

After biomass materials, barley grain, oak leaf, and straw were milled using mechanical grind grinder, the powders were produced. Then, particle size distributions were measured using Geotech Sand Shaker with standard sieve screen sizes chosen. However, jute is a long rope. Therefore, jute cannot be tested in grind grinder because it does not have grains or leaves like other biomass materials used, and it cannot be applied in Geotech Sand Shaker due to silky fibers and their light weight that it is not convenient to flow through screen sizes of the shaker. The particle size distribution of jute is approximated by measuring with caliper and microscopy from 1.5 to 2.5 mm length and diameter is between 0.017 to 0.02 mm.

According to the previous studies, a milled powder that contains too many fine particles creates light and thin particles while a powder, which is ground with too many coarse particles, produces nonhomogeneous surfaces that must be strained [127]. From the results above, the maximum particle distribution percentage of barley grains powder was 38.48 percent of the total weight percentage with standard deviation (+/- 4.234) while the particle size distribution was between dp <381 µm (pan) and dp >660.4 µm (26 OPN). The percentage values of the particle size weight percentages varied between (381 µm) and (660.4 µm) based on the sieve screens. The maximum particle size distribution percentage of oak leaves powder was 31.04 percent of the total weight percentage with standard deviation (+/- 3.131) since the particle size distribution ranged from $dp < 660.4$ µm (pan) to $dp > 1168.4$ µm (46 OPN). These values varied according to the weight percentages in Geotech Sand Shaker due to the mesh size of the sieves. Finally, the test results show that

straw powder has coarse contents due to opening mesh of the chosen sieves. Due to the morphological structure on the surfaces of straw, the fiber particles are not appropriate for superfine milling. The maximum particle distribution percentage of straw was 31.28 percent of the total weight percentage with standard deviation (+/- 6.141) while the particle distribution was between dp < 1016 μm (pan) and dp >1524 μm (60 OPN). The values of particle size distribution provided disparate weight percentages. If particles are too fine in the milled sample, small particle size will fill the empty spaces and increase bulk density [39]. The characterization of that miscellaneous percentages of the particle sizes affects particle size. The decreasing of the cohesion at the larger sieve size could be influenced by the decreasing of contact area between the larger particles, leading to a smaller area of a particular surface [39]. Thus, the three powders are not coherent due to the reduction of their contact areas. As screen size is decreased, the value of weight percentage of the powder is also reduced [35]. The milling energy increases significantly while particle size decreases [43]. Therefore, the specified power requirement of milling biomass rises with a reduction in the sieve size or softness level of the milling [123]. The higher value of the opening mesh of sieves, the greater the particle size distribution of the grinded sample. According to the results in Table 11, straw has the biggest particle size distribution based on the sieve sizes selected for each acrylic cylinder on the shaker. On the other hand, barley grain powder has the smallest particle size distribution due to small mesh of square holes. The standard sieve screen sizes are chosen for the three powders -- barley grain, oak leaf, and straw -- based on particles of each powder. For example, barley grain powder has fine particles, and the sieve screen sizes are chosen to allow the particles of powder to pass through the screen randomly from the largest sieve size to the lowest one respectively until

finding the convenient sizes like 26 OPN, 23 OPN, 20 OPN, and 15 OPN. Therefore, barley grain powder is the finest powder due to their particles passed through the lowest values of sieves chosen. The same procedure was applied for the other powders. Then, straw powder contained the coarsest particles based on the largest sieve sizes needed.

4.1.3. Microscope

Microscopic images of barley grain, oak leaf, straw, and jute are demonstrated in Figure 51 (a), (b), (c), and (d) with the size scale of 100 µm with magnification 4x objective lens. Figure 51 (a) observes barley grain powder, which has some large grains and mostly many small grains. The large grains possess many fine slits on the surfaces and appeared to have complicated structures while the small grains have no slits and indicated to have very smooth surfaces. Figure 51 (b) shows that oak leaf powder has hook fibrous particles with non-homogenous structures. Figure 51 (c) observes straw powder under microscope, and this powder has more complicated structure than the other materials. Its course-grained particles yielded long cylindrical shapes with complex ends which make the variants in shapes affecting its physical characteristics. According to the fiber morphology surface gained by microscope and as shown in Figure 51 (d), jute fibers are soft woody fibers with cylindrical shapes unequal in diameter -- rounded polygonal with a central lumen. These images distinguish between biomass powders/ cut material and indicate the variants in shapes depend on the physical structure of each material. The particle shape analysis of the biomass materials demonstrates that the actual dimensions and shapes of these biomass materials are not similar in morphology because they are different in the particle size, shape, and structure. The microscopic observations revealed that barley grain powder has very small particles and a finer-grained structure than the other materials. The microscopic

examinations demonstrate how the material reflects on the physical properties. For example, according to this test, barley grain powder has smooth particles, and this yields a perfect packing in the density cup because fine powder particles will mostly occupy the total size of that cup. Then, the bulk density result will be perfect compared to the other materials that have been examined.

a) Barley grain powder   b) Oak leaf powder

c) Straw powder   d) Jute
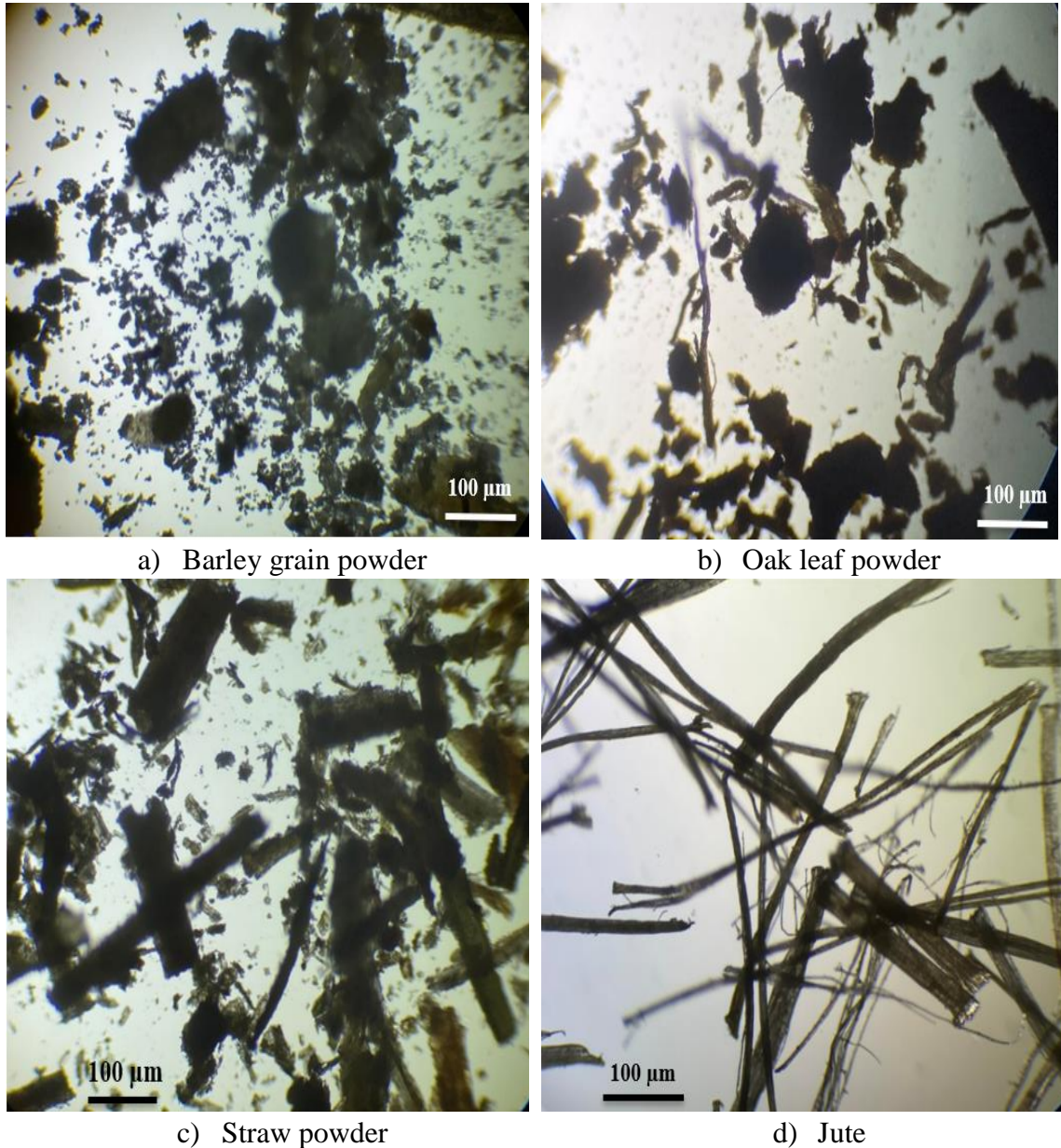
Figure 51: Biomass powders (barley grain, oak leaf, straw) and cut jut with magnification 4x objective lens.

4.1.4. Bulk Density

The average bulk density was measured. The bulk density should be determined with moisture percentage, size and shape of particles because a powder bulk density affects with its particle size and water content [26]. For instance, for the first run, and the total mass including barley grain powder was 82.09 g, and the mass of pycnometer was 50.16 g with the average moisture content was 7.1 %, and the particle size was between 381 µm and 660 µm. The net mass was 31.93 g, and the pycnometer volume was 50 cm^3. Then, the bulk density was 0.638 g/cm^3. Figure 52 presents the total mass of barley grain powder measured including the mass of the density cup.

Figure 52: Total mass of barley grains measured using Torbal Analytical balance (Run#1)

Table 15: Bulk density measurement of barley grain powder

Number of experiments	Total mass (m_1) (g)	Pycnometer mass (m_2)(g)	Net mass Mass (g) $m_{net} = m_1 - m_2$	Pycnometer volume $(V)(cm^3)$	Bulk density (g/cm^3) $\rho = m_{net}/V$
Run#1	82.0954	50.16	31.9354	50	0.638
Run#2	83.6311	50.16	33.47	50	0.669
Run#3	82.1314	50.16	31.9714	50	0.639
Run#4	82.2294	50.16	32.0694	50	0.641
Run#5	82.58805	50.16	32.42805	50	0.648
Average					0.647
Standard deviation					0.012851

Table 16: Bulk density measurement of oak leaf powder

Number of experiments	Total mass (m_1) (g)	Pycnometer mass (m_2)(g)	Net mass Mass (g) $m_{net} = m_1 - m_2$	Pycnometer volume $(V)(cm^3)$	Bulk density (g/cm^3) $\rho = m_{net}/V$
Run#1	70.5082	50.16	20.3482	50	0.406
Run#2	70.8007	50.16	20.6407	50	0.412
Run#3	71.2227	50.16	21.0627	50	0.421
Run#4	71.6307	50.16	21.4707	50	0.429
Run#5	70.68905	50.16	20.52905	50	0.410
Average					0.416
Standard deviation					0.009062

Table 17: Bulk density measurement of straw powder

Number of experiments	Total mass (m_1) (g)	Pycnometer mass (m_2) (g)	Net mass Mass (g) $m_{net} = m_1 - m_2$	Pycnometer volume (V)(cm^3)	Bulk density (g/cm^3) $\rho = m_{net}/V$
Run#1	66.5412	50.16	16.3812	50	0.327
Run#2	66.8862	50.16	16.7262	50	0.334
Run#3	67.0929	50.16	16.9329	50	0.338
Run#4	66.0993	50.16	15.9393	50	0.318
Run#5	66.0796	50.16	15.9196	50	0.318
Average					0.327
Standard deviation					0.0091

Table 18: Bulk density measurement of cut jute

Number of experiments	Total mass (m_1) (g)	Pycnometer mass (m_2)(g)	Net mass Mass (g) $m_{net} = m_1 - m_2$	Pycnometer volume (V)(cm^3)	Bulk density (g/cm^3) $\rho = m_{net}/V$
Run#1	55.2807	50.16	5.1207	50	0.102
Run#2	55.5527	50.16	5.3927	50	0.107
Run#3	55.4736	50.16	5.3136	50	0.106
Run#4	55.8162	50.16	5.6562	50	0.113
Run#5	55.2769	50.16	5.1169	50	0.102
Average					0.106
Standard deviation					0.0044

Table 19: Average bulk densities and standard deviations of the four biomass materials

Biomass materials	Run#1 (g/cm³)	Run#2 (g/cm³)	Run#3 (g/cm³)	Run#4 (g/cm³)	Run#5 (g/cm³)	n (number of runs)	Average (g/cm³)	Standard deviation
Barley grains	0.638	0.669	0.639	0.641	0.648	5	0.647	0.0128
Oak leaves	0.406	0.412	0.421	0.429	0.410	5	0.416	0.0090
Straw	0.334	0.338	0.327	0.318	0.318	5	0.327	0.0091
Jute	0.102	0.107	0.106	0.113	0.102	5	0.106	0.0044
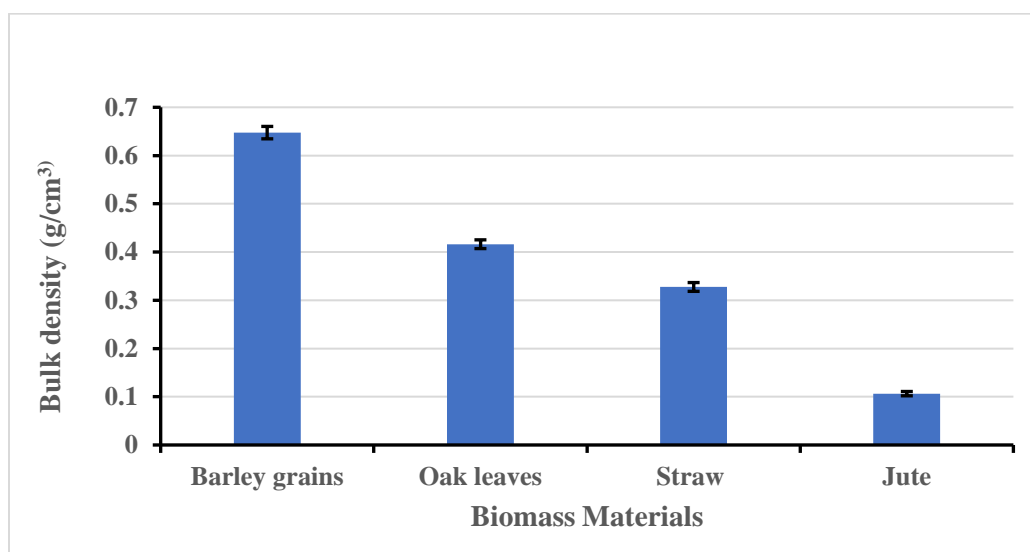
Figure 53: Bulk densities and standard deviations of biomass materials, barley grains, oak leaves, straw, and jute.

Tables 15, 16, 17, and 18 show all experiment results calculated to obtain bulk density of barley grains, oak leaves, straw, and jute respectively. Figure 50 presents the four biomass materials with the five running of experiments including standard deviation for each material. Table 19 shows the average bulk densities and standard deviations with the five runs for each sample. The bulk density of barley grains, oak leaves, straw, and jute were

0.647, 0.416, 0.327, and 0.106 g/cm^3, respectively. Barley grain powder has the highest value of the bulk density, and the standard deviation gained by repeating this experiment was under 0.013 g/cm^3 while the lowest value of bulk density was found in jute. The bulk density of a group of heterogeneous material would be impacted by the deviation values from a bulk of stems of an individual size. It was observed that the barley grain powder poured into the pycnometer comparatively more rapid than oak leaves, straw, and jute, and the primary bulk space was the lowest. Based on tapping of the biomass, barley particles had less voids to complete filling the inner small cavities to get the final enclosed system of bulk density. Therefore, barley grains are finest particles in size comparing to the other materials. The biomass materials in these experiments can be divided into types: three powders (barley grains, oak leaves, and straw) and chopped jute. The comparison of the bulk density will be in two groups according to the particle size distribution and flowability measurements. Thus, the first comparison will be presented with only three powders because the particle size distribution and flowability of chopped jute were not measured due to light weight and their silky structure, which it is not convenient to pass through both screen sizes of the shaker and the funnel of flowability test. The other comparison will include all biomass materials. While large particles of a powder are decreased to small particles, the powder occupies less volume in pycnometer and the finer particles of the powder fill the void cavities. Then, the bulk density will be increased [124]. Therefore, barley grain powder has the highest average value of bulk density (0.647 g/cm^3) compared to the biomass powders based on its smallest value of particle size distribution (381 μm < dp >660.4 μm). In contrast, straw powder has the lowest value of bulk density (0.237 g/cm^3) due to the biggest value of particle size distribution of the three powders (1016 μm

$< dp >$1524 μm). According to the results, the higher the bulk density of a powder, the lower the particle size distribution. For the second group of the overall biomass materials, barley grain powder has highest value of bulk density, and chopped jute has the lowest value of the bulk density (0.106 g/cm^3) with standard deviation (0.004 g/cm^3). The reason of that reduction in bulk density of chopped jute because it was not completely packed on the density cup due to its lightweight and string shape of the jute which make spaces inside the pycnometer while packing it in spite of totally reaching an enclosed system. The moisture content also affects the bulk density of powders. Fathollahzadeh et al. (2008) reported that the barberry bulk density increased with rising moisture content [125]. Subramanian et al (2006) also found that the bulk density of the millet flours increased logarithmically with the increase in moisture content in the moisture content range studied [126]. Lam et al (2014) studied bulk density of a biomass, such as wheat straw, switchgrass, and corn stover, that differs with its moisture content and particle size. Therefore, the bulk density of a measured product should be specified with moisture content and particle size and shape [29]. For example, the bulk density of oak leaf powder raised from 0.406 to 0.412 g/cm^3 in the first and second runs while the moisture content was increased from 10.8 to 10.6 percent. The bulk density of the biomass material decreases when the moisture decreases according to the experiments results in the tables above. Therefore, barley grain powder has the highest value of bulk density because it has the finest powder while chopped jute has the lowest value of bulk density.

4.1.5. Flowability Technique

The angle of repose was calculated for the three biomass powders (barley grains, oak leaves, and straw). The angle of repose was not calculated for the chopped jute because jute has silky formation and light mass which it makes these structures hard to pass through the funnel in flowability technique. The results are given in Table 20.

Table 20: Flowability chart of the biomass powder materials barley grains, oak leaves, and straw.

Biomass powder		H (mm)	D_1 (mm)	D_2 (mm)	R_1 (mm)	R_2 (mm)	R_{avg} (mm)	α (degrees)	Flow property
Barley Grains	Run#1	32	110	102	55	51	53	31.12˚	Moderate flow
	Run#2	33	104	102.46	52	51.23	51.61	32.59˚	Moderate flow
	Run#3	33	98.59	101.47	49.29	50.73	50.01	33.41˚	Moderate flow
	Run#4	31	104.37	97.49	52.18	48.74	50.46	31.56˚	Moderate flow
	Run#5	32	99.07	99.51	49.53	49.75	49.64	32.80˚	Moderate flow
Oak Leaves	Run#1	28	121.48	126.56	60.74	63.28	62.01	24.30˚	Excellent
	Run#2	25	126.19	121.17	63.09	60.58	61.84	22.01˚	Excellent
	Run#3	28	124.1	119.65	62.05	59.82	60.93	24.67˚	Excellent
	Run#4	26	109.78	115.33	54.89	57.66	56.27	24.79˚	Excellent
	Run#5	29	118.61	119.59	59.30	59.79	59.55	25.96˚	Good
Straw	Run#1	40	110	112.21	55	56.10	55.55	35.75	Moderate flow
	Run#2	38	110.85	108.24	55.42	54.12	54.77	34.75	Moderate flow
	Run#3	39	108	111.08	54	55.54	54.77	35.45	Moderate flow
	Run#4	38	111.82	114.41	55.91	57.20	56.55	33.89	Moderate flow
	Run#5	38	110	108	55	54	54.5	34.88	Moderate flow

The angles of repose in degrees of the three samples of biomass powders are shown in Figure 54 and Figure 55.
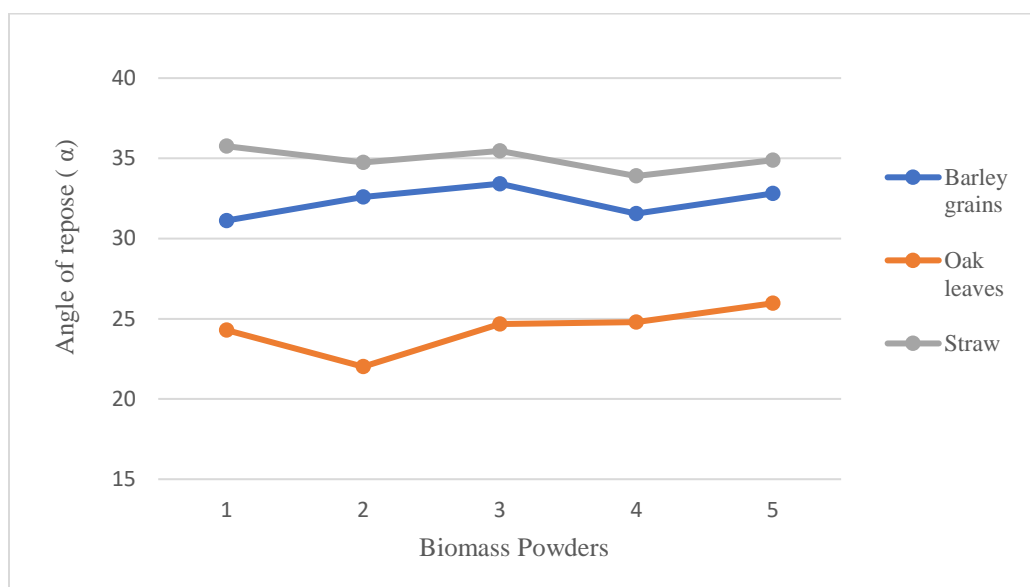
Figure 54: Angle of repose of the biomass powders with five times of tests.
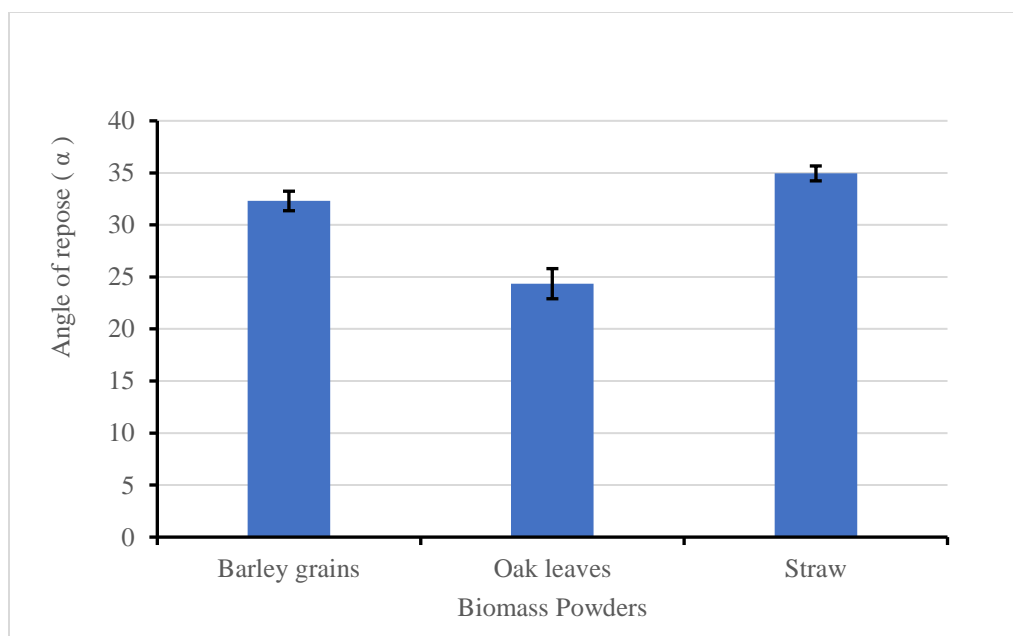
Figure 55: Angle of repose for barley grains, oak leaves, and straw

Table 21: Flowability for biomass powders, barley grains, oak leaves, and straw

Biomass powder	Angle of repose (α) (°) Run#1	Angle of repose (α) (°) Run#2	Angle of repose (α) (°) Run#3	Angle of repose (α) (°) Run#4	Angle of repose (α) (°) Run#5	Number of runs (n)	Average angle of repose (α_avg) (°)	Standard deviation	Flow property
Barley grains	31.12	32.59	33.41	31.56	32.80	5	32.29	0.9380	Moderate flow
Oak leaves	24.30	22.01	24.67	24.79	25.96	5	24.35	1.4479	Excellent flow
Straw	35.75	34.75	35.45	33.89	34.88	5	34.94	0.7168	Moderate flow

The outcomes should be due to the forces' variants on the surfaces between inter-particles [97]. The lower the cohesion forces of the powder, the better will be the flow property [127]. This physical parameter is based on the surface characteristics of singular particulates [128]. Table 20 indicates that the lowest angle of repose is found in oak leaf powder. In contrast, barley grain and straw powders have higher values of angle of repose. Also, it demonstrates that the angle of repose of oak leaves was between 22.0° and 25.96° and the average value was 24.35°. In addition, the repose angles of barley grains and straw ranged from 31.12° to 33.41° and from 33.89° to 35.75° respectively. Where the average of repose angle was 32.29° for barley grains and 34.94 for straw. According to these data collected from the tests, oak leaves have an excellent flow due to the lowest angle of repose (24.35°) while barley grains and straw have moderate flow based on the values of their angles. The smoother the powder, the lower the angle of repose. Therefore, oak leaves have

smooth surfaces that avoid accumulating particles ahead of each other, leading to the lowest angle of repose compared with the barley grains and straw powders. For these three biomass powders, barley grains, oak leaves, and straw, the lower the angle of repose of a powder, the better the flowability of the powder. There are some relationships that affect flowability.

The bulk density also affects flowability. Stufft, T. et al (1997) proved that the greater the bulk density, the lower the angle of repose and better flow of the polyethylene powder. It is inversely proportional relationship between the bulk density and flowability. In addition to being desirable during mold filling, the higher bulk density powders are preferred because of their flow characteristics. A change in the powder's bulk density changes its flow characteristics. Perfect powder will have a fluid-like movement within the mold, which ensures uniform coverage of all surfaces [129].

The flowability is affected by moisture. The higher the flowability of a powder, the lower the moisture of that powder [130]. The angle of repose of barley straw powder decreased from 35.75º to 34.75º for the first and second runs while the moisture content decreased from 10.8 to 8.8 percent. The lowest value of flowability of coal blended with wood chips in comparison with coal blended with sawdust was observed by Zulfigar et al. (2006). The long and hook shaped particles are woodchips in the experiments. Their results are alike achieved in their testing [131]. Also, results of Littlefield et al. (2011) on pecan shells of different particle sizes showed that fine particles flowed easier. The authors (Littlefield et al.) concluded that increase in moisture content resulted in a reduction in flowability of pecan shells [132]. Abdullah et al (1999) studied the effect of particle size of powder on

flowability. They found the flow rate of the powder raises with increasing particle size [133]. According to the results in Table 18, oak leaves powder has the lowest average value of angle of repose (24.35º), which means it has an excellent flow property. In addition, oak leaves powder has the highest average value of moisture content (10.36 percent) compared to barley grains and straw powders. On the other hand, Barley grains and straw powders have the high average values of angle of repose (32.29º, and 34.94º, respectively). Therefore, they are moderate flow due to their lower moisture contents.

4.1.6. Static Coefficient of Friction

The static coefficient of friction of biomass materials, oak leaves, barley grains, straw, and jute, against the four surfaces (aluminum, plywood, rubber, and paper) are represented in Table 22.

Table 22: Angle of friction and Static coefficient of friction (μ) of oak leaf, barley grain, straw powders, and chopped jute against the four various surfaces, aluminum, paper, rubber, and plywood.

Powder	Angle of friction (θ) and static coefficient of friction (μ) against the four various surfaces							
Oak leaf	Aluminum		Paper		Rubber		Plywood	
powder	θ (˚)	μ	θ (˚)	μ	θ (˚)	μ	θ (˚)	μ
Run#1	41	0.8692	40	0.8390	42	0.9004	47	1.0723
Run#2	43	0.9325	40	0.8390	42	0.9004	47	1.0723
Run#3	41	0.8692	41	0.8692	43	0.9325	47	1.0723
Run#4	40	0.8390	41	0.8692	43	0.9325	48	1.1106
Run#5	40	0.8390	42	0.9004	44	0.9656	48	1.1106
Average		0.8698		0.8634		0.9263		1.0876

n (number of runs)	5		5		5		5
Standard deviation	0.03814026		0.025591093		0.027248537		0.020946995
Standard errors	0.017056843		0.011444685		0.012185916		0.009367781

Barley grain powder	Aluminum		Paper		Rubber		Plywood	
	θ (˚)	μ	θ (˚)	μ	θ (˚)	μ	θ (˚)	μ
Run#1	34	0.6745	36	0.7265	39	0.8097	47	1.0723
Run#2	34	0.6745	36	0.7265	39	0.8097	47	1.0723
Run#3	33	0.6494	37	0.7535	40	0.8390	48	1.1106
Run#4	33	0.6494	37	0.7535	40	0.8390	48	1.1106
Run#5	33	0.6494	38	0.7812	40	0.8390	50	1.1917
Mean		0.6594		0.7482		0.8273		1.1115
n (number of runs)	5		5		5		5	
Standard deviation	0.013748342		0.02285846		0.016056814		0.048746079	
Standard errors	0.006148446		0.010222614		0.007180826		0.021799909	

Straw	Aluminum		Paper		Rubber		Plywood	
	θ (˚)	μ	θ (˚)	μ	θ (˚)	μ	θ (˚)	μ
Run#1	31	0.6008	37	0.7535	39	0.8097	41	0.8692
Run#2	31	0.6008	37	0.7535	39	0.8097	41	0.8692

	θ (°)	μ	θ (°)	μ	θ (°)	μ	θ (°)	μ
Run#3	33	0.6494	39	0.8097	40	0.8390	43	0.9325
Run#4	32	0.6248	39	0.8097	40	0.8390	43	0.9325
Run#5	32	0.6248	39	0.8097	40	0.8390	44	0.9656
Average		0.62017		0.7872		0.8273		0.9138
n (number of runs)		5		5		5		5
Standard deviation		0.020277506		0.03079843		0.016056814		0.042882974
Standard errors		0.009068376		0.013773477		0.007180826		0.019177849

Jute	Aluminum		Paper		Rubber		Plywood	
	θ (°)	μ	θ (°)	μ	θ (°)	μ	θ (°)	μ
Run#1	25	0.4663	43	0.9325	46	1.0355	47	1.0723
Run#2	24	0.4452	44	0.9656	46	1.0355	47	1.0723
Run#3	24	0.4452	43	0.9325	46	1.0355	46	1.0355
Run#4	24	0.4452	43	0.9325	45	1	49	1.1503
Run#5	25	0.4663	43	0.9325	45	1	46	1.0355
Average		0.4536		0.9391		1.0213		1.0732
N (number of runs)		5		5		5		5
Standard deviation		0.011545429		0.014835725		0.019460754		0.046889098
Standard errors		0.005163273		0.006634738		0.008703114		0.020969442

Figure 56 indicates static coefficient of friction (oak leaves, barley grains, straw and jute) on four surfaces (aluminum, paper, rubber, and plywood) with standard deviations.
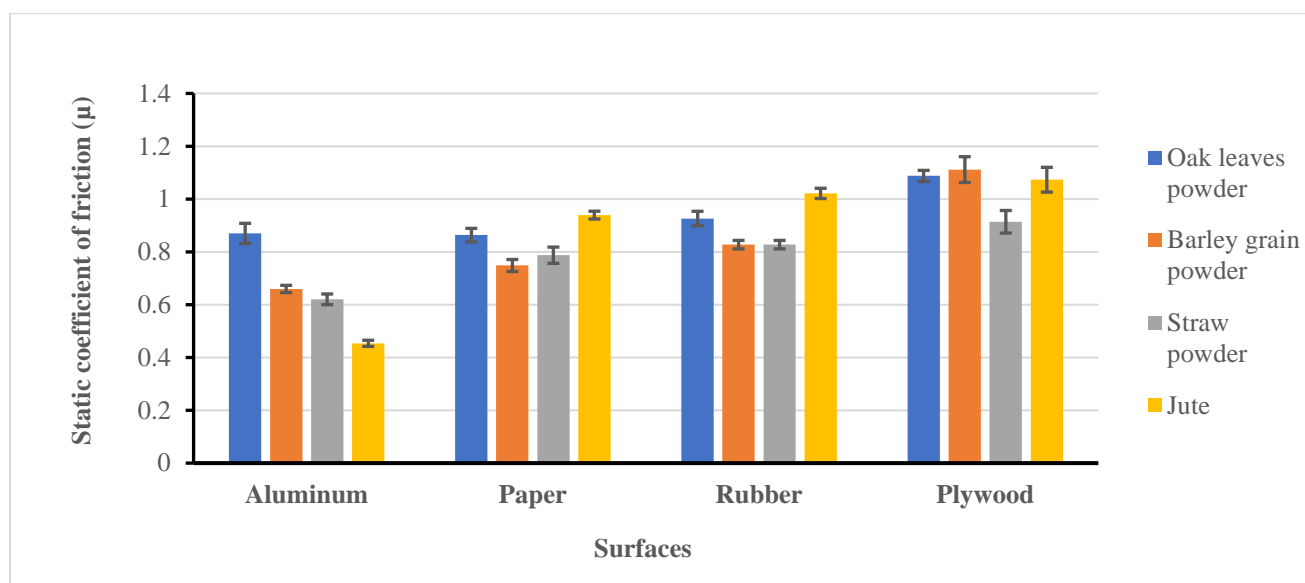
Figure 56: Static coefficient of friction (oak leaves, barley grains, straw, and jute) on four surfaces (aluminum, paper, rubber, and plywood).

The static coefficient of friction between the layer of the biomass material and surface material permits an approximation of opposing movements. There were important variances between the coefficients of friction for the tested samples that are noted. These variances between the values of coefficient of friction are determined from the size of individual particles. In the other studies, if the size increased, the surface of contact was reduced and overcome the decrease in the force required to separate the contact between particles and the surfaces of the structure materials [134]. There are other relationships affected on static coefficient of friction, like bulk density, and moisture content. Carson, J. et al (1998) proved that increase in the friction between particles led to decreases in the apparent density. Powder particles that exhibit very low friction because of their rounded shape, such as gas-atomized stainless steel powder, do not demonstrate this characteristic.

The effect of decreased particle size on density is particularly significant for particle sizes of less than 20 μm [135]. In addition, increasing of static coefficient of friction on biomass materials from maximum moisture percentage, minimum moisture percentage, and fine surface of the biomass led to easily movement on the examined surface since sticky nature of the biomass materials led to high resistance [35]. Zhang, Y. et al (2008) found the static coefficient of friction for lentils increased with an uptick in moisture content on all four surfaces (concrete, wood, rubber, and stainless steel). This might be due to the increased adhesion between the grain and the material surfaces at higher moisture values. The static coefficient of friction for lentils reduced with storage time on all four surfaces [106]. Subramanian et al (2007) studied the coefficient of static friction for the grains and flours that rose with an increase in moisture content. For both grains and flours, mild steel surface offered the maximum friction followed by galvanized steel, aluminum and stainless steel. The values of static coefficient of friction and internal coefficient of friction demonstrated a linear relationship of moisture content with higher coefficient [126]. The static coefficient of friction raised with an increase in particle size. While the static coefficient of friction increased on the surface with increasing the particle size of the grains, the adhesion between particles decreased [39]. The highest average static coefficient of friction of these materials was found on plywood surface while the lowest average was obtained on the aluminum and paper surfaces as represented in Table 19. The study indicated that the average static coefficient of friction of barley grains increased with 0.6594, 0.7482, 0.8272, and 1.1154 on the aluminum, paper, rubber, and plywood surfaces respectively. The average static coefficient of friction of oak leaves rose from 0.8634 to 1.0876 on aluminum through plywood surfaces. Also, it increased from 0.6201, 0.7872, 0.8273, and 0.9138 on

aluminum, paper, rubber, and plywood surfaces for straw, and it ranged from 0.4536 to 1.0732 on the four various surfaces for jute. It was indicated from the results that the rougher of the surface, the greater the internal angle of friction. Therefore, the static coefficients of friction of the four samples of the biomass materials on aluminum surface have the lowest values because aluminum has the smoothest surface, resulting in the plain movement on the test surface. These examinations provided ideas on how biomass materials stick to resin and how manufacture uniform composites. Jute has the highest average static coefficient value of friction on paper and rubber surfaces due to higher average value of moisture content (11.83 percent). In contrast, straw has the lowest average static coefficient value of friction on rubber and plywood surfaces due to the lower moisture content (9.93 percent) and biggest particle size distribution (1016 μm $< dp >$ 1524 μm). Barley grain powder has the highest average static coefficient value of friction on plywood surface (1.111) because it has the smallest particle size distribution, and these soft particles fill the roughness surfaces of plywood while the powder starts to slide down. Then, it makes additional resistance between the particles of the powder on the surface. Therefore, the average value of angle of friction ($\theta = 48°$) of the plywood plate reached the extreme level after sliding down the whole amount of barley grain powder.

4.2. Biomass Reinforced Composites Results

4.2.1. Density of Composites

4.2.1.1. Density Measured Using Torbal Analytical balance

The density results of composite sample measured by Torbal Density Analyzer are represented in Table 23. The average density of NEAT is 1.1528 g/cm^3. NEAT is the part

that is used without reinforced biomass, and it is made up of an undiluted clear difunctional bisphenol A/epichlorohydrin that is originated from liquid epoxy resin [121]. The density results of biomass reinforced composites are compared to NEAT. It indicates that the more biomass fibers added to NEAT, the greater the density of the composite samples. Density of biomass reinforced composites with standard deviation is presented in Figure 57. The densities' values of these composites such as NEAT, OAk10%, OAK20%, BRY10%, BRY20%, BRY30%, STR10%, STR20%, JUT2.25%, and JUT4.5% were 1.152, 0.783, 0.939, 0.636, 0.750, 0.913, 1.063, 1.017, 1.040, and 1.015 g/cm^3 respectively. From the results, the density was found to be reduced when biomass powders added to neat epoxy. The addition of 10% oak leaf powder resulted a decrease of 32.03% in density compared to that of the neat epoxy. Also, the addition of 20% oak leaf powder resulted a decrease of 18.49% in density compared to that of the neat epoxy. The addition of 10%, 20%, and 30% barley grain powder gave a decrease of 44.79%, 34.88%, and 20.74%, respectively, compared to that of the neat epoxy. The addition of 10%, and 20% straw powder gave a decrease of 7.72%, and 11.71%, respectively, in density compared to that of the neat epoxy. The addition of 2.25%, and 4.5% cut jute resulted a decrease of 9.72%, and 11.89%, respectively, compared to that of the neat epoxy. The lowest average density was obtained in BRY10%, and the highest average density was found in STR10% compared to the neat epoxy.

Table 23: Density measured by Torbal Analytical balance of the samples of biomass reinforced composites, NEAT, OAK10%, OAK20%, BRY10%, BRY20%, BRY30% STR10%, STR20%, JUT2.25%, and JUT4.5% [g/cm^3].

Name of composite	Density1 (g/cm^3)	Density2 (g/cm^3)	Density3 (g/cm^3)	Density4 (g/cm^3)	Density5 (g/cm^3)	n	Average density (g/cm^3)	Standard Deviation	Standard Error
NEAT	1.153	1.152	1.154	1.150	1.153	5	1.152	0.0012	0.0005
OAK 10%	0.784	0.787	0.786	0.772	0.787	5	0.783	0.0066	0.0029
OAK 20%	0.906	0.955	0.935	0.959	0.941	5	0.939	0.0210	0.0094
BRY 10%	0.614	0.638	0.651	0.643	0.636	5	0.636	0.0138	0.0061
BRY 20%	0.761	0.730	0.758	0.751	0.751	5	0.750	0.0120	0.0053
BRY 30%	0.919	0.917	0.902	0.913	0.913	5	0.913	0.0065	0.0029
STR 10%	1.067	1.063	1.066	1.050	1.068	5	1.063	0.0071	0.0032
STR 20%	1.011	1.012	1.023	1.020	1.018	5	1.017	0.0049	0.0022
JUT 2.25%	1.037	1.043	1.037	1.040	1.042	5	1.040	0.0028	0.0012
JUT 4.5%	1.016	1.013	1.011	1.017	1.019	5	1.015	0.0030	0.0013
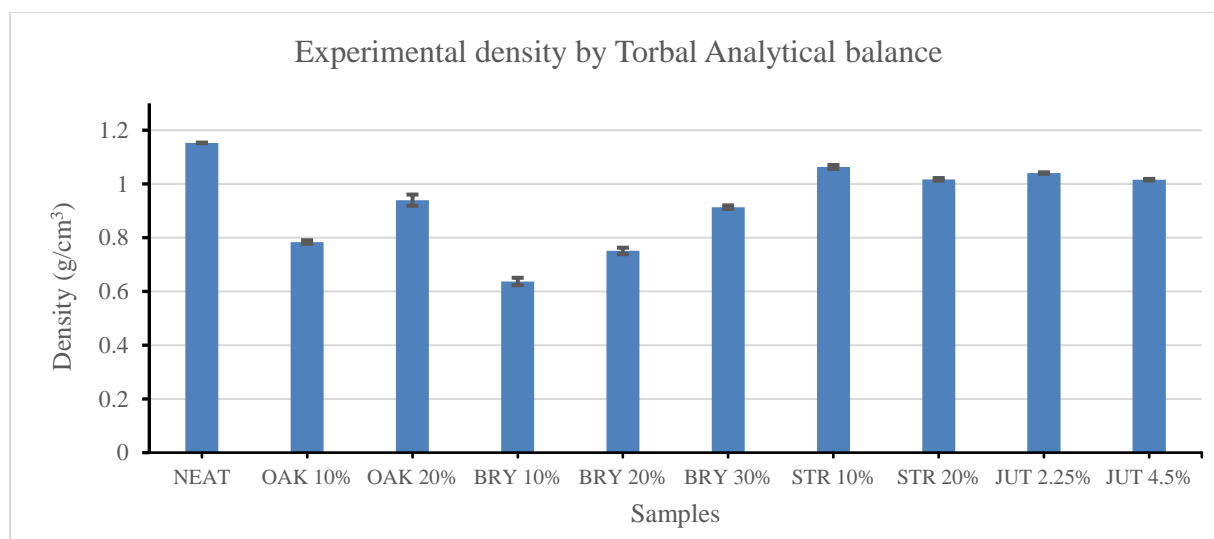
Figure 57: Density of the samples of biomass reinforced composites, NEAT, OAK10%, OAK20%, BRY10%, BRY20%, BRY30%, STR10%, STR20%, JUT2.25%, and JUT4.5% [g/cm^3]

4.2.1.2. Theoretical Density

The other results were measured by calculating the theoretical density as following:

The dimensions of BRY30% were:

m (mass)= 33.4741 g

D_1 (diameter of small circle) = 43.15 mm $\implies$ R_1=21.575 mm

D_2 (diameter of large circle) = 52.74 mm $\implies$ R_2= 26.37 mm

H (height of the truncated cone) = 20.53 mm

$$V = \frac{\pi}{3}(R_1^2 + R_1.R_2 + R_2^2).H \dots\dots\dots\dots\dots\dots\dots (2)$$

Applying equation (1) [102], the volume of truncated cone is:

V= 37169.84875 mm^3 = 37.16984875 cm^3

$$\rho = \frac{m}{V} = \frac{33.4741}{37.16984875} = 0.900571327 \text{ g/cm}^3$$

The same calculations for the other samples, and the densities were found in Table 24.

Table 24: Theoretical calculations of composite sample densities, NEAT, OAK10%, OAK20%, BRY10%, BRY20%, BRY30%, STR10%, STR20%, JUT2.25%, and JUT4.5% [g/cm³].

	m	D1	D2	R1	R2	H	V	V	density	Average	Standard
	(g)	(mm)	(mm)	(mm)	(mm)	(mm)	(mm³)	(cm³)	(g/cm³)	density (g/cm³)	deviation (g/cm³)
NEAT											
Run#1	48.125	43.02	54.3	21.51	27.15	23.24	43390.08	43.390	1.109	1.130	0.0183
Run#2	48.808	42.82	54.26	21.41	27.13	23.06	42848.35	42.848	1.139		

Run#3	48.804	41.27	54.41	20.635	27.205	23.63	42720.61	42.720	1.142		
OAK10%											
Run#1	31.621	42.68	54.07	21.34	27.035	22.34	41228.4	41.228	0.766	0.763	0.0616
Run#2	31.387	43.26	53.41	21.63	26.705	20.73	38157.98	38.157	0.822		
Run#3	33.554	44.46	54.92	22.23	27.46	24.66	47973.51	47.973	0.699		
OAK20%											
Run#1	35.15	43.43	53.33	21.715	26.665	21.05	38812.02	38.812	0.905	0.907	0.0032
Run#2	36.204	42.65	54.09	21.325	27.045	21.65	39948.41	39.948	0.906		
Run#3	36.305	42.45	53.85	21.225	26.925	21.78	39823.93	39.823	0.911		
BRY10%											
Run#1	27.046	43.35	53.65	21.675	26.825	22.2	41146.73	41.146	0.657	0.631	0.0304
Run#2	27.125	43.22	54.15	21.61	27.075	22.68	42376.33	42.376	0.640		
Run#3	21.243	43.29	53.8	21.645	26.9	19.125	35518.38	35.518	0.598		
BRY20%											
Run#1	22.697	43.39	51.08	21.695	25.54	16.6	29138.27	29.138	0.778	0.737	0.0457
Run#2	25.95	43.13	52.52	21.565	26.26	19.35	34854.07	34.854	0.744		
Run#3	24.594	43.77	52.43	21.885	26.215	19.62	35729.78	35.729	0.688		
BRY30%											
Run#1	33.474	43.15	52.74	21.575	26.37	20.53	37169.85	37.169	0.900	0.896	0.0104
Run#2	33.479	43.11	52.91	21.555	26.455	20.4	37039.8	37.039	0.903		
Run#3	30.992	41.41	51.23	20.705	25.615	20.73	35045.29	35.045	0.884		
STR10%											

Run#1	47.856	42.65	54.77	21.325	27.385	24.54	45942.58	45.942	1.041	1.051	0.0124
Run#2	49.127	42.63	54.96	21.315	27.48	24.54	46110.48	46.110	1.065		
Run#3	45.061	40.95	53.3	20.475	26.65	24.55	43042.99	43.042	1.046		
STR20%											
Run#1	49.709	42.94	55.26	21.47	27.63	25.31	48150.12	48.150	1.032	1.016	0.0192
Run#2	49.512	43.3	55.16	21.65	27.58	25.36	48481.27	48.481	1.021		
Run#3	45.377	41.48	53.6	20.74	26.8	25.57	45610.48	45.610	0.994		
JUT2.25%											
Run#1	57.793	43.13	56.76	21.565	28.38	29.08	57297.42	57.297	1.008	1.013	0.0053
Run#2	58.144	43.19	56.96	21.595	28.48	28.96	57363.85	57.363	1.013		
Run#3	25.896	42.09	48.78	21.045	24.39	15.65	25406.74	25.406	1.019		
JUT4.5%											
Run#1	52.719	43.34	57	21.67	28.5	27.58	54831.09	54.831	0.961	0.970	0.0218
Run#2	52.846	43.13	56.6	21.565	28.3	27.05	53120.41	53.120	0.994		
Run#3	48.214	41.41	55.85	20.705	27.925	27.03	50547.96	50.547	0.953		
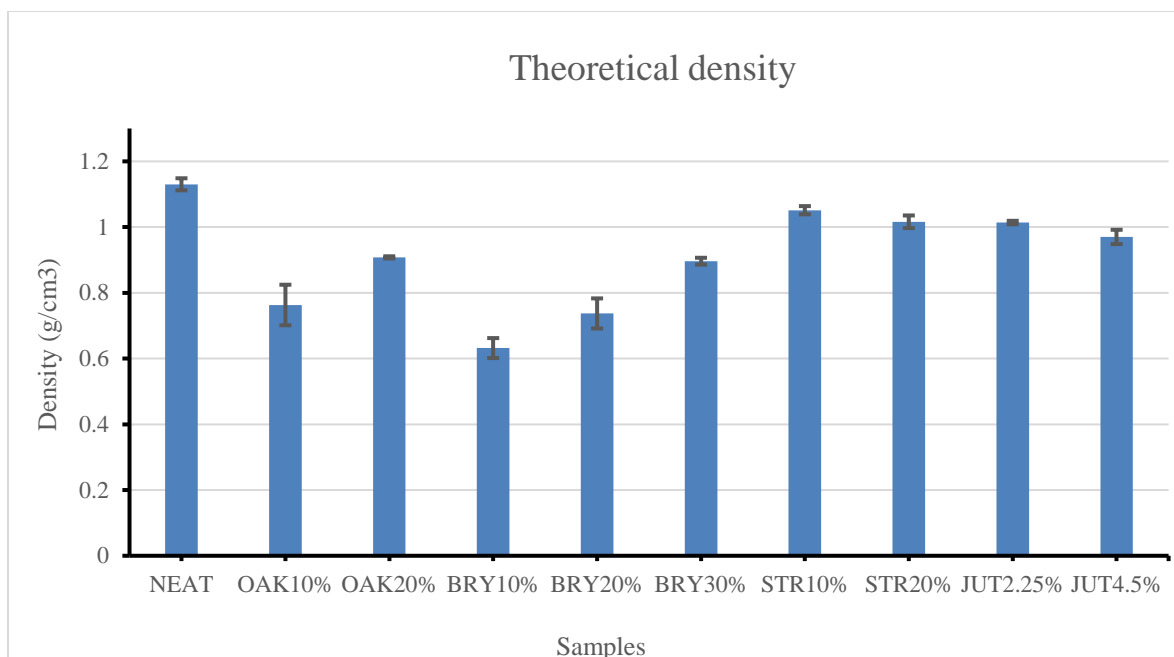
Figure 58: Calculations of theoretical densities of composites materials, NEAT, OAK10%, OAK20%, BRY10%, BRY20%, BRY30%, STR10%, STR20%, JUT2.25%, and JUT4.5% [g/cm³].

Table 25: Comparison of densities measured from Torbal Analytical balance and theoretical calculations

Samples	NEAT	OAK 10%	OAK 20%	BRY 10%	BRY 20%	BRY 30%	STR 10%	STR 20%	JUT 2.25%	JUT 4.5%
Torbal Density (g/cm³)	1.152	0.782	0.939	0.636	0.750	0.913	1.063	1.017	1.040	1.015
Theoretical density (g/cm³)	1.130	0.763	0.907	0.631	0.737	0.896	1.051	1.016	1.013	0.970
Difference	1.99%	2.59%	3.44%	0.79%	1.81%	1.93%	1.14%	0.09%	2.61%	4.71%

According to data presented in Table 25, densities measurements in both experimentally

(Torbal Analytical balance) and theoretical calculations showed small differences between

the two measurements. The lowest average density was found in BRY10% while the highest average density was measured in STR10% compared to the neat epoxy.

4.2.2. Porosity

The porosity results were shown after calculating theoretical solid density for each composite material.

| NEAT | OAK 10% | OAK 20% | BRY 10% | BRY 20% | BRY 30% |

| STR10% | STR20% | JUT2.25% | JUT4.5% |
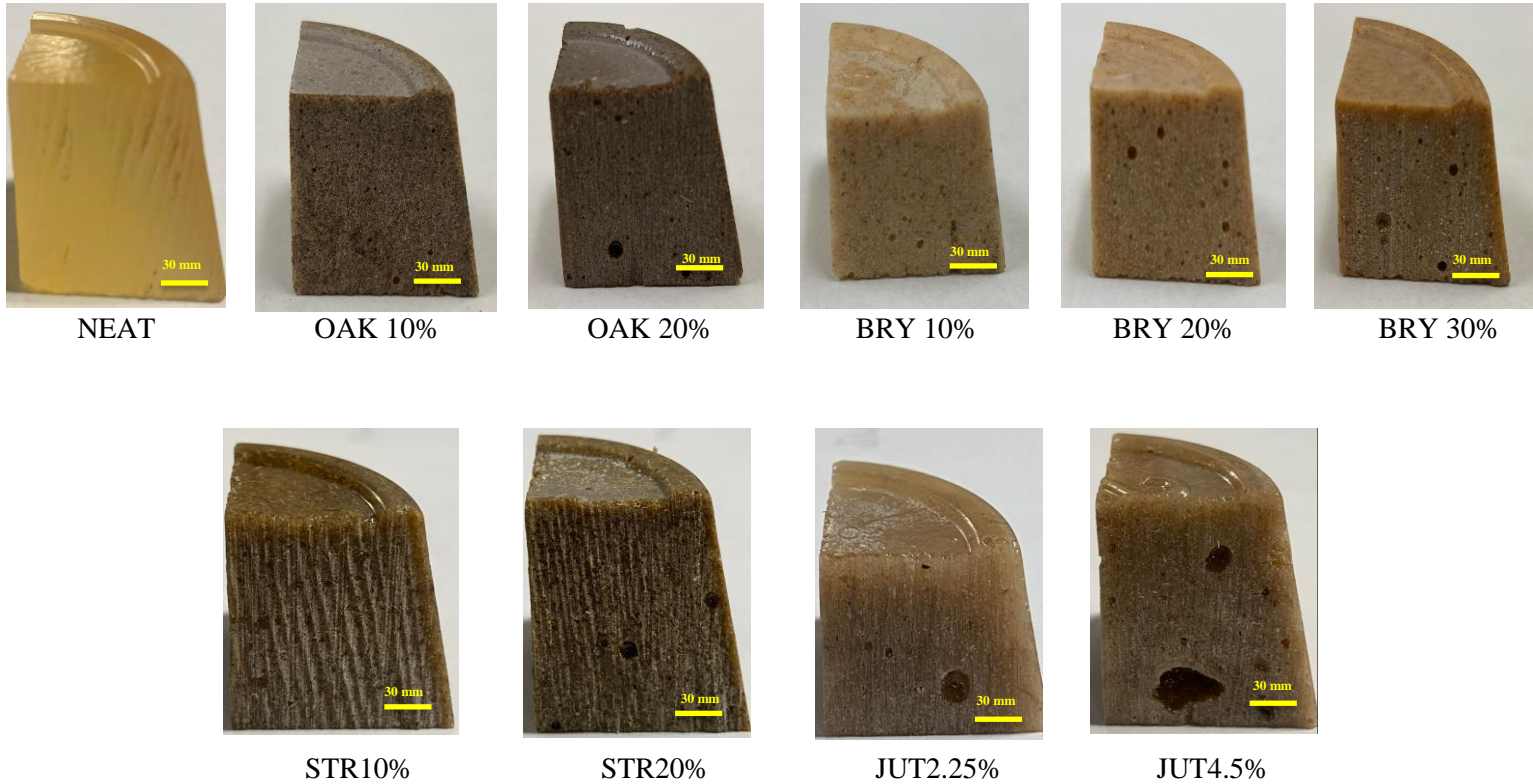
Figure 59: Porosity of biomass reinforced composites, NEAT, OAK10%, OAK20%, BRY10%, BRY20%, BRY30%, STR10%, STR20%, JUT2.25%, and JUT4.5%.

The porosity that was mentioned in section three was calculated according to the following equation:

$$P = \left(1 - \frac{\rho_{Torbal}}{\rho_{TheoreticalSolidDensity}}\right) x\ 100 \qquad (10)$$

Where P is the porosity (%)

ρ_{Torbal}: density measured by Torbal Analytical balance (g/cm^3)

$\rho_{therotical}$: theoretical solid density calculation (g/cm^3)

The value of oak particle density is 0.593 g/cm^3 [117], barley particle density is 1.2 g/cm^3 [118], straw particle density is 1.323 g/cm^3 [119], jute particle density is 1.46 g/cm^3 [120], and Neat EPON particle density is 1.16 g/cm^3 [121].

The results of theoretical solid density calculations ($\rho_{TheoreticalSolidDensity}$) were shown in the following:

Density of OAK10% = ((10/100) x 0.593) + ((90/100) x 1.16) = 1.1033 g/cm^3

Density of OAK20% = ((20/100) x 0.593) + ((80/100) x 1.16) = 1.0466 g/cm^3

Density of BRY10% = ((10/100) x 1.2) + ((90/100) x 1.16) = 1.164 g/cm^3

Density of BRY20% = ((20/100) x 1.2) + ((80/100) x 1.16) = 1.168 g/cm^3

Density of BRY30% = ((30/100) x 1.2) + ((70/100) x 1.16) = 1.172 g/cm^3

Density of STR10% = ((10/100) x 1.323) + ((90/100) x 1.16) = 1.1763 g/cm^3

Density of STR 20% = ((20/100) x 1.323) + ((80/100) x 1.16) = 1.1926 g/cm^3

Density of JUT2.25% = ((2.25/100) x 1.46) + ((97.75/100) x 1.16) = 1.16675 g/cm^3

Density of JUT4.5% = ((4.5/100) x 1.46) + ((95.5/100) x 1.16) = 1.1735 g/cm^3

Table 26: Porosity calculations of biomass reinforced composites, NEAT, OAK10%, OAK20%, BRY10%, BRY20%, and BRY30%

Sample	density (Torbal) (g/cm^3)	Theoretical density (g/cm^3)	Porosity	Porosity (%)
NEAT	1.152	1.16	0.006	0.620
OAK10%	0.782	1.1033	0.290	29.044
OAK20%	0.939	1.0466	0.102	10.266
BRY10%	0.636	1.164	0.452	45.284

BRY20%	0.750	1.168	0.357	35.734
BRY30%	0.913	1.172	0.220	22.048
STR10%	1.063	1.176	0.096	9.603
STR20%	1.017	1.192	0.147	14.715
JUT2.25%	1.040	1.166	0.108	10.829
JUT4.5%	1.015	1.1735	0.134	13.441
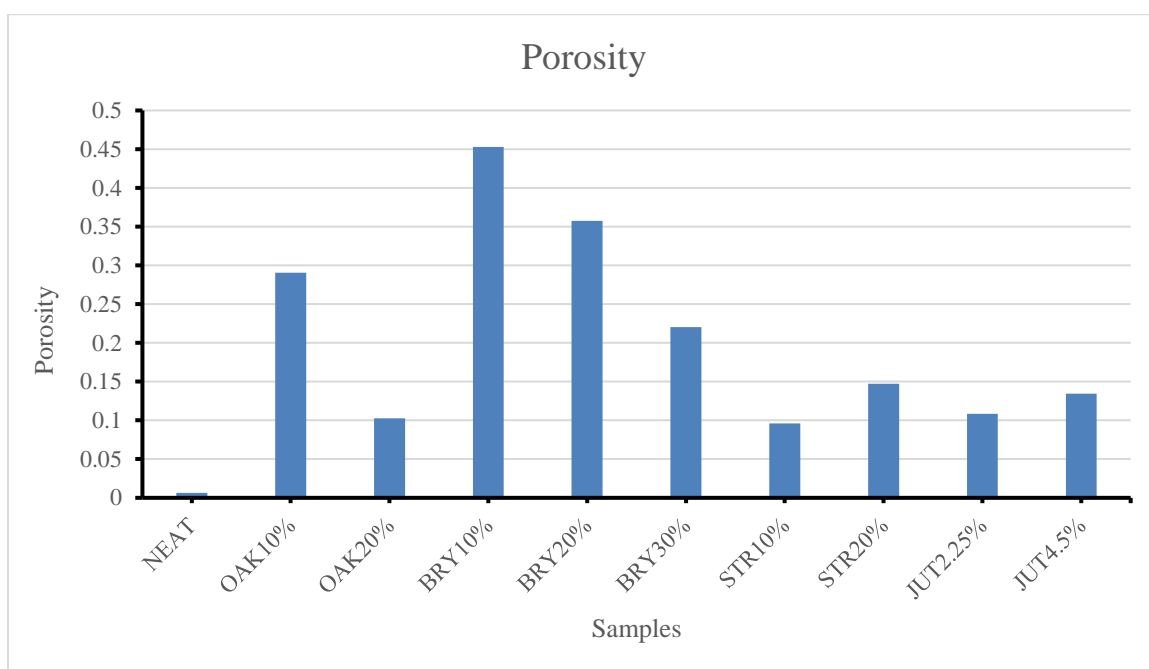
Figure 60: Porosity of the composites' materials, NEAT, OAK10%, OAK20%, BRY10%, BRY20%, BRY30%, STR10%, STR20%, JUT2.25%, and JUT4.5%

The results from Table 26 and Figure 60 show that STR10% has the lowest porosity while the highest porosity was measured in BRY10% compared to NEAT.

4.2.3. Thermal Conductivity of Biomass Reinforced Composites

The thermal conductivity tests were conducted by Dr. Dikici. Figure 61 shows the thermal conductivity values and standard deviations of each composite.
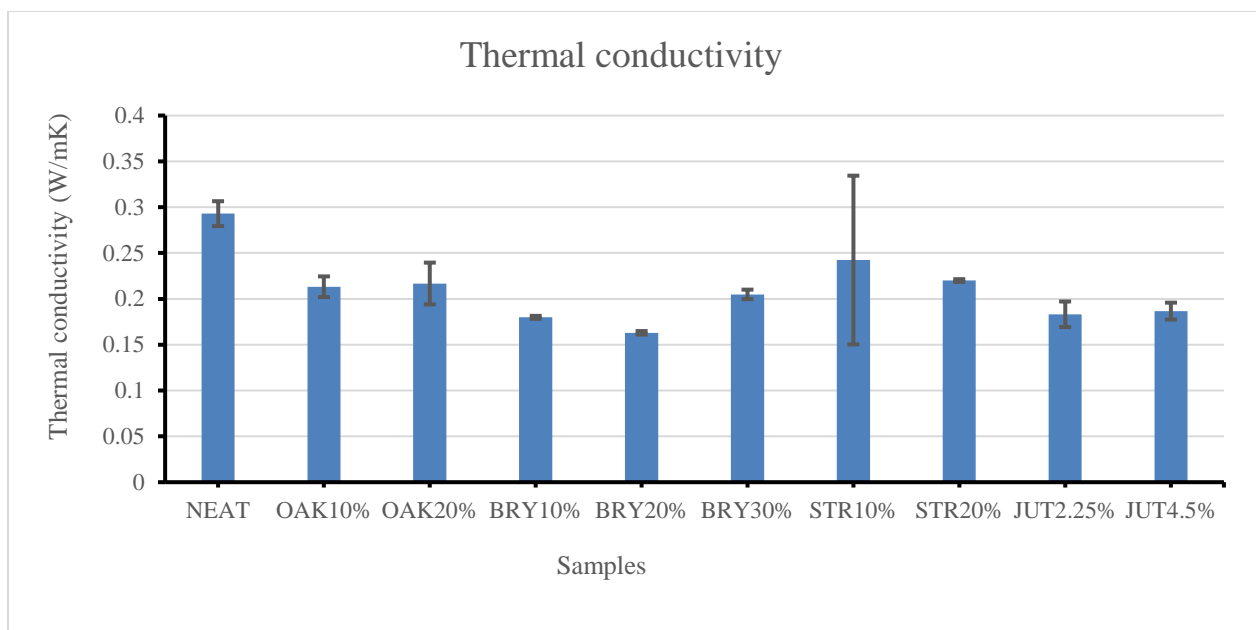
Figure 61: Thermal conductivity of the six samples of composite samples [W/m.K]

Table 27: Thermal conductivity of biomass reinforced composites

Sample	Average thermal conductivity (W/m.K)	Standard deviation
NEAT	0.292	0.0135
OAK10%	0.213	0.0112
OAK20%	0.216	0.0228
BRY10%	0.179	0.0016
BRY20%	0.162	0.0019
BRY30%	0.204	0.0051
STR10%	0.242	0.0920
STR20%	0.22	0.0014
JUT2.25%	0.183	0.0139

JUT4.5%	0.186	0.0092

According to results from Figure 61 and Table 27, the values of thermal conductivity of these composites such as NEAT, OAk10%, OAK20%, BRY10%, BRY20%, BRY30%, STR10%, STR20%, JUT2.25%, and JUT4.5% were 0.2929, 0.2132, 0.2167, 0.1798, 0.1629, 0.2049, 0.2423, 0.22, 0.1832, and 0.1866 W/m.K, respectively.

It could be indicated that the material properties measured are not exact quantities. Even if TPS 2500 S Thermal Constants Analyzer is an accurate device and highly controlled examination process, there is usually some scattered material. The thermal conductivity of OAK10% is 0.213 W/m.K while the thermal conductivity of OAK20% is 0.216 W/m.K compared to NEAT (0.292 W/m.K). There is a small difference between OAK10% and OAK20%. Thus, the thermal conductivity was found to be decreased slightly between these two samples when biomass powders were added to neat epoxy. The reduction percentage in thermal conductivity was calculated from OAK10% (27.21%) to OAK20% (26.01%). The addition of 10 percent oak leaf powder resulted a decrease of approximately 27.21% in thermal conductivity compared to that of the neat epoxy while the addition of 20 percent oak leaf powder produced 26.01%. It is an unexpected result because the air gaps in composites could be changed from one sample to another. Air has lower thermal conductivity ($k_{air} = 0.025$ W/m.K). It has a significant effect on the results. Fabricating more composites and obtaining thermal conductivity results will be the solution.

The addition of 10%, 20%, and 30% barley grain powder produced a reduce of approximately 38.61%, 44.36%, and 30.05% in thermal conductivity compared to that of

the neat epoxy. The addition of 10% straw powder yielded an increase of 17.27% in thermal conductivity compared to that of the neat epoxy while the addition of 20% straw powder resulted a decrease 24.9% in thermal conductivity compared to that of the neat epoxy.

The addition of 2.25% jute yielded a decrease of approximately 37.46% while the addition of 4.5% jute produced a decrease of 36.28% in thermal conductivity compared to that of the neat epoxy. It can be concluded that the lowest value of the thermal conductivity of biomass reinforced composites is barley reinforced composite with 20 percent (BRY20%) where it has 0.1629 W/m.K, and the highest average thermal conductivity was found in STR10% (0.2423 W/m.K).

Table 28 indicated the aggregate results of biomass powders (barley grains, oak leaves, straw, and jute) and reinforced composites (NEAT, OAK10%, OAK20%, BRY10%, BRY20%, BRY30%, STR10%, STR20%, JUT2.25%, and JUT4.5%.

Table 28: Overall calculations of biomass powders and reinforced composites.

Sample	Angle of repose $(\alpha)(°)$	Static coefficient of friction (μ)				Bulk density (g/cm^3)	Moisture content (%)	Experimental density (Torbal Analytical balance) (g/cm^3)	Theoretical density (g/cm^3)	Porosity	Thermal conductivity (W/m.K)
		Aluminum	Paper	Rubber	Plywood						

Oak leaf powder	24.30	0.869	0.863	0.926	1.087	0.410	10.36	----	----	----	----
Barley grain powder	31.12	0.659	0.748	0.827	1.111	0.648	7.13	----	----	----	----
Straw powder	35.75	0.620	0.787	0.827	0.913	0.327	9.93	----	----	----	----
Jute (chopped)	----	0.453	0.939	1.021	1.073	0.106	11.83	----	----	----	----
NEAT								1.152	1.130	0.006	0.292
OAK10%								0.782	0.763	0.290	0.213
OAK20%								0.939	0.907	0.102	0.216
BRY10%								0.636	0.631	0.452	0.179
BRY20%								0.750	0.737	0.353	0.162
BRY30%								0.913	0.896	0.220	0.204
STR10%								1.063	1.0513	0.096	0.242
STR20%								1.0171	1.016	0.147	0.22
JUT2.25%								1.040	1.013	0.108	0.183
JUT4.5%								1.015	0.970	0.134	0.186

4.3. Relations of Thermal Conductivity on Moisture Content, Porosity, and Density

4.3.1. Effect of Moisture Content

There is a proportional relation between thermal conductivity, and both moisture content

and temperature due to the thermal conductivity of water ($k_{water} = 0.598$ W/m·K at 20 °C)

[136]. Markowski et al (2013) found that the value of the thermal conductivity of malting barley increases with rising moisture content and temperature. The thermal conductivity of *Mauritia* barley type increases from 0.124 to 0.155 W/m.K with raising water content and temperature [137]. Troppova et al (2015) studied the effect of temperature and moisture content on the thermal conductivity of wood-based fibreboards, and they found that the thermal conductivity increases with rising moisture content and temperature [138]. Mňahončáková et al (2016) studied the influence of moisture content on the thermal conductivity measurements of the carbon fiber reinforced cement composite material. The values of thermal conductivity are implemented based on moisture content between dry state and entirely water saturated state utilizing an impulse method. Then, the achieved information is analyzed using formulas of Brugemann and Wiener homogenization. The implemented homogenization methods are evaluated by comparing the experimental and theoretical results. Then, Mňahončáková et al (2016) found that the thermal conductivity of the cementitious composite increases with increasing temperature and water content [139]. MacLean (1941) and Vay et al (2015) found there is a linear correlation between moisture in wood and thermal conductivity under the fiber saturation point. They found that the thermal conductivity is raised with increasing water amounts in wood because water is considered as a good conductor [140][141]. Alagusundaram et al (1991) mentioned in their study that the higher the thermal conductivities of the three seeds types (barley, lentils, and peas), the greater the moisture content or temperature [65]. Gel (2016) mentioned that the thermal conductivity of cellulose insulation materials raised from 0.040 to 0.066 W/mK based on the moisture content which was increased from 0 to 5 % [142]. In addition, the effect of thermal conductivity with moisture content has been investigated

by Grelat et al (2004) on straw bales [143], and Palumbo et al (2016) on board composed of barley straw [144]. Thermal performance of different samples of sheep wool materials varied according to thickness and density was assessed by Zach et al (2012). They found that while moisture content is increased, the thermal conductivity is also raised [145]. According to the previous investigations, there is an obvious linear relationship between thermal conductivity and moisture content or temperature. The higher the thermal conductivity of biomass reinforced composites, the greater the moisture content or temperature.

4.3.2. Effect of Porosity

The other relation is the effect porosity on thermal conductivity. The wood porosity is a significant factor because air is considered as a weak thermal conductor compared to wood due to thermal conductivity of air ($k_{air} = 0.025$ W/m.K) [146]. Therefore, porous woods possess lower values of thermal conductivity. The thermal conductivity of several Indian trees was examined by Vasubsbu et al. (2015), and they noted that the lowest thermal conductivities were gained from the most porous woods. Where the curry tree showed about 73 percent porosity with the lowest thermal conductivity about 0.0615 W/mK [147]. There is an inverse relationship between thermal conductivity and porosity. Wei et al (2015) studied the effect of the thermal conductivity with porosity. The thermal conductivity raises while the porosity of the insulation structure of rice straw decreases. The greater the thermal conductivity, the lower the porosity of rice straw [148]. The thermal properties of biocomposites were robustly affected by the porosity [149]. Chikhi et al (2018) numerically investigated the porosity of composites materials made from gypsum and date palm fibers as natural fibers. They indicated that the porosity impacts on

the thermal conductivity of biocomposites [150]. The higher the porosity in the composites, the lower the thermal conductivity [151] [152].

4.3.3. Effect of Density with Orientation

The measurement of orientation is a crucial factor for thermal conductivity, which is mostly higher in the axial orientation. Samuel et al. (2012) studied the direction of three various wood products measurements, and they found the thermal conductivity has the maximum value in the axial plane and rises with density [153]. The effect of the density on the thermal conductivity of straw bales with respecting orientation was studied by Andersen et al (2001). Two groups of samples were investigated: the first one had a density of 75 kg/m^3; the other density was 90 kg/m^3. The value of thermal conductivity of the first group of samples was 0.052 W/m.K while perpendicular to the fibers, and it was 0.056 W/m.K while parallel to the fibers. The thermal conductivity of the second group of samples was a little higher: it was 0.056 W/m.K while perpendicular, and 0.06 W/m.K parallel. Then, Anderson et al found that the thermal conductivity of straw bales was increased by 7.69 percent when the examined direction shifts from perpendicular to parallel with the density of 75 kg/m^3. On the other hand, the thermal conductivity of the other set of samples was increased with the same percent of the variation from perpendicular to parallel direction for 90 kg/m^3 density [154]. Yapici et al. (2011) mentioned getting higher thermal conductivity value perpendicular to the grain (0.195 W/m.K) with density (0.450 g/cm^3). Yapici et al. also reported that the thermal conductivity values of Scots pine (0.182 W/m.K) and chestnut (0.196 W/m.K) showed slightly higher values compared to Cavus et al (0.132 - 0.114 W/m.K) [155] [156]. Sair et al (2018) studied thermal characterizations of hemp fiber

reinforced polyurethane composites, and they found the thermal conductivity of these composites materials grows linearly with density [157].

The more the thermal conductivity, the greater the density of the composites. The thermal conductivity possesses the maximum value in the axial plane with the density. The higher value of the thermal conductivity is obtained in parallel orientation to the biomass-reinforced composites with the density based on the previous studies. According to the results from previous studies, the relationships could be summarized by the following:

From the results measured of thermal conductivity (k), density (ρ), and porosity (P) of the reinforced composites materials, experimental results indicated that both the thermal conductivity and density of composites materials rise after increasing the weight ratios of biomass fibers, but porosity decreased after adding more weight ratios of fibers. Based on the relationships between (k), (ρ), and (P), these results are compatible with the results of the previous studies where both the thermal conductivity and density increased, and the porosity decreased.

Table 29: The thermal conductivity and density of biomass samples

Biomass	Thermal conductivity (W/m.K)	Density (kg/m^3)
White oak wood (*Quercus alba*)	0.148 W/m.K [156]	
Oak wood (*Quercus petreae L.*)	0.197 W/m.K [156]	
European oak (*Quercus sp.*)	0.372 W/(m.K) Longitudinal plane [141]	744 (±46) kg/m^3 [141]
European oak (*Quercus sp.*)	0.174 W/ (m.K) Radial plane [141]	744 (±46) kg/m^3 [141]

Oak wood	0.209 W/ (m.K) [158]	850 kg/m^3 [158]
Mauritia barley	0.124 - 0.155 W/m K [137]	596.8- 599.6 kg/m³ [137]
Mauritia barley	0.169 to 0.232 W/(m.K) [65]	
Mauritia barley		600 kg/m³ [159]
Prestige barley		646.5-637.1 kg/m³ [137]
Straw bale	0.0353- 0.0539 W/m.K [67]	
Straw bale	0.0487 W/m.K perpendicular 0.0605 W/m.K parallel [160]	130 kg/m^3 [160]
Straw bale	0.052 W/m.K perpendicular 0.056 W/m.K parallel [154]	75 kg/m^3 [154]
Straw bale	0.056 W/m.K perpendicular 0.06 W/m.K parallel [154]	90 kg/m^3 [154]
Straw bale	0.066 parallel [161]	75 kg/m^3 [161]
Jute	0.038-0.055 W/m.K [67]	
Jute	0.046–0.055 W/m.K [162]	
Jute		1.45 g/cm^3 [163] (1450 Kg/m^3) [164]
Jute		1.3 g/cm^3 (1300 Kg/m^3) [165]
Jute		1.46 g/cm^3 [120]
Jute		1.34 g/cm^3 [166]

Table 30 provides some data from the other studies related to some experimental data of the thermal conductivity and density of biomass samples (barley, oak, straw, and jute). These data have variant values relied on the type of biomass material and the experimental

conditions (ambient temperature, and relative humidity). Oak wood has different values of thermal conductivity. For example, European oak has higher thermal conductivity in longitudinal plane than radial plane with the density. Also, thermal conductivity value of straw bale increased from perpendicular to parallel plane with the density. According to the thermal conductivity results, the lowest value of the thermal conductivity of biomass reinforced composites is barley-reinforced composite with 20 percent (BRY20%) where it has 0.1629 W/m.K, and the highest average thermal conductivity was found in STR10% (0.2423 W/m.K). These values of thermal conductivity and density of biomass reinforced composites were found to be close to the thermal conductivity and density values of biomass samples collected in Table 28, and the properties of biomass composites have slightly variants from that properties in Table 28 because the properties in that table are raw biomass materials without any additive materials.

Table 30: Some common insulation materials with thermal conductivities and densities

Common commercial insulation materials	Biomass reinforced composites materials	Density (g/cm^3)	Thermal conductivity (W/m.K)
Polyurethane foam (SPF)[167]		0.03	0.027
Expanded Polystyrene (EPS) [168]		0.028-0.045	0.030
Extruded Polystyrene (XPS) [169]		1.05	0.034 – 0.036
Earth (diatomaceous) [170]		2.25	0.126

	Kingspan OPTIM-R [174]		0.17-0.21	0.007
	Mineral Wool [175]		0.114	0.035
	Phenolic foam [176]		0.18-0.44	0.018-0.023
	Silicone rubber [172]		1.2	0.35
	Polyurethane rubber [172]		1.2	0.29
	Glass foam [177]		0.30–1.20	0.052-0.024
	Fiberglass [114]		2.44	0.035
	Calcium Silicate [178]		2.9	0.053
✓	Plaster board [171]		0.688	0.19
✓	Fluoroelastomer [172]		0.885	0.19
✓	Neoprene rubber [172]		1.23	0.19
✓	Bakelite [173]		1.27	0.233
		NEAT	1.152	0.292
		OAK 10%	0.782	0.213
		OAK 20%	0.939	0.216
		BRY 10%	0.636	0.178
		BRY 20%	0.750	0.162
		BRY 30%	0.913	0.204
		STR 10%	1.063	0.240
		STR 20%	1.017	0.242
		JUT 2.25%	1.040	0.183

	JUT 4.5%	1.015	0.186

Table 30 shows the experimental results of densities and thermal conductivities of the biomass-reinforced composed materials compared with the common traditional insulation materials. The densities' values of biomass reinforced composites were measured ranged from 0.636 (g/cm^3) to 1.063 (g/cm^3), and the thermal conductivities were between 0.1629 (W/m.K) and 0.242 (W/m.K). These properties measured have been compared to the common commercial insulation materials, and they were found to be close to the properties like density and thermal conductivity of bakelite, fluoroelastomer, plaster board, and neoprene rubber [179]. The composite density and the thermal conditivity were found to be reduced when biomass powders were added to neat epoxy. Barley grain, oak leaf, straw, and jute reinforced composites are shown to be good potential insulation materials.

4.4. Uncertainty and error analysis

Despite the use of the most accurate measuring devices and highly controlled examination processes, data could have a few variables even in samples of the same material. It could be observed that each result of the physical properties of the powders -- density, porosity, and thermal conductivity of composites -- contained slightly variations. There are some factors that led to uncertainties in measured data: containing the testing; differences in specimen- manufacturing procedures; uneven device calibration; and operator bias. There are inhomogeneities might be happened within the same portion of the materials and/ or simple composition and variations from portion to another. Convenient measures should be required to minimize the likelihood of measurement error, eliminating factors that could lead to data variations.

It is important to understand that scatter and variability of physical characteristics and properties of composites are unavoidable, and it is mandatory to deal with suitably.

It is necessary to identify a typical value and level of scatter from some measured parameter, and this is usually achieved by calculating the standard deviation of each result. While a measurement is repeated several times (the largest and lowest numbers are not taken to quantify the uncertainty), the standard deviation (σ) is calculated [180]

$$\sigma = \sqrt{\frac{\sum_{i=1}^{N}(x_i - \overline{x})^2}{N - 1}} \qquad (11)$$

Where N is the number of measurements of the experiment is repeated

x_i is the value of a discrete measurement.

$\overline{x}$ is the average of the measurements.

A large value of the standard deviation is related to a high degree of scatter. The standard error could be calculated due to the standard deviation values. While the standard error is small, the data is more demonstrative to the true result.

Also, the error types that are specified by the manufacturers are presented in Table 31.

Table 31: Errors parameters of devices used in the experiments

Device	details	error limits
Relative humidity meter PCE-MA	Readability	10 mg / 0.01 g
110	Readability moisture	0.1 %
Lab oven from Quincy Lab, Inc. MODEL 10GC	Temperature Stability: @ 150 ℃	+/- 3.0 ℃

Torbal Analytical	Readability	0.0001g
balance	Verification	0.001g
(AGZN220 Model)	Repeatability	0.0001g
	Linearity	+/- 0.0002g
	Percent Weighing (% Resolution Displayed)	0.1% (10mg to 700mg), 0.01% (700mg to 7g), 0.001% (>7g)
TPS 2500 S	Accuracy	+/- 5%
	Reproducibility	1 %

5. Section Two: Thermal Insulation and Carbon Footprint Optimization

5.1.Introduction

Currently, new materials have been developed with the goal of decreasing heat transfer and energy loss. Then, heat power can be transferred effectively, and energy usage can be decreased [181]. Heat transfer is defined as an energy form that can be transferred from a system to another due to a temperature variance. It can be classified into three modes: conduction, convection, and radiation. The heat transfer modes need the presence of the temperature variance, and the amount of energy transfers gradually from high-temperature to lower-temperature mediums for all three modes. This amount of heat transfer stops if the two systems have the same temperature. The first mode is conduction which is when energy transfers from more active particles of a material to the less active ones by direct contact. Conduction can occur in solids, liquids, or gases. Conduction happens due to the integration of molecular vibrations in a lattice and the power transfer by free electrons. The heat conduction rate across a medium relies on the geometry, thickness, and the materials of the medium in addition to the temperature difference through the medium. Convection is the second mode of heat transfer and occurs between a solid surface and the close liquid or gas that is in motion. This includes the combined influences of conduction mode and motion of fluid. If the fluid motion is rapid, the amount of heat transfer will be greater. The last mode of heat transfer is radiation. It refers to the amount of heat emitted by the form of photons (electromagnetic waves) due to the variations in the electronic shapes of the molecules or atoms. Radiative heat transfer differs from the other modes like conduction

and convection because it does not need the existence of the interfering surroundings. Also, radiation mode is the fastest mode due to the speed of light and it does not weaken in a vacuum. Thermal radiation refers to radiation energy that bodies emit because of their own temperature. All bodies above absolute zero emit radiation. Radiation is treated as electromagnetic waves, just like radio or sound waves. Radiation is defined as a volumetric phenomenon, and all cases like solids, liquids, and gases emit, absorb or transfer radiation to different degrees [114]. The amount of heat transfer could be optimized by using a technique called Genetic Algorithms (GA). Genetic Algorithms (GA) are robust adaptive search techniques that mimic the idea of Darwinian evolution using rules of natural selection to investigate highly complex multidimensional problems. As a non-gradient-based optimization technique, the usage of GA is advantageous for this until a better fit is obtained for an application. The parameters that may be progressively altered by the operators of the GA maximize its fitness function. Using Genetic Algorithms technique is good as an example design application.

5.1.1. Single objective function

In this study, design parameters are constructed of two, large, thick steel plates divided by steel bars, and an insulation material filled between the steel plates with a temperature difference between the inner and outer surfaces. The amount of heat transfer rate through that design is initially optimized. An insulation material can be selected by collecting conventional insulation materials which have thermal conductivity ranged from minimum to maximum values. According to the three modes of heat transfer mentioned above, the convection of heat transfer does not apply for this design because there is no liquid or gas reacting with the solid surfaces. Radiative heat transfer does not occur because there is no

source to emit thermal radiation. Therefore, heat transfer conduction will be applied in this design because it has solid surfaces with an insulation material between the steel plates with the temperature difference between inner and outer surfaces.

The first step to optimize this design begins by selecting an insulation material. Air is selected as a material to keep between the two large plate. The thermal conductivity of air is 0.025 W/m.K [146]. Air is also considered as a good conductor. Therefore, the rate of heat transfer will not be optimized because an insulation material should be filled in the design. The other idea is to fill the remain spaces with a powder insulation material, which can be manufactured as biomass-reinforced composites known for low thermal conductivity, or manufacturing matrix suited with design dimensions like calcium silicate insulation ($CaSiO_3$) [182]. Numerical optimization framework of a design has been performed based on Genetic Algorithms (GA) to systematically alter geometric parameters with the goal of maximizing the insulation capacity of a set design (single objective thermal optimization) (minimizing heat transfer) within a design space that includes several parameters such steel width, steel height, insulation width, insulation height, and thermal conductivity of an insulation material.

5.1.2. Multi-objective function

In recent years, the temperature of global warming has raised by 1-2 °C with continued irritation from the greenhouse influence [183]. Multiple studies have illuminated this subject worldwide [184]. Based on the statistics from the International Energy Agency, carbon dioxide emissions produced from electrical and heat energies reached 40 percent in 2014 [185].

Carbon footprint can be classified into two groups: embodied in building materials including the manufacture, transport, and insulation of construction materials, and operations containing building energy consumption, as shown in Figure 62.

Figure 62: Embodied and operational carbon footprint [186].

Improving clean energy resources is essential key to achieve sustainability [187]. The International Energy Agency has proposed reducing renewable resources to 65 percent of the world's overall energy source by 2050 [188]. Carbon dioxide gas is one of the toxic gases released into the atmosphere, helping create the greenhouse effect and boosting global warming [189]. Climate change is a main environmental crisis which threatens the world economy and could lead to international conflict s along with its detrimental effect on society [190]. Multiple countries have signed the Kyoto Protocol of 1997, committing to decreasing greenhouse gases to overcome climate change [191]. A second agreement was later signed in Paris as the global response to climate change. The target is to hold the increase in global temperature below 2 °C [192]. Efforts are being made to measure the "carbon footprint," which reflects direct and indirect emissions of greenhouse gases on any

level. These gases can be created by activity of human or be accumulated across the life cycle of the product [193]. The carbon footprint can be detected directly through the power plant operation, and at non-operational levels of the life cycle. Fossil-fueled techniques like oil, gas, and coal leave a large carbon footprint. Techniques with non-fossil fuel as biomass, solar, wind, nuclear, hydro, and wave/tidal are known as low carbon while they do not produce carbon dioxide during their operation [194].

Researchers looking for an optimal solution to climate change problems are exploring the value of countering one objective or multi-objective functions. Problems that possess more than one objective are represented as multi-objective optimization. These kinds of problems are found in many fields like mathematics, engineering, economics, agriculture, and automobile. There are several methods to create multi-objective optimization like Pareto and scalarization. In Pareto Front technique, there are two solutions like dominated solutions and non-dominated solutions that can be attained by the continuously updated algorithms [195]. Therefore, multi-objective optimization entailing maximizing insulation (minimizing heat transfer) and simultaneously maximizing sustainability (minimizing the carbon footprint) of a designed insulation structure will be performed by using a numerical technique like Genetic Algorithms (GA) with multi-objective optimization way such as Pareto Front Optimization.

5.2. Review of the Relevant Literature

Several studies have been performed to use multi-objective optimization by using Genetic Algorithms GA which use the way of optimization modelling.

5.2.2. Single Objective Optimization

Divo et al (2015) addressed transient multi-dimensional heat conduction problems in both composite and heterogeneous media by using a computational technique based on the localized radial-basis function (RBF) collection (LRC) meshless way merged with a volume-of-fluid scheme. While the localized radial collection meshless methods drive inherent benefits of spectral convergence and plain of automation, the volume-of-fluid scheme provides one to simulate efficiently and effectively the location, size, and shape of cavities, voids, or detachments in the conducting media without the need to regenerate point distributions, boundaries, or interpolation matrices. An optimization code relied on the genetic algorithms method (GA) will lead the LRC-VoF meshless algorithms. GA can efficiently search for the optimal group of design parameters (location, size, shape, etc.) within a predefined design space. The proposed method permitted solving the arduous computational inverse geometric problem in a very efficient and robust manner while allowing its performance in modest computational platforms. Thus, realizing the disruptive potential of the proposed multidimensional high-fidelity nondestructive evaluation (NDE) technique [196]. Akpinar (2019) used Genetic Algorithms to solve heat transfer problems of insulation material selection and the determination of laminar boundary layer thickness. His aim is to evaluate the optimal parameters by performing GA. The first case of his work involved the thickness of insulation material selection and the maximum value of heat loss

that can be affected by various thicknesses of the insulating material with respecting the boundary conditions and assumptions. GA can be applied to find the thickness or the outer temperature of the insulation material. The second case of that study was to determine the boundary layer thickness for airflow with a laminar flow, where the boundary layer parameters are constant, it is assumed as neglectable irradiation, and air and plate temperatures are constant in the continuous system on the plate. The results for both cases prove that Genetic Algorithms provide optimal goals as well as minimum and maximum values, Therefore, GA were applicable in heat transfer optimization problem [181].

5.2.3. Multi-objective Optimization

Zhang et al (2017) investigated the relationships between three factors: processing time, the consumption of power energy, and the carbon emissions from the milling process through dry milling steps. Energy consumption and carbon footprint emissions parameters were also examined. The functions such the minimum energy, maximum efficiency, and minimum carbon emissions were independently built. Then, the model of multi-objective optimization was created to record minimum energy, maximum efficiency, and minimum carbon emissions. The process was constructed to characterize the coefficients of the experimental model function with empirical data obtained through fundamental components and regression analyses. According to the procedure, the effective flow scheme followed constrains from machine tool performance and machining quality to an the optimum model utilizing Genetic Algorithms. The optimal analysis and cutting constrains program were beneficial to the optimum implementation of the machine equipment with the cutter and used to seek sustainable industrialization [197]. The goals of the multi-objective optimization of the multi-passes cylindrical tuning presented by

Perdomo et al (2019) included economic, environmental, and social aspects to maximize sustainability. The initial aspect is the cost followed by environmental effects like carbon dioxide emission. The other is the social sustainability, such as operational safety. Furthermore, the constrains resultant from the technical impacts of the turning procedure were considered. For this purpose, the optimization process applied is a Pareto Front technique, which is used to identify the most convenient solution relied on the certain conditions. The non-sorting genetic algorithm was applied, and the most important achievement of this study was the utilization of a tridimensional Pareto Front to choose the best cutting situations while taking into consideration the three pillars of the sustainability [198]. In addition, multi-objective optimization of a suggested multi-generation cycle like powder, heating/cooling, and desalination was introduced by Anvari et al (2021). The optimization was implemented by using Genetic Algorithms (GA) and choosing 10 design constrains with two objective functions. The purpose of the optimization was to detect the design variables relied on Pareto diagrams such as performance enhancement, cost decrease, and carbon dioxide emissions that will raise the exergy effectiveness since decreasing cost and carbon dioxide emissions. Objective functions optimization can be introduced by scatter charts of the decision parameters for the population. Optimum amount of the objective functions can be determined by choosing lower amounts of the heat exchanger and evaporator's pinch-point temperature variances and higher amounts for the compressor pressure ratio, inlet temperature of the gas turbine, isentropic effectiveness of gas turbine and air compressor, and Rankine cycle evaporator temperature [199]. Limleamthong et al (2017) also studied the three aspects of sustainable systems simultaneously -- economic, environmental and social factors. The model of a multi-

objective optimization is presented by using a group of points of Pareto front, and these points display the property of enhancing the multi-objective functions simultaneously. The researchers proposed the first rigorous technique that relied on bilevel optimization to detect Pareto points. That technique permits distinguishing in a systematic approach non-dominated solutions that are especially attractive for decision-makers, and also computing the space between any sensible point of a multi-objective optimization model and its Pareto front. Finally, the study sought to determine enhancement goals for suboptimal results of a multi-objective optimization that would be optimum if they were attained. Their method analyzed Pareto fronts and chose a final point of Pareto front to be performed practically without needing to identify private weights in an obvious way. Their methodology was applied across the United Kingdom electricity combine and was based on economic, environmental, and social aspects [200].

5.3. Methodology

Genetic Algorithms

5.3.1   Genetic Algorithms

The minimization of the objective function $\dot{Q}(t)$ in equation (8) to optimize the heat transfer rate may be achieved by a non-gradient based technique like the Genetic Algorithms (GA) [201]. Genetic Algorithms is a powerful non-conventional optimization method in which the set of algorithms imitates the evolution procedure. This approach to biological systems can be implemented in engineering optimization [202]. GA are robust adaptive search techniques that mimic the idea of Darwinian evolution using rules of natural selection to investigate highly complex multidimensional problems. As a non-gradient-based optimization technique, the usage of GA is advantageous for this until a best-fit is found for that application. The parameters may be progressively adjusted by the operators of the GA to maximize a fitness function. This fitness function can be directly and simply defined as the following:

$$R = \frac{L}{kA} \qquad (12)$$

 The GA optimization process starts by setting a random set of possible solutions, called the population, with number of individuals or a fixed initial size. Each individual is defined by optimization parameters and is represented as a chromosome or a bit string, as shown in Figure 63. An objective function, Z_{GA}, is estimated for every individual in the present population, defining their fitness or their probability of survival. At every iteration of the GA, the updating the population of designs is processed through selection, 26 cross-over, and mutation operators. A selection operator is first applied to the population in order to

determine and choose the individuals who are going to pass information in a mating process with the rest of the individuals in the population. This mating process is called the crossover operator, and it allows the genetic information contained in the best individuals to be combined to form offspring. Furthermore, the information obtained by the mating of individuals is affected randomly by a mutation operator. This is a crucial step for continuous improvement.
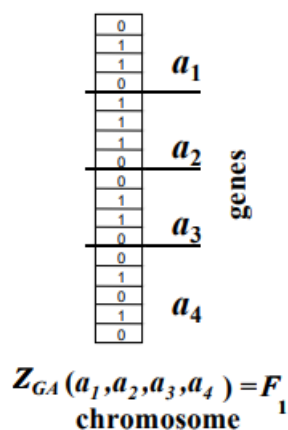
Figure 63: Example of an individual in the population characterized by four parameters (genes) encoded in a chromosome yielding the individual's fitness value F1.

A series of parameters are initially set in the GA code, and the performance of the genetic optimization process is determined and affected by these parameters. Parameters that control the optimization process varies, including the size of the bit string or chromosome that defines each individual, the number of individuals or population size per generation, the number of children from each mating, the probability of crossover, and the probability of mutation. This set of operations is carried out generation after generation until either a convergence criterion (a preset level of acceptable fitness) is satisfied or a maximum number of generations is reached. Also, it is important to refer that three significant features

characterize GA from the others evolutionary algorithms, namely: (1) binary representation of the solution, (2) the proportional method of selection, and (3) mutation and crossover as primary methods of generating variations.

In nature, the properties of an organism are characterized by a string of genes in the chromosomes. Therefore, if scientists are trying to simulate nature using computers, they must encode the design variable in a convenient approach. A haploid model is adopted using a binary vector to model a single chromosome. The length of the vector is dictated by the number of design variables and the required precision of each design variable. Each design variable has to be bounded with a minimum and a maximum value. In the process, the precision of the variable is determined. The number of divisions used in the discretization has to be integer power of two. This procedure allows an easy mapping from real numbers to binary strings and vice versa. This coding process represented by a binary string is one of the distinguishing features of GA and differentiates it from other evolutionary approaches. The haploid GA places all design variables into one binary string, called a chromosome or off-spring. The information contained in the string of vectors comprising the chromosome characterizes an individual in a population. In turn, each individual is equipped with a given set of design variables that corresponds to a value of the objective function. This value is the measure of "fitness" of the individual design. In GA, poorly fit designs are not discarded. Instead, they are kept, as in nature, to provide genetic diversity in the evolution of the population. This genetic diversity is required to provide forward movement of the population during the mating, cross-over, and mutation processes that characterize the GA.

The initial population size may grow or diminish to mimic actual biological systems. However, in the GA used here, the population size is not allowed to change while the program is running. Once the population size is fixed, the algorithm initializes all of the chromosomes. This operation is carried out by assigning a random value of 0 or 1 for each bit contained in each of the chromosomes. After initializing the population, evaluation of the fitness of each individual is performed by computing the objective (or fitness) which represents a set of possible solutions. Having the values of the objective function for each individual, the selection process can be started. First values of the fitness function for each individual have to be added, and then the probability of being a selected individual is calculated as the ratio between the value of the fitness function of each individual and the sum of all objectives function values. This is given by:

$$P_{selected_i} = \frac{Z(z_i)}{\sum_{i=1}^{pop-size} Z(z_i)} \qquad (13)$$

Where z_i is the ith member of the population, and $Z(z_i)$ is the measure of the fitness of that member under its currently evolved parameter set configuration. A weighted roulette wheel is generated, where each member of the current population is assigned a portion of the wheel in proportion to its probability of selection. The wheel is spun as many times as there are individuals in the population to select which members mate. Obviously, some chromosomes would be selected more than once. The best chromosomes get more copies, the average stay even, and the worst die off. Once selection has been applied, cross-over and mutation occur to the surviving individuals. These operations further expand genetic diversity in the current population. All other probabilities referred to in the description of

the GA adopted in this research are computed in an analogous fashion as the selection probability.

The probability of crossover P_c is a critical parameter that defines the expected population size of chromosomes undergoing crossover operation. This is a mating process that allows individuals to interchange intrinsic information contained in the chromosomes. The operation might be performed in two steps: (1) a random selection based on the probability of crossover is implemented to gain pairs of individuals, and (2) a random number is created between the first position of the binary vector and the last one to point out the location of the crossing point that delineates the location about which genetic information is interchanged between two chromosomes.

The mutation operator is the final operator performed. The probability of mutation P_m provides the expected number of mutated bits and every bit in all chromosomes in the whole population has an equal chance to undergo mutation: switch of a bit from 0 to 1 or vice-versa. This process is executed by creating a random number within the range (0...1) for each bit within the chromosome. If the generated number is smaller than P_m the bit is mutated. When the mutation is done on a bit-by-bit basis is called the creep mutation. Another kind of mutation is the jump mutation which is used to an individual selected to be mutated from this perspective. In this case all bits within the chromosome are switched from 0 to 1 and vice-versa. Following selection, crossover and mutation the new population is ready for its next evolution until the convergence criteria "fitness" is reached. It is the very nature of the binary representation of the design variables of the objective function and the random search process which provide yet another but implicit degree of regularization in this optimization process. The sensitivity of the objective function can be

tuned depending on the size of each element of the chromosome. Thus, low bit representation is insensitive to large variations in input (regularized but may lead to poor solution due to low resolution), while high bit representation is sensitive to large variations in input (not regularized and therefore may lead to poor solution as well). There is a range of bit size which produces a regularized and sensitive response leading to stable solutions. In the GA employed in this research, the following parameters are chosen: population size of *150* individuals per generation, with strings of *8* bits for the x and y location of the anchored grid pattern as well as for the *8* rays of the pattern. The mating process generates one offspring per mating using uniform crossover which creates a higher level of diversity than single point crossover, a *4%* probability of jump mutation, *20%* probability of creep mutation, and *50%* probability of crossover. The population is not permitted to develop (static population) and elitist generation (the best parent survives to the next generation). The population is totally eliminated after *100* generations if there is no further enhancement, maintaining the best member of the population (restart). This combination of GA parameters has been indicated to provide robust results in heat transfer optimization [205].

5.3.2. Direct Problem Solution

A design is constructed of two large 2-cm-thick steel plates ($k =15\ W/m.°C$) separated by 1-cm-thick and 20-cm wide steel bars placed 99 cm apart as shown in Figure 64. The remaining space between the steel plates is filled with an insulation material. If the temperature difference between the inner and the outer surfaces of the design is *22 °C*. The rate of heat transfer through the following design should be determined and optimized.

Steel plates

Insulation material

99 cm

1 cm

2 cm
20 cm
2 cm
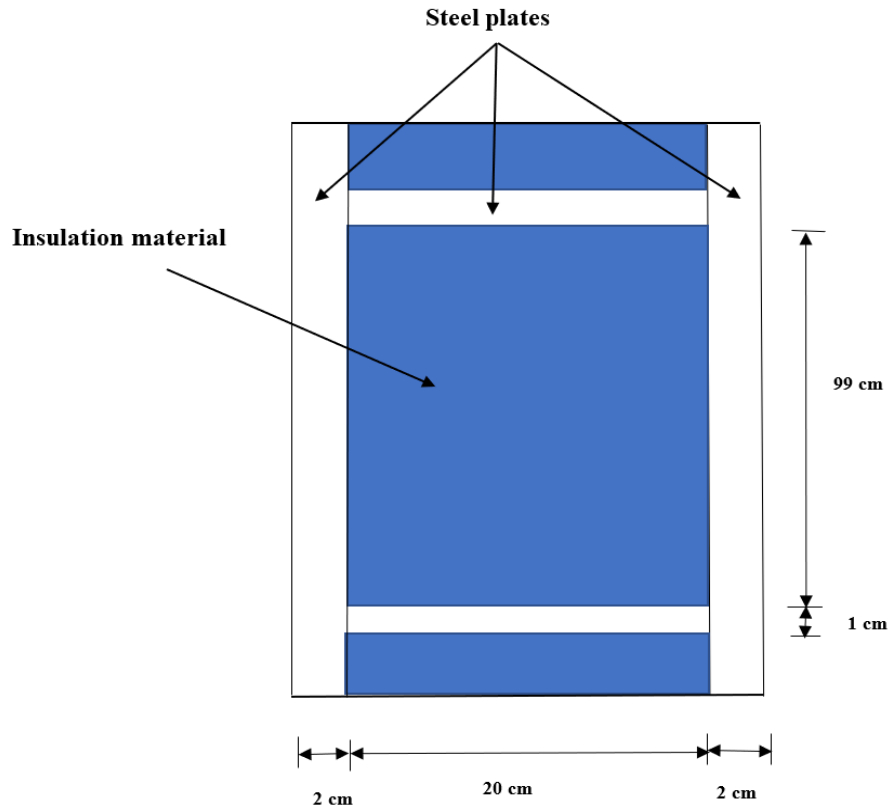
Figure 64: Design parameters with an insulation material

The assumptions for this direct problem are the followings: Heat transfer is steady since there is no indication of change with time, heat transfer through the design can be approximated to be one-dimensional, and the surfaces of this design are maintained at constant temperatures. The thermal conductivities are given to be $k=15$ $W/m.°C$ for steel plates.

The direct method could be solved theoretically if the insulation material has been chosen. For example, the thermal conductivity of fiberglass insulation (k) is 0.035 W/m.K. The theoretical solution is the following:

$$\dot{Q} = \frac{\Delta T}{R_{total}} \qquad (8)$$

Where: $\dot{Q}$ = Heat transfer rate (W)

ΔT = Temperature difference in (ºC)

$$R = \frac{L}{kA} \qquad (12)$$

Where: R = Thermal resistance $(°C/W)$

L = Length (m)

A = Cross-sectional area (m²)

$$R_1 = R_4 = R_{steel} = \frac{L}{kA} = \frac{0.02\ m}{(15\ W/m.°C)(1*1)m^2} = 0.00133\ °C/W$$

$$R_2 = R_{steel} = \frac{L}{kA} = \frac{0.20\ m}{(15\ W/m.°C)(0.01*1)m^2} = 1.33333\ °C/W$$

$$R_3 = R_{insulation} = \frac{L}{kA} = \frac{0.20\ m}{(0.035\ W/m.°C)(0.99*1)m^2} = 5.77201\ °C/W$$

$$\frac{1}{R_{equ.}} = \frac{1}{R_2} + \frac{1}{R_3} = \frac{1}{1.33333} + \frac{1}{5.77201}$$

$$R_{equ.} = 1.08313\ °C/W$$

$$R_{total} = R_1 + R_{equ.} + R_4 = 0.00133 + 1.08313 + 0.00133 = 1.0858\ °C/W$$

The rate of heat transfer per m² surface area of the design is

$$\dot{Q} = \frac{\Delta T}{R_{total}} = \frac{22\,°C}{1.0858\,°C/W} = 20.26\,W$$

5.3.3. Types of optimizations

a) Single-objective optimization

Single objective thermal optimization has been performed to arrive at a design by using Genetic Algorithms to maximize insulation (minimize heat transfer) within a design space that includes several parameters: steel width (w_s), steel height (h_s), insulation width (w_i), insulation height (h_i), and thermal conductivity of an insulation material (k_i). Figure 65 shows design parameters with an insulation material. Therefore, this method used the same design, and it will be solved numerically by using single thermal objective optimization.
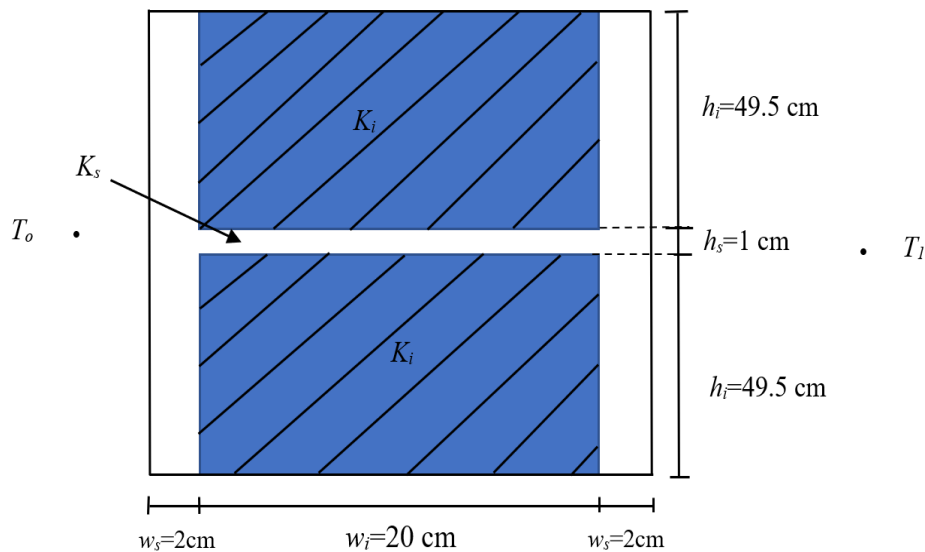
Figure 65: Parameters of the design.

The design constrains are the following:

$$2w_s + w_i = 24\,cm \qquad\qquad (13)$$

$$h_s + 2h_i = 100 \; cm \hspace{3cm} (14)$$

The parameters constrains used in Genetic Algorithm implimentation are determined in Table 32.

Table 32: Parameter's constrains

Design space	Minimum value	Maximum value
Steel width (w_s)	1 cm	4 cm
Insulation material width (w_i)	16 cm	22 cm
Steel height (h_s)	0.5 cm	4 cm
Insulation material height (h_i)	48 cm	49.75 cm
Thermal conductivity of the insulation material (K_i)	0.007 W/m.K	0.1 W/m.K

The values of thermal conductivity of insulation materials are collected for different traditional insulation materials based on the constrains for minimum value (0.007 W/m.K) and maximum value (0.1 W/m.K) as shown in Table 33.

Table 33: Some insulation materials as sandwich.

No	Insulation material	k (W/m.ºC)	reference
1	Silicone rubber (Glass fiber filled)	0.35 W/m.ºC	[172]
2	Polyurethane rubber	0.29 W/m.ºC	[172]
3	Nitrile rubber (NBR)	0.24 W/m.ºC	[172]
4	Plaster board (Gyproc Fireline) (single)(double)	0.24 W/m.ºC	[171]
5	Plaster board (Gyproc Wallboard) (single)(double)	0.19 W/m.ºC	[171]

6	Fluoroelastomer	0.19 W/m.°C	[172]
7	Neoprene rubber (Polychloroprene)	0.19 W/m.°C	[172]
8	Silicone rubber	0.14 W/m.°C	[172]
9	Wood shavings	0.09 W/m.°C	[204]
10	Butyl rubber (IIR)	0.09 W/m.°C	[172]
11	Wood barks	0.061 W/m.°C	[204]
12	RCF fibers-Pyro-Bloc	0.06 W/m.°C	[205]
13	Superwool- AES fibers-Pyro-Bloc	0.06 W/m.°C	[205]
14	Glass foam	0.052 W/m.°C	[204]
15	Blok Superwool	0.05 W/m.°C	[205]
16	Cork boards	0.04 W/m.°C	[204]
17	Phenol foam	0.04 W/m.°C	[204]
18	Rock wool	0.04 W/m.°C	[204]
19	Cork	0.035 W/m.°C	[206]
20	Polyurethane	0.035 W/m.°C	[204]
21	Mineral Wool	0.035 W/m.°C	[175]
22	Fiberglass	0.035 W/m.°C	[114]
23	Expanded Polystyrene (EPS)	0.030 W/m.°C	[168]
24	XPS (extruded polystyrene)	0.029 W/m.°C	[169]
25	Fire Master	0.026 W/m.°C	[205]
26	Extruded Polystyrene (XPS)	0.025 W/m.°C	[207]
27	Polyurethane foam (PU)	0.024 W/m.°C	[208]

28	WDS Lambda Flex	0.024 W/m.°C	[205]
29	Polyisocyanurate (PIR)	0.022 W/m.°C	[169]
30	WDS Rigid Board	0.022 W/m.°C	[205]
31	WDS Flexible	0.020 W/m.°C	[205]
32	Phenolic foam	0.018 W/m.°C	[224]
33	Kooltherm	0.018 W/m.°C	[169]
34	Natural rubber (Unvulcanized)	0.01 W/m.°C	[172]
35	Kingspan OPTIM-R	0.007 W/m.°C	[169]

a) Multi-objective Optimization

A multi-objective optimization needs the simultaneous satisfaction of number of different and often conflicting objectives. These objectives are characterized by specified measures of performance that may be dependent and/or incommensurable.

After performing numerical optimization framework based on Genetic Algorithms (GA) which is discussed to systematically alter geometric parameters with the goal of maximizing the insulation capacity of a set design (single objective thermal optimization) (minimizing heat transfer) within a design space that includes several parameters: w_s, h_s, w_i, h_i, and k_i.

A Pareto Front Optimization Multi-objective will be used to perform optimization entailing maximizing insulation (minimizing heat transfer) and simultaneously maximizing sustainability (minimizing carbon footprint) of a predesigned insulation structure.

The two resulting nonlinear competing objective functions will be maximized by means of evolutionary optimization techniques within a predefined design space. The multi-

objective optimization is achieved by building a Pareto Front and determining the points of best compromise between the two objectives.

To apply the multi-objective optimization, the design has two objective functions. The first objective function is represented by thermal objective function with the same predesign with five constrains of the design spaces. The second objective function is represented by minimizing carbon footprint to maximizing the sustainability with constrain of carbon dioxide gas emissions. The design was performed by using GA with a Pareto front optimization by using the two objective functions, the objective thermal and the carbon footprint objective functions. The Pareto front optimization technique does not contain multiple criteria using weights. The Pareto front method presents optimal solutions for each criterion.

Table 34 contains the values of the thermal conductivity and the carbon footprint estimations of conventional insulation materials.

Table 34: Carbon footprint estimations and thermal conductivity of traditional insulation materials.

No.	Insulation materials	Carbon footprint (kgCO$_2$/kg)	Thermal conductivity W/m.K	References
1	Nitrile rubber (NBR)	5.90 kgCO$_2$/kg		[235]
	HNBR		k=0.2317 W/m.K	[236]
2	Plaster board (Gyproc	2.15 X 10^{-1}		[209]
	Fireline) (single)(double)	kgCO$_2$/kg	k=0.24 W/m.K	[171]
3	Neoprene rubber	1.6 – 1.8 (kgCO$_2$/kg)		[210]
	(Polychloroprene)		k=0.19 W/m.K	[172]
4	Silicone	2.67 kg CO$_2$/kg		[211]

			k=0.024 W/mK	[212]
5	Wood	1.65 to 1.8 kgCO$_2$/kg		[213]
			k= 0.1-0.2 W/mK	[214]
6	Butyl rubber (IIR)	1.577 kgCO$_2$/kg		[215]
			k=0.19 W/m.K	[172]
7	Glass foam	1.565 KgCO$_2$/kg		[216]
			k=0.052 W/m.K	[204]
8	Cork boards	0.17 kgCO$_2$/kg	k= 0.0392 W/m·K	[233]
9	Phenol foam	2.98 (kg CO$_2$/kg)		[217]
			k=0.04 W/m.K	[172]
10	Rock wool	1.12 (kg CO$_2$/kg)		[217]
			k=0.04 W/m.K	[172]
11	Fiberglass	1.54 kgCO$_2$/kg		[217]
			k=0.04 W/m.K	[234]
12	Cork	1.156 kgCO$_2$/kg		[216]
			k=0.035-0.043 W/m.K	[206]
13	Polyurethane	4.307 kgCO$_2$/kg		[216]
			k=0.035 W/m.K	[217]
14	Mineral Wool	1.16 kgCO$_2$/kg	k= 0.039 W/m.K	[218]
15	Sheep wool	1.8 kg CO$_2$/kg		[219]
			k=0.038-0.054 W/m.K	[220]
16	Expanded Polystyrene (EPS)	3.51 kgCO$_2$/kg	k=0.036 W/m.K	[218]
17	Extruded polystyrene (XPS)	3.83 kgCO$_2$/kg	k= 0.035 W/m.K	[218]
18	Flexible Polyurethane foam (PU)	0.43 kg CO$_2$/kg		[221] [208]

		k=0.022-0.028 W/m.K		
19	Polyisocyanurate (PIR)	1.32 kg CO_2/kg		[222]
		k= 0.0236 W/m·K	[182]	
20	Phenolic foam	7.021 kgCO_2/kg		[223]
		k=0.018-0.023 W/m.K	[224]	
21	Kooltherm	3.74 kgCO_2/kg		[225]
		k=0.019 W/m.K	[226]	
22	Natural rubber	3.34 kg CO_2/ kg		[227]
		k=0.01 W/m.K	[172]	
23	Calcium silicate	0.158 kgCO_2/kg		[228]
		k= 0.084-0.173 W/mK	[229]	
24	Cellulose fiber	0.704 kgCO_2/kg		[230]
		k= 0.04 W/m.K	[231]	
25	Vacuum Insulation Panels (VIP)	0.99 kgCO_2/kg		[232]
		k=0.003 W/m.K	[231]	

Table 35: Parameter's constrains of multi-objective functions

Design space	Minimum value	Maximum value
Steel width (w_s)	1 cm	4 cm
Insulation material width (w_i)	16 cm	22 cm
Steel height (h_s)	0.5 cm	4 cm
Insulation material height (h_i)	48 cm	49.75 cm
Thermal conductivity of the insulation material (K_i)	0.003 W/m.K	0.24 W/m.K
Carbon dioxide gas emissions	0.15 KgCO_2/Kg	6.0 KgCO_2/Kg

5.4. Results and Discussions

5.4.1. Single Objective Optimization Result

Maximizing the fitness function (R_{total}) is achieved by executing Genetic Algorithms (GA), which is setup to run 100 generations with 150 individuals per generation and 8-bits per design variable. This problem is steady state since there is no indication of change with time. The design variables like steel width (w_s), steel height (h_s), an insulation material width (w_i), the insulation material height (h_i), and the thermal conductivity of the insulation material (k_i) that exemplify the rate of heat transfer are modified by Genetic Algorithms operators until the maximum number of fitness is attained. Figure 66 indicates evolution of Genetic Algorithims fitness function (R_{total}) with 100 generations.
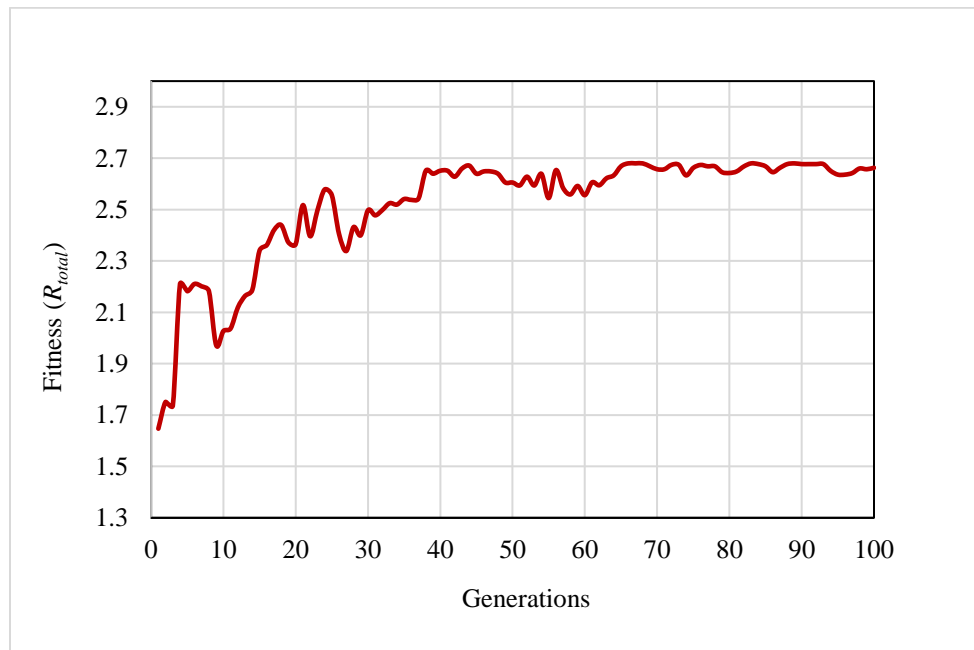
Figure 66: Evolution of GA fitness function

The Genetic Algorithms (GA) was implemented to adjust the design variables (w_s, h_s, w_i, h_i, and k_i). These variables were yielded steel width (w_s=0.010235 m), steel height (h_s=0.005 m), the width of the insulation material (w_i=0.219529 m), the height of the insulation material (h_i=0.4975 m), and the thermal conductivity of the insulation (k_i=0.007 W/m.°C) as shown in Figure 67. According to the value of the thermal conductivity of the insulation material found, this value indicates to Kingspan OPTIM-R as the insulation material which is used to fill the remaining area between the steel plates [226]. Therefore, the maximum fitness (the total thermal resistance (R_{total})) produced by GA is 2.6797 °C/W. The minimum objective function ($\dot{Q}_t$) was obtained by applying equation (4) and it was 8.209 W, and this value is considered as the minimum amount of heat transferred through the design.

K_i=0.007 W/m.°C

h_i=49.75 cm

T_o

h_s=0.5 cm

T_l

K_s=15 W/m.°C

h_i=49.75 cm

w_s=1.023cm w_i=21.95 cm w_s=1.023cm
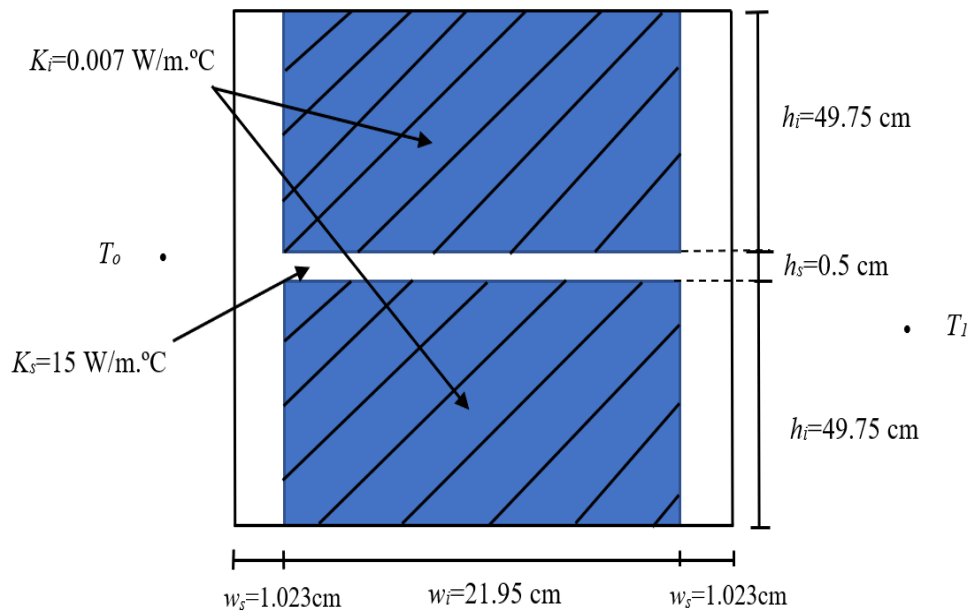
Figure 67: Design Parameters altered by GA

Table 36: Optimized values of the design space

Design space	Optimized values
Steel width (w_s)	0.010235 m
Insulation material width (w_i)	0.219529 m
Steel height (h_s)	0.005 m
Insulation material height (h_i)	0.4975 m
Thermal conductivity of the insulation material (K_i)	0.007 W/m.K

5.4.2. Multi-Objective Optimization Result

The effects of thermal design parameters as well as carbon footprint parameters on the Pareto front optimization based on Genetic Algorithms are estimated utilizing the developed program code. The design was implemented again using Genetic Algorithms for single objective optimization with 100 generations with 150 individuals per generation and 8-bits per design variable based. Also, the thermal conductivity constrains were provided and based on carbon dioxide gases emissions measured by some studies as shown in Table 31. However, there are not enough details provided on carbon footprint calculations of insulation materials. Therefore, the thermal conductivity values are collected with other constrain related to the carbon dioxide emissions.

Figure 68 illustrates that the minimum value of fitness function (minimum total thermal resistance) of the single objective optimization was 0.4944 °C/W, and the maximum value of fitness function (maximum total thermal resistance) was 2.6856 °C/W.
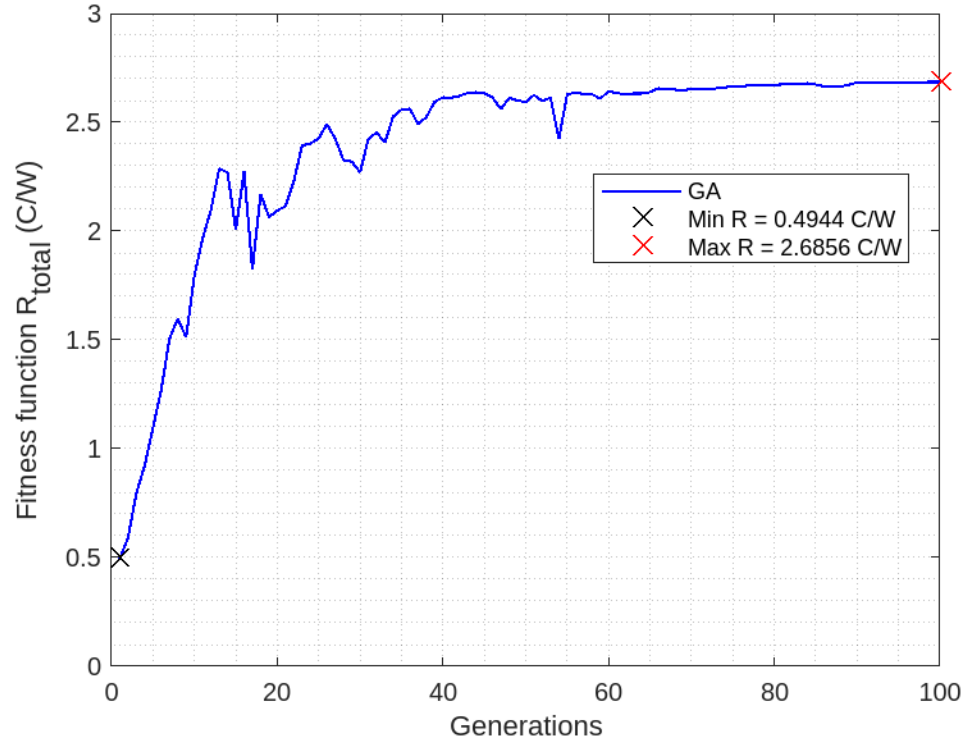
Figure 68: Evolution of GA fitness function with minimum total thermal resistance

Based on the equation (8), the maximum and minimum values of heat transfer rate (W) are shown in Figure 69. The maximum value of heat transfer rate of the single thermal objective optimization was 44.495 W, and the minimum value of $\dot{Q}_t$ was 8.192 W, which is considered as an optimum value.
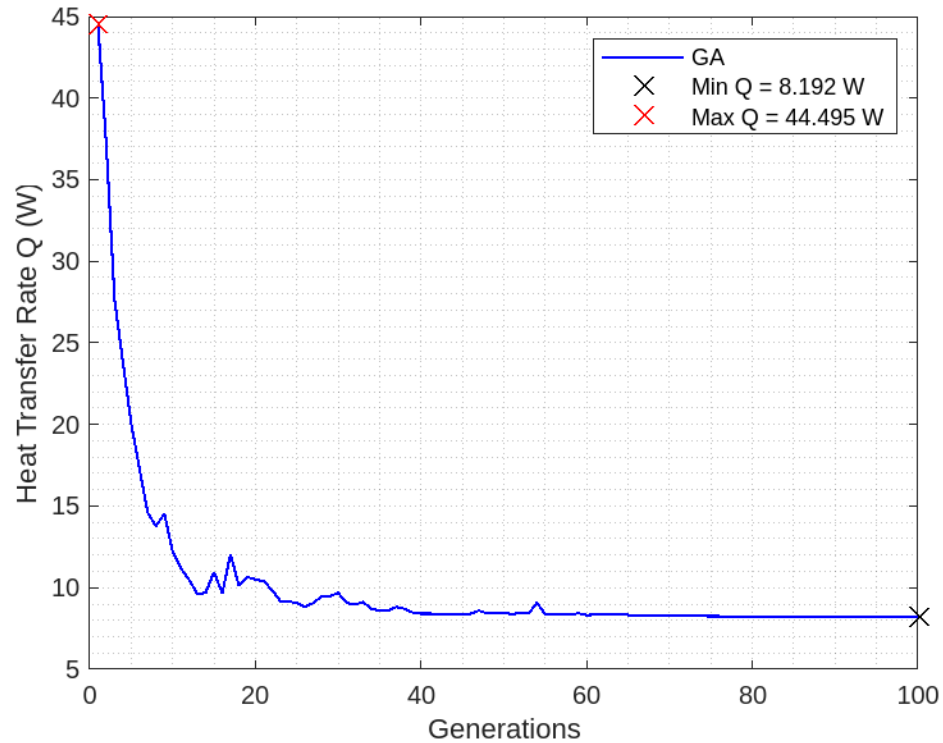
Figure 69: Evolution of GA heat transfer rate

After implementing the thermal objective optimization, the multi-objective optimization was also performed in the same number of generations with 150 individuals using 8 bits of design variables. The carbon footprint estimations were collected based on some studies which have measured carbon dioxide gas emissions based on $kgCO_2$ per kg of industrial insulation material as indicated on Table 34. Pareto front optimization has been executed with constrains of thermal objective function of the same predesign such as w_i, w_s, h_i, and h_s with the values of (k_i) as shown in Table 34 . The other objective function is represented by the constrains of carbon dioxide gas emissions of conventional insulation materials that range from 0.15 to 6.0 $KgCO_2/Kg$. Pareto front optimization was implemented by entailing minimizing heat transfer rate and minimizing carbon footprint of that designed insulation structure. This optimization solution results reflect a compromise between the two

objective functions, and this process is implemented to formulate the function to accomplish this required compromise. Pareto verified that it is impossible to get a better solution for the two objective functions, but it finds a group of solutions that are called non-dominated solutions or Pareto solutions.

The population is classified in fronts, and each individual takes a sign of the front where it exists. After that, all individuals are compared, and dominated ones are chosen as an optimal solution. [238].
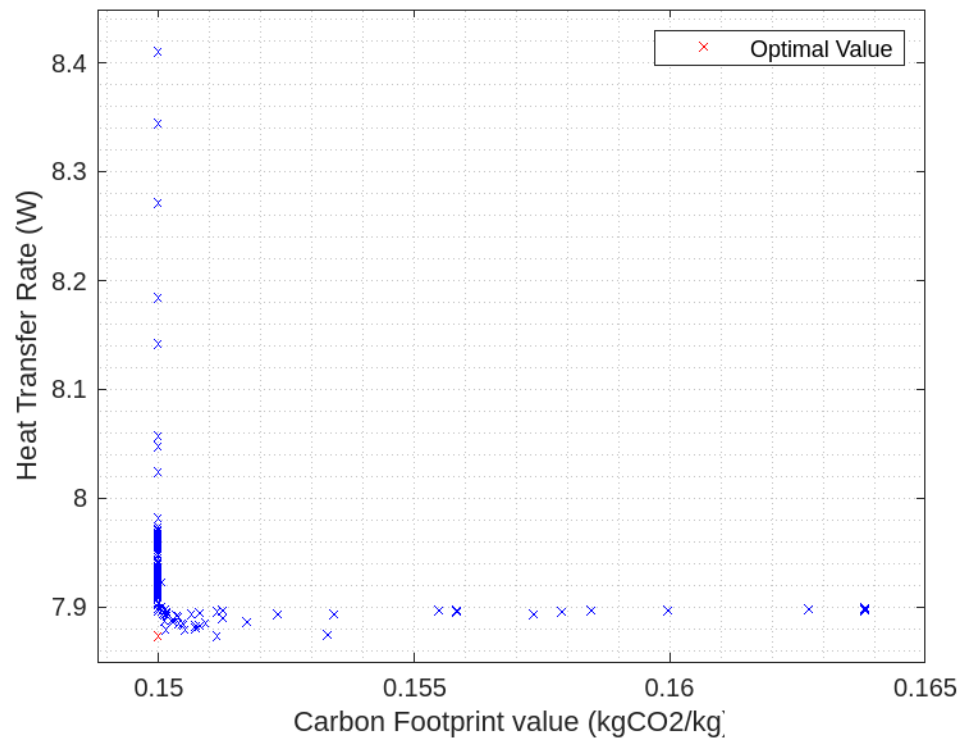
Figure 70: Pareto front optimization of minimizing heat transfer rate and minimizing carbon footprint.

In this evolutionary method, it should find a set of points first before making any decision.

So, the range of points have been optimized. Then, the point can be chosen.

The first goal of optimization algorithms is to have algorithm convergence for Pareto front optimization. For example, a set of points is considered a very good distribution, but none of these points is close to the Pareto front because none of them are close to being optimum. The set of points should have to get a good convergence and a good diversity. The closest value of these points to the origin point is considered the optimum value. The two resulting nonlinear competing objective functions were maximized by means of evolutionary optimization techniques within a predefined design space. The multi-objective optimization was achieved by building a Pareto Front and determining the points of best compromise between the two objectives as shown in Figure 70.

Therefore, all points are considered as the optimum solution, and the closest point to the origin determined of the nonlinear competing objective functions is (0.15, 7.872). The heat transfer rate was 7.872 W, and from this value, the total thermal resistance became 2.8252 W/˚C. Any constrains are presented in Table 37.

Table 37: Optimized values of the design space with carbon footprint

Design space	Optimized values
Steel width (w_s)	0.010235 m
Insulation material width (w_i)	0.219529 m
Steel height (h_s)	0.005 m
Insulation material height (h_i)	0.4975 m
Thermal conductivity of the insulation material (k_i)	0.003 W/m.K
Carbon footprint estimation	0.15 kgCO$_2$/kg

According the results and based on Table 37, cork board or vacuum insulation panels could be used in the design to gain the optimum result.

6. Summery

In this section, the following tables contain the maximum and minimum values of biomass characteristics, properties of biomass reinforced composites, and optimization of thermal insulation and carbon footprint with their limitations.

Table 38 summarizes the minimum and maximum values of physical properties limitations with their results

Table 38: Summarize of minimum and maximum values of properties limitations

No.	Property	Minimum value	Maximum value	Details
1	Moisture content	7.13 % (barley grain powder)	11.83 % (jute)	It should not be exceeded than 15% [237]
2	Particle Size Distribution (dp)	381 μm $< dp <$660.4 μm (barley grain powder)	$1500 < dp < 2500$ μm (jute)	$53.3 < dp < 4749.8$
3	Bulk density (ρ)	0.106 g/cm^3 (jute)	0.647 g/cm^3 (finest powder)	
4	Angle of repose (α)	24.35° (oak leaf powder)	34.94 ° (straw powder)	$20 < \alpha < 40$ [102]
	Flowability	Excellent flow (oak leaf powder)	Moderate flow (straw powder)	
5	Static coefficient of friction (μ)	0.4536 (jute against aluminum surface)	1.1115 (barley grain against plywood surface)	μ is more than one for powder.

Table 39 summarizes the minimum and maximum values of biomass reinforced composites limitations with their results.

Table 39: Minimum and maximum values of experimental limitations

No.	Property	Minimum value	Maximum value	Details
1	Density of biomass reinforced composites (ρ)	BRY10% (0.636 g/cm^3)	STR10% (1.063 g/cm^3)	compared to the neat epoxy (1.152 g/cm^3)
2	Porosity of biomass reinforced composites (P)	STR10% (0.096)	BRY10% (0.452)	compared to the neat epoxy (0.006)
3	Thermal conductivity of biomass reinforced composites (k)	BRY20% (0.162 W/m.K)	STR10% (0.2423 W/m.K)	compared to the neat epoxy (0.292 W/m.K)

The original design has limitations as shown in Table 40

Table 40: Limitations of the original problem

Design space	Minimum value
Steel width (w_s)	2 cm
Insulation material width (w_i)	20 cm
Steel height (h_s)	1 cm
Insulation material height (h_i)	49.5 cm
Thermal conductivity of steel (k_i)	15 W/m.K
Temperature difference (ºC)	22 ºC

Table 41 summarizes the minimum and maximum values of design optimization limitations

Table 41: Minimum and maximum values of optimization limitations.

Design space	Minimum value	Maximum value	Optimized value
Steel width (w_s)	1 cm	4 cm	1.0235 cm
Insulation material width (w_i)	16 cm	22 cm	21.9529 cm
Steel height (h_s)	0.5 cm	4 cm	0.5 cm
Insulation material height (h_i)	48 cm	49.75 cm	49.75 cm
Thermal conductivity of the insulation material (k_i)	0.003 W/m.K	0.24 W/m.K	0.003 W/m.K
Carbon footprint ($KgCO_2/Kg$)	0.158 $KgCO_2/Kg$	8.10 $KgCO_2/Kg$	0.15 $kgCO_2/kg$

7. Conclusion

Characterization techniques of four kinds of biomass materials, barley grains, oak leaves, straw, and jute were discussed. Moisture content, particle size distribution, bulk density, microscopy, flowability, and static coefficient of friction resulted physical properties to characterize the behavior of each powder. The composite density, porosity, and the thermal conductivity were found to be decreased when biomass powders added to neat epoxy. Barley grain, oak leaf, straw and jute reinforced composites are demonstrated to be good potential insulation materials. A numerical optimization framework (single objective optimization) based on Genetic Algorithms (GA) was presented to alter systematically geometric parameters with the goal of maximizing the thermal insulation capacity of a set design. Multi-objective optimization entailing maximizing insulation (minimizing heat transfer) and simultaneously maximizing sustainability (minimizing carbon footprint) of a predesigned insulation structure was performed by using a Pareto Front Optimization. The two resulting nonlinear competing objective functions were maximized by means of evolutionary optimization techniques within a predefined design space. The multi-objective optimization was achieved by building a Pareto Front and determining the points of best compromise between the two objectives. Therefore, cork board or vacuum insulation panels could be used in the design to gain the optimum result.

8. Recommendations and Future Work

This study demonstrates that biomass reinforced composites can be naturally sustainable alternatives to conventional insulation materials by characterizing the physical properties of these biomass materials. The biomass materials chosen are manufactured with Epon resin 828 and Epikure Curing Agent 3140. However, bio-resin like biobased epoxy, ecopoxy, and eco-resin could be used as a future work with the hardener to make a bio-composite materials with different weight ratios of barley grain, oak leaf, straw, and jute to reach sustainability goals. Also, other natural fibers such as hemp, kenaf, and flax could be used as biomass materials. Chemical treatments could be applied to modify these bio-composites. The adhesion of biomass and the matrix surface could be enhanced by chemical modification such as using alkali treatment (mercerization) or acetylation. Alkali treatment could add sodium hydroxide (NaOH) to decrease the hydrogen content of the cellulose bio-composites. Mold on bio-composites could be treated by adding distilled white vinegar. Enhancing the fire resistance of the composites could be accomplished by adding coating layers of ceramic, silicone, ablative, and glass mats. To avoid degradation and shrinkage, these bio-composites could be used in interior applications like buildings, airplanes, and automobiles to ensure the temperatures will not reach above (200º C). Mechanical properties, such as flexural, tensile, and compressive loading, could be tested. The research could be expanded further to determine how this can be used in building applications. For example, these composite materials can be used as applications in ACE lab exterior building wall to demonstrate a biomass-insulated wall of a building, as shown in Figure 71.

Figure 71: ACE lab exterior.

For the Genetic Algorithms section, the exact parameters of the predesign could be applied using conduction with convection and radiation, and the total thermal objective function of the heat transferred from that design could be calculated that way. In addition, one of the biomass reinforced composites manufactured in section-1, OAK10%, OAK20%, BRY10%, BRY20%, BRY30%, STR10%, STR20%, JUT2.25%, or JUT4.5%, for the objective thermal function could be applied as insulation material, and carbon footprint emissions could be calculated for the sustainable objective function to build a code of Genetic Algorithms using Pareto front optimization to solve multi-objective optimization. Another way could be recommended for using an insulation material. The powder (oak leaf, barley grain, or straw, as in section 1) could be applied directly without mixing with resin by trapping that powder in bags, cartons, containers, or plastic.

The other way utilized in the application could be a spray form with oak leaves placed experimentally between the design bars. Then, the work could be executed numerically using other techniques like Nash equilibrium, Non-discriminating Sort Genetic Algorithms, or Scalarization to solve multi-objective optimization.

Finally, the carbon footprint could be measured experimentally for the biomass reinforced composites materials, OAK10%, OAK20%, BRY10%, BRY20%, BRY30%, STR10%, STR20%, JUT2.25%, and JUT4.5% by estimating carbon dioxide gas emissions for each sample. The carbon footprint of composite samples is estimated using a weighted sum based on the mass fraction of industrial constituents. In addition, using the thermal conductivity values, which have been measured according to the data gained from the current study, could be applied. Then, the predesign can include one of these materials to fill the space between steel bars without using conventional insulation materials. After that, multi-objective optimization entailing maximizing insulation, minimizing heat transfer, and simultaneously maximizing sustainability, minimizing carbon footprint, of a predesigned insulation structure could be performed using a Pareto Front Optimization. The two sections of this work (biomass composites and GA optimization studies) could be merged together. These future works will help to process new concepts of insulation materials and their properties.

References

[1]   Ojha, S.; Raghavendra, G.; Acharya, S.K. A Comparative Investigation of Bio Waste Filler (Wood Apple-Coconut) Reinforced Polymer Composites. Polym. Compos. 2014, 35, 180–185.

[2]   Molaba, T.P.; Chapple, S.; John, M.J. Aging Studies on Flame Retardant Treated Lignocellulosic Fibers. J. Appl. Polym. Sci. 2016, 133.F. Lastname, Book Title, Publisher, Year.

[3]   Sriramamurthy, Lokesh Kanchugaranahally, et al. "Experimental and Statistical Evaluation of the Mechanical Performance of (Jute and Cocopeat) Plant and (Silk) Animal-Based Hybrid Fibers Reinforced with Epoxy Polymers." Journal of Natural Fibers, June 2022, https://doi.org/10.1080/15440478.2022.2073501.

[4]   Mohammed, L., Ansari, M., Grace, G., Jawaid, M., and Islam, M., "A Review on Natural Fiber Reinforced Polymer Composite and Its Applications." Hindawi Publishing Corporation International Journal of Polymer Science Volume 2015, Article ID 243947, 15 pages http://dx.doi.org/10.1155/2015/243947

[5]   Asim, Mohammad, et al. "Potential of Natural Fiber/Biomass Filler-Reinforced Polymer Composites in Aerospace Applications." Sustainable Composites for Aerospace Applications, Page 253, Elsevier Science & Technology, 1 May 2018, assets.erau.edu/federror/index.html?docID=5379881.

[6]   T.G. Yashas Gowda, M.R. Sanjay, K. Subrahmanya Bhat, P. Madhu, P. Senthamaraikannan & B. Yogesha | Duc Pham, Polymer matrix-natural fiber composites: An overview, Cogent Engineering, Volume 5, 2018 - Issue 1.

[7]   Senthilrajan, S., et al. "Parametric Study of Different Fiber Parameters and Their Influence on Acoustics and Vibration Behavior of Jute Fiber/Polyester Resin Composites." Journal of Natural Fibers, 2022, pp. 1–13. Crossref, https://doi.org/10.1080/15440478.2022.2085225.

[8]   Hai, Ho Dinh. "THE WORLDWIDE VEGETABLES." Hordeum Vulgare Barley, 20 May 2015, theworldwidevegetables.weebly.com/hordeum-vulgare---barley.html.

[9]   "Barley | Department of Plant Sciences | College of Agriculture and Natural Resources | University of Wyoming." *FORAGE IDENTIFICATION: BARLEY*, www.uwyo.edu/plantsciences/uwplant/forages/small-grains/barley.html. Accessed 12 July 2022.

[10] "Center of Food Safety." Barley Growing and Seed Saving Tips, www.globalseednetwork.org/seed-tips-detail.php?id=3. Accessed 12 July 2022.

[11] Worldlistmania. "World's Largest Barley Producing Countries." WorldlistMania, 19 Nov. 2021, www.worldlistmania.com/worlds-largest-barley-producing-countries.

[12] Briggs DE (1978) The morphology of barley; the vegetative phase. In: "Barley" Briggs DE, Chapman and Hall, London, pp 1–38. ISBN-13: 978-94-009-5717-6

[13] "Worldwide Wheat Production." Wheat Production by Country 2022, 2022, worldpopulationreview.com/country-rankings/wheat-production-by-country.

[14]   Wallach, Omri. "Visualizing the World's Biggest Rice Producers." Visual Capitalist, 23 Feb. 2022, www.visualcapitalist.com/worlds-biggest-rice-producers.

[15]   "World Corn Production by Country." Atlas Big, 2022, www.atlasbig.com/en-us/world-corn-production-map.

[16]   Haryasz, John. "19 Different Types of Oak Trees With Photos for Identification." Gardening Chores, 7 June 2022, www.gardeningchores.com/types-of-oak trees/?fbclid=IwAR2tCaFeD4TWquvkixrOZlAlbYh1WTHj_bjmoQMwIap7ys a4mk3zqtjj2X8.

[17]   Qi, Yadong; Favorite, Jammie; Chin, Kit L.; Xiao, Ying, Physiological, anatomical, and ecological characteristics of southern live oak, Proceedings of the 13th biennial southern silvicultural research conference. U.S. Department of Agriculture, Forest Service, Southern Research Station. 640 p Augest, 2006

[18]   Gray, Terry L. "SOUTHERN PRIDE TREE FARM, INC." Live Oak Tree Characteristics, www.sptreefarm.com/quercus-virginiana-live-oak-tree-characteristics.html?fbclid=IwAR32F_5dKEcHUp2mDiykr8A3Flg1bZVDZls ZcOmqjzu6x-sHbFQYQTgIzNY. Accessed 12 July 2022.

[19]   Serra-Parareda, F.; Julian, F.; Espinosa, E.; Rodriguez, A.; Espinach, F.X.; Vilaseca, F. Feasibility of Barley Straw Fibers as Reinforcement in Fully Biobased Polyethylene Composites: Macro and Micro Mechanics of the Flexural Strength. Molecules 2020,25, 2242.

[20] "Barley and Rice Straw." Strategies for Preventing and Managing Harmful Cyanobacterial Blooms (HCB-1), hcb-1.itrcweb.org/barley-and-rice-straw. Accessed 21 July 2022. https://hcb-1.itrcweb.org/barley-and-rice-straw/

[21] "Food and Agriculture Organization of the United Nation." Future Fibres: Jute, www.fao.org/economic/futurefibres/fibres/jute/en. Accessed 12 July 2022.

[22] "Jute Yarn : Natural Colour Brown, Raddies and off-White and Dyed but We Prefer Natural Colour Brown , For Making Jute Fabric, Carpet, Rug, Rope so on , Natural Vegetable Fiber Suppliers 1476220 - Wholesale Manufacturers and Exporters." Fibre2Fashion, www.fibre2fashion.com/yarns/jute-yarn-suppliers-1476220. Accessed 12 July 2022.

[23] Sewport. "What Is Jute Fabric: Properties, How Its Made and Where." Sewport, 6 Dec. 2019, sewport.com/fabrics-directory/jute-fabric.

[24] Nag, Oishimaya Sen. "What Is Jute Used For, And Where Is It Grown?" WorldAtlas, 25 Apr. 2017, www.worldatlas

[25] Tabrej Khan, Mohamed Thariq Bin Hameed Sultan, Ahmad Hamdan Ariffin, "The challenges of natural fiber in manufacturing, material selection, and technology application: A review." Journal of Reinforced Plastics and Composites. April 16, 2018.

[26] Lam PS, Sokhansanj S, Chapter 2 Engineering Properties of Biomass, Y. Shastri et al. (eds.), Engineering and Science of Biomass Feedstock 17 Production and Provision, DOI 10.1007/978-1-4899-8014-4_2, Springer Science+Business Media New York 2014.

[27] Kalia, S., Kaith, B.S., Kaur, I., 2011a. Cellulose Fibers: Bio- and Nano-polymer Composites Green Chemistry and Technology. Springer-Verlag, Berlin Heidelberg, UK

[28] F. M. Al-Oqla and S. M. Sapuan, "Natural fiber reinforced polymer composites in industrial applications: feasibility of date palm fibers for sustainable automotive industry," Journal of Cleaner Production, vol. 66, pp. 347–354, 2014.

[29] Mateusz Stasiak, Marek Molenda, Maciej Ban´da, Ewa Gondek. Mechanical properties of sawdust and woodchips. / Fuel 159 (2015) 900–908. http://dx.doi.org/10.1016/j.fuel.2015.07.044.

[30] Yaning Zhang, A.E. Ghaly, and Bingxi Li. Physical Properties of Wheat Straw Varieties Cultivated Under Different Climatic and Soil Conditions in Three Continents. American Journal of Engineering and Applied Sciences, 2012, 5 (2), 98-106 https://thescipub.com/pdf/ajeassp.2012.98.106.pdf

[31] Wu MR, Schott DL, Lodewijks G et al (2011) Physical properties of solid biomass. Biomass. Bioenergy 35:2093–2105.

[32] Anon, ETIP Bioenergy. Torrefied Pellets DEFINITION and PROPERTIES, 2020. https://www.etipbioenergy.eu/images/ETIP_B_Facsheet_Torrefied-pellets_13022020.pdf

[33] S Marwen Bouasker, Naima Belayachi, Dashnor Hoxha, and Muzahim Al-Mukhtar, Physical Characterization of Natural Straw Fibers as Aggregates for

Construction Materials Applications. Materials 2014, 7, 3034-3048; doi:10.3390/ma7043034.

[34] D.C. Joshi, S.K. Das, R.K. Mukherjee, Physical properties of pumpkin seeds. J. Agric. Eng. Res. 54(3), 219–229 (1993).

[35] Naraganti Snehitha, Murlidhar Meghwal, Determination of Engineering Properties of Coffee Beans and Coffee Powder. Journal of Food Processing & Technology, Vol.12 Iss.7 No:547, 2021.

[36] K. Carman, Some physical properties of lentil seeds. J. Agric. Eng. Res. 63(2), 87–92 (1996).

[37] H. Ogut, Some physical properties of white lupin. J. Agric. Eng. Res. 69, 237–277 (1998)

[38] R.K. Gupta, S.K. Das, Fracture resistance of sunflower seed and kernel to compressive loading. J. Food Eng. 46(1), 1–8 (2000).

[39] Z. Ghorbani, A. Hemmat, and A. A. Masoumi. Physical and Mechanical Properties of Alfalfa Grind as Affected by Particle Size and Moisture Content, Journal of Agricultural Science and Technology, (2012) Vol. 14: 65-76.

[40] E.A. Baryeh, Physical properties of Bambara groundnuts. J. Food Eng. 47, 321–326 (2001).

[41] J.D. Olajide, J.C. Igbeka, Some physical properties of groundnut kernels. J. Food Eng. 58(2), 201–204 (2003)

[42] H. Ahmadi, K. Mollazade, Some physical and mechanical properties of fennel seed (Foeniculum vulgare). J. Agric. Sci. 1(1), 66–75 (2009)

[43] Sudhagar Mani,Lope G. Tabil, Shahab Sokhansanj, Grinding performance and physical properties of wheat and barley straws,corn stover and switchgrass. Biomass and Bioenergy 27 (2004) 339 – 352. doi:10.1016/j.biombioe.2004.03.007.

[44] An extensive analysis of mechanical, thermal and physical properties of jute fiber composites with different fiber orientations. Gukendran Rangasamy, Sambathkumar Mani, Sasikumar Kondayampalayam Senathipathygoundar Kolandavelu, Mohammad S. Alsoufi, Ahmed Mohamed Mahmoud Ibrahim, Suresh Muthusamy, Hitesh Panchal, Kishor Kumar Sadasivuni, Ammar H. Elsheikh. Case Studies in Thermal Engineering 28 (2021) 101612. https://doi.org/10.1016/j.csite.2021.101612

[45] Kalia, S., Avérous, L., Njuguna, J., Dufresne, A., Cherian, B.M., 2011b. Natural fibers, bio- and nanocomposites. Int. J. Polymer Sci. 2011. http://dx.doi.org/10.1155/ 2011/735932. Article ID 735932.

[46] Faruk O, Bledzki AK, Fink H-P, Sain M (2012) Biocomposites reinforced with natural fibers: 2000–2010. Prog Poly Sci 37(11):1552–1596

[47] Campilho RDSG (2015) Natural fiber composites. CRC Press, Boca Raton

[48] Alves, C., Ferrão, P.M.C., Silva, A.J., Reis, L.G., Freitas, M., Rodrigues, L.B., Alves, D.E., 2010. Ecodesign of automotive components making use of natural jute fiber composites. J. Cleaner Prod. 18, 313e327

[49] MIR, A., Zitoune, R., Collombet, F., Bezzazi, B., 2010. Study of mechanical and thermomechanical properties of jute/epoxy composite laminate. J. Reinforc. Plast. Compos. 29, 1669e1680.

[50] Pickering, K.L., Beckermann, G.W., Alam, S.N., Foreman, N.J., 2007. Optimising industrial hemp fibre for composites. Compos. A Appl. Sci. Manuf. 38, 461e468.

[51] Sarikanat, M., 2010. The influence of oligomeric siloxane concentration on the mechanical behaviors of alkalized jute/modified epoxy composites. J. Reinforc. Plast. Compos. 29, 807e817.

[52] Yao, F., et al. Thermal decomposition kinetics of natural fibers: Activation energy with dynamic thermogravimetric analysis. Polymer Degradation and Stability 93 (2008) pages 90-98.

[53] 6 Natural, Safe Mold Treatment Solutions to use Instead of Bleach. Colorado Property Group. www.beyondtoxics.org/wpcontent/uploads/GreatNaturalMoldCleaners-Instead-of-Bleach.pdf.

[54] Kozłowski R, Władyka-Przybylak M (2008) Flammability and fire resistance of composites reinforced by natural fibers. Polym Adv Technol 19(6):446–453

[55] Mohanty AK, Misra M, Drzal LT (2001) Surface modifications of natural fibers and performance of the resulting J Mater Sci (2020) 55:829–892 881 biocomposites: an overview. Compos Interfaces 8(5):313–343

[56] Stark NM (1999) Wood fiber derived from scrap pallets used in polypropylene composites. For Prod J 49:39–46

[57] Araujo JR, Waldman WR, De Paoli MA (2008) Thermal properties of high density polyethylene composites with natural fibres: coupling agent effect. Polym Degrad Stab 93(10):1770–1775

[58] Yildiz S, Gezer ED, Yildiz UC (2006) Mechanical and chemical behavior of spruce wood modified by heat. Build Environ 41(12):1762–1766

[59] Al-Khanbashi, A., Al-Kaabi, K., Hammami, A., 2005. Date palm fibers as polymeric matrix reinforcement: fiber characterization. Polymer Compos. 26, 486e497.

[60] Foisal A M, Ali M A, Byung S K and Jong I S 2009 Recent Developments in Natural Fiber Reinforced Composites. The Korean Society for Composite Materials 22 4.

[61] Broeren M L, Dellaert S N, Cok B, Patel M K, Worrell E, and Shen L 2017 Life cycle assessment of sisal fibre–Exploring how local practices can influence environmental performance J Clean Prod 149 818-827

[62] Hobani, A.I., Tolba, M.H., 1995. Bulk thermal conductivity and diffusivity or barley. Research Bulletin of Agricultural Research Center at King Saud University, Saudi Arabia 73, 5–18.

[63] Kayisoglu, B., Kocabiyik, H., Akdemir, B., 2004. The effect of moisture content on the thermal conductivities of some cereal grains. J. Cereal Sci. 39, 147–150

[64] Jiriˇ cková, ˇ M., Pavlík, Z., Cern ˇ y, ´ R., 2006. Thermal properties of biological agricultural materials. In: Proceedings of the Thermophysics 2006, Meeting of the Thermophysical Society Working Group of the Slovak Physical Society, pp. 68–71.

[65] K. Alagusundaram, D. S. Jayas, W. E. Muir, N. D. G. White. Thermal conductivity of bulk barley, lentils, and peas. Transactions of the ASAE. 34 (4): (1991) 1784-1788. (doi: 10.13031/2013.31801)

[66] Zach J, Hroudova J, Brožovskýc J, Krejzad Z, Gailiuse A. Development of thermal insulating materials on natural base for thermal insulation systems. Proceedia Eng 2013;57:1288–94.

[67] S. Schiavoni, F. D'Alessandro, F. Bianchi, F. Asdrubali, Insulation materials for the building sector: A review and comparative analysis. Renewable and Sustainable Energy Reviews 62, (2016) 988–1011.

[68] Korjenic A, Petránek V, Zach J, Hroudová J. Development and performance evaluation of natural thermal-insulation materials composed of renewable resources. Energy Build 2011;43:2518–23.

[69] Xu J, Sugawara R, Widyorini R, Han G, Kawai S. Manufacture and properties of low-density binderless particleboard from Kenaf core. J Wood Sci 2004;50 (1):62–7

[70] Dikici B., Motagi S., Kantamani, P., and Al-Haik, M., Thermal Conductivity Study of Biomass Reinforced Polymer Composites, ASME 2020 18th

International Conference on Nanochannels, Microchannels, and Minichannels, HT2020-9065, V001T11A008, September 25, 2020.

[71] Collet, F., and Pretot, S., "Thermal Conductivity of Hemp Concretes: Variation with Formulation, Density and Water Content." Construction and Building Materials. Volume 65, Pages 612–619, ScienceDirect, 29 Aug. 2014.

[72] T. I. Ogedengbe, E. O. Fatomilola, and O. R. Bello. Evaluation of Thermal Conductivity of Selected Biomass Composites. Research Journal in Engineering and Applied Sciences 2(4) 326-335. Emerging Academy Resources (2013).

[73] Metter Toledo, Thermal Analysis of Polymers, Selected Applications Thermal Analysis, Applications Handbook, 2016.

[74] Gotmare V D, Kole S S. Applications of biomass and recycled fibers in construction engineering: an overview. J Textile Eng Fashion Technol. 2017;1(5):198-201. DOI: 10.15406/jteft.2017.01.00032

[75] Vázquez-Núñez E, Avecilla-Ramírez AM, Vergara-Porras B, López-Cuellar M del R. Green composites and their contribution toward sustainability: A review. Polymers and Polymer Composites. 2021;29(9_suppl):S1588-S1608. doi:10.1177/09673911211009372

[76] Blanco, Ignazio, and Valentina Siracusa. "The Use of Thermal Techniques in the Characterization of Bio-Sourced Polymers." Materials, vol. 14, no. 7, 2021, p. 1686–, https://doi.org/10.3390/ma14071686.

[77] Relative Humidity Meter PCE-MA 110." PCE Instruments, PCE Deutschland GmbH, 2021. Accessed 21 Apr. 2021.

[78] Geotech Environmental Equipment, Inc." Geotech Sand Shaker, 2021, www.geotechenv.com.

[79] "AmScope Microscope & Accessory Supplier, B120 Model." Microscopic User's Manual, 2021Pdf, Accessed 4 Apr. 2021.

[80] "Vision on Quality." TQC, Specific Gravity Cup ISO 2811 DIN 53217 ASTM D 1475, www.tqc.eu. Accessed 2 July 2022.

[81] Sergio C. Capareda "Introduction to Biomass Energy Conversions" CRC Press, 2014 by Taylor & Francis Group, ISBN 978-1-4665-1333-4 (alk. Paper) (Biomass Properties for Thermal Conversion) Pages 85-90.

[82] K. Ibsen, A. McAloon, E. Taylor, R. Wooley, W. Yee, Determining the cost of producing ethanol from corn starch and lignocellulosic feedstocks, NREL/TP-580-28893, US Department of energy, National Renewable Energy Laboratory, Golden, CO, 2000

[83] A. Demirbas, Biomass resource facilities and biomass conversion processing for fuels and chemicals, Energy Conversion and Management 42 (2001) 1357–1378.

[84] T. Christopher, P.A. Pryfogle, N.A. Stevens, J.R. Hess, C.W. Radke, Value of distributed preprocessing of biomass feedstocks to a biorefinery industry, Paper No. 066151, American Society of Agricultural Engineers, St. Joseph, MI, 2006.

[85] S. Sokhansanj, J. Cushman, L. Wright, Collection and delivery of biomass for fuel and power production, The CIGR Journal of Scientific Research and Development V (2003) 1–22.

[86] M. Knauf, M. Moniruzzaman, Lignicellulosic biomass processing: a perspective, International Sugar Journal 106 (2004) 147–150.

[87] G.V. Barbosa-Canovas, E. Ortega-Rivas, P. Juliano, H. Yan, Food Powders: Physical Properties, Processing, and Functionality, Kluwer Academic Plenum Publishers, New York, NY, 2005.

[88] Duncan A, Pollard A, Fellouah H (2013) Torrefied, spherical biomass pellets through the use of experimental design. Appl Energy 101:237–243

[89] Gil M, Schott D, Arauzo I et al (2013) Handling behavior of two milled biomass: SRF poplar and corn stover. Fuel Process Technol 112:76–85

[90] Chevanan N, Womac AR, Bitra VSP et al (2009) Flowability parameters for chopped switchgrass, wheat straw and corn stover. Powder Technol 193:79–86

[91] Illeleji KE, Zhou B (2008) The angle of repose of bulk corn stover particles. Powder Technol 187:110–118

[92] Carr RL (1976) Powder and granule properties and mechanics. In: Marchello JM, Gomezplata A (eds) Gas–solids handling in the processing industries. Marcel Dekker, New York.

[93] Lam PS, Sokhansanj S, Bi X et al (2008) Effect of particle size and shape on physical properties of biomass grinds. Paper No. 080014, Providence, Rhode Island, American Society of Agricultural and Biological Engineers, St. Joseph, MI, June 29–July 2.

[94] Geldart, D. (2007). Powder Characteristics, Experts in powder technology, Powder Research Ltd. Derek Geldart. http://powderresearch.com/aor.html.

[95] Frette V, Christensen K, Malthesorenssen A, Feder J, Jossang T, Meakin P. Avalanche dynamics in a pile of rice. Nature 1996;379:49–52.

[96] Jaeger H, Liu C, Negel S. Relaxation at the angle of repose. Phys Rev Lett 1989;62:40–3.

[97] Makse HA, Havlin S, King PR, Stanley HE. Spontaneous stratification in granular mixtures. Nature 1997;386:379–81.

[98] Baxter J, Tuzun U, Heyes D, Hayati I, Fredlund P. Stratification in poured granular heaps. Nature 1998;391:136.

[99] Jullien R, Meakin P, Pavlovitch A. Particle size segregation by shaking in twodimensional disc packings. Europhys Lett 1993;22:523–8.

[100] Samadani A, Kudrolli A. Angle of repose and segregation in cohesive granular matter. Phys Rev E 2001;64:1301–10.

[101] H.M. Beakawi Al-Hashemi, O.S. Baghabra Al-Amoudi, A review on the angle of repose of granular materials, Powder Technology 330 (2018) 397–417.

[102] Arun Raj R.*, Nandkishore K. "Formulation and Evaluation of Meloxicam Crystals Using Spherical Crystallization for Solubility Enhancement" Research & Reviews: A Journal of Drug Formulation, Development and Production ISSN: 2394-1944, Page 18, Volume 3, Issue 2.

[103] Volume of a Circular Truncated Cone Calculator." High Accuracy Calculation for Life or Science., 2019, keisan.casio.com/exec/system/1223372110.

[104] J O Bird, P J Chivers, Newnes Engineering and Physical Science Pocket Book, 28 – Friction, published online 27 June 2014, Pages 235-237.

[105] V.N.Malyshev, 8 - Tribological aspects in friction stir welding and processing, Advances in Friction-Stir Welding and Processing Woodhead Publishing Series in Welding and Other Joining Technologies, ISBN: 9780857094544, published online 12 December 2014, Pages 329-386.

[106] Yang Zhang, L.G. Tabil, Decheng Wang, Effect of Moisture Content, Postharvest Treatment and Storage Time on Physical Properties and Dehulling Quality of Red Lentil. An ASABE Annual International Meeting, Presentation Paper Number: 085261, June 29 – July 2, 2008.

[107] Jan Erik Mattsson (1990) Basic handling characteristics of wood fuels: Angle of repose, friction against surfaces and tendency to bridge for different assortments, Scandinavian Journal of Forest Research, 5:1-4, 583-597, DOI: 10.1080/02827589009382641.

[108] "Model GCE Digital Series Lab Ovens." Quincy Lab, Inc., 2016, img1.wsimg.com/blobby/go/158de9bd-2322-4539-84a4-5adaf0187e1a/downloads/Lab%20Oven%20GC%20Operating%20Manual_%20REV%20F%200917_COPY.pdf?ver=1661193939066.

[109] Material Safety Data Sheet, E408 Dry Film Mold ReleaseTM, Stoner http://www.moglice.com/sds/sds_accessories/DevittSeparatorTF-E408.pdf

[110] "EPONTM Resin 828." HEXION, Technical Data Sheet, 6 Mar. 2015, miller stephenson.com/wp-content/uploads/2016/08/828.pdf.

[111] "Technical Data Sheet EPIKURETM Curing Agent 3140." HEXION, Responsible Chemistry, 20 May 2020,

https://www.hexion.com/CustomServices/PDFDownloader.aspx?type=tds&pi
d=f6ca273c-5814-6fe3-ae8a-ff0300fcd525

[112] TORBAL Scales. "TORBAL DENSITY ANALYZER KITS." Torbal Balances, Si Division of Scientific Industries, Inc., www.torbalscales.com/backup-center/download.

[113] Density Determination Guide - TORBAL Scales. "Https://Www.torbalscales.com/Backup-Center/Download..." Torbal AD Series Precision Balances, Si Division of Scientific Industries, Inc., [PDF].

[114] Cengel, Yunus, Ghajar, Afshin, Heat and Mass Transfer: Fundamentals and Applications 5th Edition, 2015.

[115] Hot Disk Thermal Constants Analyzer Instruction Manual. (2015) Hot Disk AB https://www.hotdiskinstruments.com/products-services/instruments/tps-2500-s/

[116] Tekce, Kumlutas, D., & Tavman, I. H. (2007). Effect of Particle Shape on Thermal Conductivity of Copper Reinforced Polymer Composites. Journal of Reinforced Plastics and Composites, 26(1), 113–121. https://doi.org/10.1177/0731684407072522

[117] Density of wood in kg/m^3, g/cm^3, lb/ft^3 – the ultimate guide-https://matmatch.com/learn/property/density-of-wood

[118] M.P. Felizardo, J.T. Freire. Characterization of barley grains in different levels of pearling process. Journal of Food Engineering,Volume 232, September 2018, Pages 29-35 https://doi.org/10.1016/j.jfoodeng.2018.03.017

[119] Kingsley Iroba, Lope Tabil, Meda Venkatesh, and Baik Oon-Doo, Thermal properties of lignocellulosic biomass barley straw. 2013 ASABE Annual International Meeting Paper. https://www.researchgate.net/publication/271434562_Thermal_properties_of_li gnocellulosic_biomass_barley_straw

[120] M. K. Guptaa, R. K. Srivastavaa, and Himanshu Bisaria, Potential of Jute Fibre Reinforced Polymer Composites: A Review. International Journal of Fiber and Textile Research 2015; 5(3): 30-38. https://www.researchgate.net/publication/320526159_Structural_analysis_and_ mechanical_properties_of_lignite_fly-ash-added_jute-epoxy_polymer_matrix_composite.

[121] HEXION, EPONTM RESIN 828, Technical Data Bulletin. (2005). https://www.spacematdb.com/spacemat/manudatasheets/Epon828.pdf

[122] S.G. Walde, K. Balaswamy, V. Velu, D.G. Rao "Microwave drying and grinding characteristics of wheat (Triticum aestivum) Journal of Food Engineering." Volume 55, Issue 3, December 2002, Pages 271-276.

[123] H. Tavakoli, S. S. Mohtasebi, A. Jafari, M. Nazari Galedar. SOME ENGINEERING PROPERTIES OF BARLEY STRAW. APPLIED ENGINEERING IN AGRICULTURE, 2009 American Society of Agricultural and Biological Engineers ISSN 0883-8542, Vol. 25(4): 627-633.

[124] Mani, S., Tabil, L. G. and Sokhansang, S.2004b. Mechanical Properties of CornStover Grind. Trans. ASAE, 45(6): 1983-1990

[125] Fathollahzadeh, H., Mobli, H., Beheshti, B., Jafari, A. and Borghei, A. M. 2008. Effect of Moisture Content on Some Physical Properties of Apricot kernal (CV. Sonnati salmas). Manuscript FP 08008, Agricultural Engineering International, The CIGR Ejournal, Vol. X.

[126] Subramanian, & Viswanathan, R. (2007). Bulk density and friction coefficients of selected minor millet grains and flours. Journal of Food Engineering, 81(1), 118–126. https://doi.org/10.1016/j.jfoodeng.2006.09.026

[127] E. Hadjittofis, S. C. Das, G.G. Z. Zhang, J.Y.Y. Heng, Chapter 8 – Interfacial Phenomena "Developing Solid Oral Dosage Forms (Second Edition)" Pharmaceutical Theory and Practice. 2017, Pages 225-252

[128] Tadesse F. Teferra, "Engineering Properties of Food Materials" in Handbook of Farm, Dairy and Food Machinery Engineering (Third Edition), Pages 45-89, 2019.

[129] Stufft, T. J., & Strebel, J. (1997). How grinder variables affect bulk density and flow properties of polyethylene powder. Plastics Engineering, 53(8), 29. Retrieved from

http://ezproxy.libproxy.db.erau.edu/login?url=https://www.proquest.com/trade-journals/how-grinder-variables-affect-bulk-density-flow/docview/213915702/se-2

[130] Crouter A, Briens L. The effect of moisture on the flowability of pharmaceutical excipients. AAPS PharmSciTech. 2014 Feb;15(1):65-74. doi: 10.1208/s12249-013-0036-0. Epub 2013 Oct 3. PMID: 24092523; PMCID: PMC3909156.

[131] Zulfigar M, Moghtaderi B, Wall TF. Flow properties of biomass and coal blends. Fuel Process Technol 2006;87:281–8.

[132] Littlefield, B., Fasina, O. O., Shaw, J., Adhikari, S., & Via, B. (2011). Physical and flow properties of pecan shells—Particle size and moisture effects. Powder Technology, 212, 173–180.

[133] E.C. Abdullah, D. Geldart. The use of bulk density measurements as flowability indicators. Powder Technology 102 (1999) 151–165.

[134] Stasiak M, Molenda M, Bańda M, Horabik J, Wiącek J, Parafiniuk P, Wajs J, Gancarz M, Gondek E, Lisowski A, Oniszczuk T. Friction and Shear Properties of Pine Biomass and Pellets. Materials (Basel). 2020 Aug 12;13(16):3567. doi: 10.3390/ma13163567. PMID: 32806744; PMCID: PMC7475855.

[135] John W. Carson and Brian H. Pittenger, Bulk Properties of Powders. ASM Handbook, Volume 7: Powder Metal Technologies and Applications. p 287-301, 1998.https://materialsdata.nist.gov/bitstream/handle/11115/193/Bulk%20Properti es%20of%20Powders.pdf?sequence=3&isAllowed=y

[136] Huber, M.L., Perkins, R.A., Friend, D.G., and Sengers, J.V., Assael, M.J., Metaxa, I.N., Miyagawa, K., Hellmann, R., and Vogel, E. "New International Formulation for the Thermal Conductivity of H2O," J. Phys. Chem. Ref. Data, 41(3), 033102, 2012. doi: 10.1063/1.4738955

[137] Marek Markowski, Ireneusz Białobrzewski. Bulk thermal conductivity of malting barley. Industrial Crops and Products 42 (2013) 369–372. http://dx.doi.org/10.1016/j.indcrop.2012.06.017

[138] Troppová E, Švehlík M, Tippner J, Wimmer R. Influence of temperature and moisture content on the thermal conductivity of wood-based fibreboards. Mater Struct 2015;48:4077–83.

[139] Mňahončáková, E., Jiřičková, M., Pavlík, Z., Fiala, L., Rovnaníková, P., Bayer, P., Černý, R., Effect of moisture on thermal conductivity of a cementitious composite. July 2006 International Journal of Thermophysics 27(4):1228-1240. DOI: 10.1007/s10765-006-0073-y.

[140] MacLean, J. D. (1941). "Thermal conductivity of wood," Heating, Piping & Air Conditioning 13(6), 380-391.

[141] Vay, O., De Borst, K., Hansmann, C., Teischinger, A., and Müller, U. (2015). "Thermal conductivity of wood at angles to the principal anatomical directions," Wood Science and Technology 49(3), 577-589. DOI: 10.1007/s00226-015-0716-x.

[142] B.P. Jelle, (2016) https://doi.org/10.1016/B978-0-08-100546-0.00008-X

[143] Grelat, A. Using Sustainable Materials as Walling for Individual Housing With Wood Structure; Final report; Centre D'expertise du Batiment et des Travaux Public: Saint-Remy-Les-Chevreuse, France, 2004.

[144] Palumbo, M.; Lacasta, A.M.; Holcroft, N.; Shea, A.; Walker, P. Determination of hygrothermal parameters of experimental and commercial bio-based insulation materials. Constr. Build. Mater. 2016, 124, 269–275.

[145] Zach J, Korjenic A, Petránek V, Hroudová J, Bednar T. Performance evaluation and research of alternative thermal insulations based on sheep wool. Energy Build 2012;49:246–53

[146] Air – Density – Heat Capacity – Thermal Conductivity, Nuclear Power | Thermal Engineering | Radiation Dosimetry, 2022 https://material-properties.org/air-density-heat-capacity-thermal-conductivity/

[147] Vasubsbu, M., Nagaraju, B., Kumar, J. V., and Kumar, R. J. (2015). "Experimental measurement of thermal conductivity of wood species in India: effect of density and porosity," International Journal of Science, Environment and Technology 4(5), 1360-1364.

[148] Wei, K.; Lv, C.; Chen, M.; Zhou, X.; Dai, Z.; Shen, D. Development and performance evaluation of a new thermal insulation material from rice straw using high frequency hot-pressing. Energy Build. 2015, 87, 116–122.

[149] Abanto, Ginés A., et al. "Thermal Properties of Adobe Employed in Peruvian Rural Areas: Experimental Results and Numerical Simulation of a Traditional Bio-Composite Material." Case Studies in Construction Materials, vol. 6, no. C, 2017, pp. 177–91, https://doi.org/10.1016/j.cscm.2017.02.001.

[150] M Chikhi, F Chekired, N Metidji, and F Mokhtari. Numerical investigation of porous materials composites reinforced with natural fibers. International Conference on Nanomaterials and Biomaterials (ICNB 2017), IOP Conf. Series: Materials Science and Engineering 350 (2018) 012003 doi:10.1088/1757-899X/350/1/012003

[151] Chen G, Li F, Jing P, Geng J, Si Z. Effect of Pore Structure on Thermal Conductivity and Mechanical Properties of Autoclaved Aerated Concrete. Materials (Basel). 2021 Jan 11;14(2):339. doi: 10.3390/ma14020339. PMID: 33440871; PMCID: PMC7827858.

[152] Smith, D., Alzina, A., Bourret, J., Nait-Ali, B., Pennec, F., Tessier-Doyen, N., . . . Gonzenbach, U. (2013). Thermal conductivity of porous materials. Journal of Materials Research, 28(17), 2260-2272. doi:10.1557/jmr.2013.179.

[153] Samuel, O. S., Ramon, B. O., and Johnson, Y. O. (2012). "Thermal conductivity of three different wood products of Combretaceae family; Terminalia superba, Terminalia ivorensis and Quisqualis indica," Journal of Natural Sciences Research 2(4).

[154] Andersen, B.M.; Munch-Andersen, J. Halmballer og Muslinger som Isoleringsmaterialer; Report 2001-06–21; Statens Byggeforskningsinstitut: Copenhagen, Denmark, 2001.

[155] Yapici, F. I., Ozcifci, A., Esen, R., and Kurt, S. (2011). "The effect of grain angle and species on thermal conductivity of some selected wood species," BioResources 6(3), 2757-2762. DOI: 10.15376/biores.6.3.2757-2762

[156] Çavuş, V., Şahin, S., Esteves, B., and Ayata, U. (2019). "Determination of thermal conductivity properties in some wood species obtained from Turkey," BioRes. 14(3), 6709-6715.

[157] S. Sair, A. Oushabi, A. Kammouni, O. Tanane, Y. Abboud, A. El Bouari. Mechanical and thermal conductivity properties of hemp fiber reinforced

polyurethane composites. Case Studies in Construction Materials 8 (2018) 203–212 https://doi.org/10.1016/j.cscm.2018.02.001

[158] Clara-Eugenia Ferrández-García , Antonio Ferrández-García, Manuel Ferrández-Villena, Juan Fernando Hidalgo-Cordero, Teresa García-Ortuño, and María-Teresa Ferrández-García. Physical and Mechanical Properties of Particleboard Made from Palm Tree Prunings. Forests 2018, 9, 755; doi:10.3390/f9120755

[159] Density of Grain Barley (material), 2022. https://www.aqua-calc.com/page/density-table/substance/grain-blank-barley

[160] McCabe, J. Thermal Resistivity of Straw Bales for Construction. Master's Thesis, University of Arizona, Tucson, AZ, USA, 1993.

[161] Conti, L.; Barbari, M.; Monti, M. Steady-State Thermal Properties of Rectangular Straw-Bales (RSB) for Building. Buildings 2016, 6, 44 https://www.mdpi.com/2075-5309/6/4/44.

[162] Felippe Fabrício dos Santos Siqueira , Renato Lemos Cosse , Fernando Augusto de Noronha Castro Pinto, Paulo Henrique Mareze, Caio Frederico e Silva and Lívio César Cunha Nunes. Characterization of Buriti (Mauritia flexuosa) Foam for Thermal Insulation and Sound Absorption Applications in Buildings. Buildings 2021, 11, 292. https://doi.org/10.3390/buildings11070292.

[163] Surya D Pandita, Xiaowen Yuan, Munirah A Manan,Chun H Lau, Alamelu S Subramanian and Jun Wei. Evaluation of jute/glass hybrid compositesandwich: Water resistance, impactproperties and life cycle assessment. Journal of Reinforced Plastics and Composites 2014, Vol 33(1) 14–25

https://www.researchgate.net/publication/274499529_Evaluation_of_juteglass_hybrid_composite_sandwich_Water_resistance_impact_properties_and_life_cycle_assessment.

[164] Sanjoy Debnath, M. Madhusoothanan, Water Absorbency of Jute–Polypropylene Blended Needle-punched Nonwoven. JOURNAL OF INDUSTRIAL TEXTILES, Vol. 39, No. 3—January 2010 https://www.researchgate.net/publication/249776964_Water_Absorbency_of_Jute-Polypropylene_Blended_Needle-punched_Nonwoven

[165] M. Jawaid, and H. P. S. Abdul Khalil. Effect of Layering Pattern on The Dynamic mechanical Properties and Thermal Degradation of oil Palm-Jute Fibers Reinforced Epoxy Hybrid composite. BioResources 6(3), 2309-2322 https://www.researchgate.net/publication/216884887_Effect_of_layering_pattern_on_the_dynamic_mechanical_properties_and_thermal_degradation_of_oil_palm-jute_fibers_reinforced_epoxy_hybrid_composite

[166] Azam Ali, Khubab Shaker, Yasir Nawab, Munir Ashraf, Abdul Basit, Salma Shahid and Muhammad Umair. Impact of hydrophobic treatment of jute on moisture regain and mechanical properties of composite material. Journal of Reinforced Plastics and Composites, 2015

[167] Lasance, Clemens. The Thermal Conductivity of Thermal Insulators. 1 May 2022, www.electronics-cooling.com/2002/05/the-thermal-conductivity-of-thermal-insulators. https://www.electronics-cooling.com/2002/05/the-thermal-conductivity-of-thermal-insulators/.

[168] "Expanded Polystyrene - EPS - Thermal Insulation." Nuclear Power, 2 June 2022, www.nuclear-power.com/nuclear-engineering/heat-transfer/heat-losses/insulation-materials/expanded-polystyrene-eps.

[169] "Types of Insulation - a Guide." Kingspan Group, 30 June 2022, www.kingspan.com/gb/en/knowledge-articles/types-of-insulation-a-guide.

[170] Thermal Conductivity of Non-metallic Solids. 2 Jan. 2020, www.piping-designer.com/index.php/properties/878-tables/2728-thermal-conductivity-of-non-metallic-solids.

[171] I. Rahmanian, Y. Wang, Thermal Conductivity of Gypsum at High Temperatures A Combined Experimental and Numerical Approach, Acta Polytechnica Vol. 49 No. 1/2009. http://ctn.cvut.cz/ap/

[172] Lasance, Clemens. "The Thermal Conductivity of Rubbers/Elastomers." Electronics Cooling, 1 Nov. 2001, www.electronics-cooling.com/2001/11/the-thermal-conductivity-of-rubbers-elastomers/?fbclid=IwAR0POCZPA5qDsawc00uBWHbF1QFRO6MzsVEE_Fnuro5vvm_UuGCxlpkWNpE.

[173] Wang, RT., Wang, JC. Analysis of thermal conductivity in HI-LEDs lighting materials. J Mech Sci Technol 31, 2911–2921 (2017). https://doi.org/10.1007/s12206-017-0534-1.

[174] "OPTIM-R Vacuum Insulation Panels." Kingspan Insulation, 2022, www.kingspan.com/gb/en/business-groups/kingspan-insulation/optim-r.

[175] Maurice Stewart, Material requirements: Piping materials, Surface Production Operations. Volume 3: Facility Piping and Pipeline System, 2016, Pages 159-192 https://doi.org/10.1016/B978-1-85617-808-2.00003-1

[176] "Phenolic Foam Insulation." Designing Buildingd, July 2022, www.sciencedirect.com/topics/engineering/mineral-wool.

[177] Le Duong Hung Anh, Zoltan Pasztory, An overview of factors influencing thermal conductivity of building insulation materials, Journal of Building Engineering 44 (2021) 102604. https://doi.org/10.1016/j.jobe.2021.102604.

[178] GeorgeWypych, 2 - Fillers – Origin, Chemical Composition, Properties, And Morphology, Handbook of Fillers (Fourth Edition), 2016, Pages 13-266. https://doi.org/10.1016/B978-1-895198-91-1.50004-X.

[179] Saad, Hussein Ak, Dikici, Birce, Villarroel, Gustavo, and Divo, Edurado, "Characterization Methods for Biomass Materials and Optimizing Heat Transfer By Using Genetic Algorithms" 7th Thermal and Fluids Engineering Conference (TFEC), ASTFE Digital Library, pages 448-451. DOI: 10.1615/TFEC2022.emt.040794.

[180] William Callister, David Rethwisch, Materials Science and Engineering, An Introduction. 10 Edition, Wiley, Chapter 6, page 172, 2020.

[181] Akpinar M., Application of Genetic Algorithm for Optimization of Heat-Transfer Parameters, Sakarya University Journal of Science, 2019, 23(6), doi: https://doi.org/10.16984/saufenbilder.500643

[182] Biswas, Kaushik et al. "Insulation materials for commercial buildings in North America: An assessment of lifetime energy and environmental impacts." Energy and Buildings 112 (2016): 256-269.

[183] King, A.D., Karoly, D.J., Henley, B.J., 2017. Australian climate extremes at 1.5 degrees C and 2 degrees C of global warming. Nat. Clim. Change 7, 412

[184] Mostafa, M.M.,2016 Post-materialism, religiosity, political orientation, locus of control and concern for global warming: a multilevel analysis across 40 nations Soc. Indicat. Res., 128 (2016), pp. 1273-1298.

[185] Santos-Alamillos, F.J., Archer, C.L., Noel, L., Budischak, C., Facciolo, W., 2017. Assessing the economic feasibility of the gradual decarbonization of a large electric power system. J. Clean. Prod. 147, 130–141.

[186] Long, Katherine. "New Apps Help Builders Reduce Carbon Footprint." University of Washington, 21 Nov. 2019, https://urban.uw.edu/news/new-apps-help-builders-reduce-carbon-footprint/

[187] Aviso, K.B., Sy, C.L., Tan, R.R., Ubando, A.T., 2020. Fuzzy optimization of carbon management networks based on direct and indirect biomass co-firing, 132. Renewable & Sustainable Energy Reviews.

[188] Lund, P.D., 2011. Boosting new renewable technologies towards grid parity - economic and policy aspects. Renew. Energy 36, 2776–2784.

[189] Fluorides, G. A., and P. Christodoulides. 2009. Global warming and carbon dioxide through sciences. Environ. Int 35 (2):390–401. doi:10.1016/j.envint.2008.07.007.

[190] Lima, M. A., L. F. R. Mendes, G. A. Mothé, F. G. Linhares, M. P. P. Castro, M. G. Silva, and M. S. Sthel. 2020. Renewable energy in reducing greenhouse gas emissions: Reaching the goals of the Paris agreement in Brazil. Environ. Dev 33:100504. doi:10.1016/j. envdev.2020.100504.

[191] Babiker, M. H. 2005. Climate change policy, market structure, and carbon leakage. J. Int. Econ 65 (2):421–45. doi:10.1016/ j.jinteco.2004.01.003.

[192] Rogelj, J., O. Fricko, M. Meinshausen, V. Krey, J. J. J. Zilliacus, and K. Riahi. 2017. Understanding the origin of Paris agreement emission uncertainties. Nat. Commun 15748:1–12.

[193] Wang, S., Fang, C., Ma, H., Wang, Y., Qin, J., 2014. Spatial differences and multi-mechanism of carbon footprint based on GWR model in provincial China. J. Geogr. Sci. 24, 612–630.

[194] Kerem, A., 2022. Investigation of carbon footprint effect of renewable power plants regarding energy production: A case study of a city in Turkey. Journal of the Air & Waste Management Association. Vol. 72, No. 3, 294–307

[195] Gunantara. Nyoman (2018). A review of multi-objective optimization: Methods and its applications. Cogent Engineering, 5(1), 1502242–. https://doi.org/10.1080/23311916.2018.1502242.

[196] Eduardo Divo, Hussein Awad Kurdi Saad, Sandra Boetcher, Jeff Brown, and Alain J. Kassab. Inverse Vof Meshless Method For Efficient Nondestructive Thermographic Evaluation, Computational Thermal Sciences: An International Journal. Volume 7, 2015 Issue 2. pp. 105-121.

[197] Zhang, Deng, Z., Fu, Y., Lv, L., & Yan, C. (2017). A process parameters optimization method of multi-pass dry milling for high efficiency, low energy and low carbon emissions. Journal of Cleaner Production, 148, 174–184. https://doi.org/10.1016/j.jclepro.2017.01.077

[198] La Fé Perdomo, Quiza, R., Haeseldonckx, D., & Rivas, M. (2019). Sustainability-Focused Multi-objective Optimization of a Turning process. International Journal of Precision Engineering and Manufacturing - Green Technology, 7(5), 1009–1018. https://doi.org/10.1007/s40684-019-00122-4

[199] Anvari, Mahian, O., Solomin, E., Wongwises, S., & Desideri, U. (2021). Multi-objective optimization of a proposed multi-generation cycle based on Pareto diagrams: Performance improvement, cost reduction, and CO_2 emissions. Sustainable Energy Technologies and Assessments, 45, 101197–. https://doi.org/10.1016/j.seta.2021.101197

[200] Limleamthong, and Guillén-Gosálbez, G. (2017). Rigorous analysis of Pareto fronts in sustainability studies based on bilevel optimization: Application to the redesign of the UK electricity mix. Journal of Cleaner Production, 164, 1602–1613. https://doi.org/10.1016/j.jclepro.2017.06.134.

[201] Goldberg, D.E., Genetic Algorithms in Search, Optimization and Machine Learning, Addison-Wesley, Reading, MA, 1989.

[202] Balaji, C. Essentials of Thermal System Design and Optimization, Chapter 8, Non-traditional optimization techniques, Page 261, 2011

[203] Saad, Hussein Awad Kurdi. Inverse Volume-of-Fluid Meshless Method for Efficient Non-Destructive Thermographic Evaluation. Embry-Riddle Aeronautical University, 2014.

[204] Özlüsoylu, İ., & İstek, A. 2019c. The Effect of Hybrid Resin Usage on Thermal Conductivity in Ecological Insulation Panel Production. 4th International Conference on Engineering Technology and Applied Sciences (ICETAS) April 24-28 2019 Kiev Ukraine 292-296.https://www.researchgate.net/publication/333164278_The_Effect_of_Hybrid_Resin_Usage_on_Thermal_Conductivity_in_Ecological_Insulation_Panel_Production/figures?fbclid=IwAR3ib3IaOij2YebTUPhUuRi7Ucli2gMDz_SsxS0hO9JCBiZVw_uQaOGdGL4

[205] Advancing Materials Science | Morgan Advanced Materials. www.morganadvancedmaterials.com.

[206] Thermal Conductivity of Cork Insulation, Nuclear Power, 3 June 2022, www.nuclear-power.com/nuclear-engineering/heat-transfer/heat-losses/insulation-materials/thermal-conductivity-of-cork-insulation/?fbclid=IwAR3t3xyAFGcKfHEzP0ME8fs7uXRWZPemvzDvHfQ0KhwRRzPyeNhDVPIYdRE.

[207] "Extruded Polystyrene - XPS - Thermal Insulation." Nuclear Power, 2 June 2022, www.nuclear-power.com/nuclear-engineering/heat-transfer/heat-losses/insulation-materials/extruded-polystyrene-xps.

[208] Thermal Conductivity Rigid Polyurethane Foam, Low thermal conductivity www.poliuretano.it/EN/thermal_conductivity_polyurethane.html.

[209] Cho S-H, Chae C-U. A Study on Life Cycle CO2 Emissions of Low-Carbon Building in South Korea. Sustainability. 2016; 8(6):579. https://doi.org/10.3390/su8060579

[210] https://www.polybags.co.uk/environmentally-friendly/useful-numbers-for-environmental-studies.pdf

[211] Albassam. www.albassam.ae/public/file/products/28545_GRP+Panel+Brochure.pdf. Accessed 6 Oct. 2022.

[212] Melito, Steve. "Post Author: Steve Melito." Elastoproxy, 8 Apr. 2022, www.elastoproxy.com/thermally-conductive-silicones-explained.

[213] "How Much CO2 Is Stored in 1 Kg of Wood?" Kaltimber, 2 Mar. 2021, www.kaltimber.com/blog/2017/6/19/how-much-co2-is-stored-in-1-kg-of-wood.

[214] Pásztory. "The Effect of Heat Treatment on Thermal Conductivity of Paulownia Wood." SpringerLink, 20 Nov. 2019, link.springer.com/article/10.1007/s00107-019-01470-3?error=cookies_not_supported&code=984e55c1-854c-4dc2-b6fc-eace754b3955.

[215] Ecocosts for Butyl Rubber (IIR) Waste Incineration With Electricity | Design-4-Sustainability. www.design-4-sustainability.com/ecocosts/50334. Accessed 6 Oct. 2022.

[216] https://link-springer-com.ezproxy.libproxy.db.erau.edu/content/pdf/10.1007/s12053-017-9536-1

[217] Hammond, Geoffrey, and Craig Jones. "The Inventory of Carbon and Energy (ICE)." A BSRIA Guide Embodied Carbon, Jan. 2021, greenbuildingencyclopaedia.uk/wp-content/uploads/2014/07/Full-BSRIA-ICE-guide.pdf.

[218] Ioannis Axaopoulos, Petros Axaopoulos, John Gelegenis, and Emmanouil D Fylladitakis. Optimum external wall insulation thickness considering the annual CO2 emissions. Journal of Building Physics 42(4), p527-544, 2019

[219] "WOOL AND THE CARBON CYCLE." The Woolmark Company, Mar. 2019, www.paulo-oliveira.pt/assets/content/wool-carbon-cycle.pdf.

[220] Dénes, Tünde-Orsolya. "Analysis of Sheep Wool-Based Composites for Building Insulation." MDPI, www.mdpi.com/2073-4360/14/10/2109. Accessed 6 Oct. 2022.

[221] Niklas von der Assen, André Sternberg, Arne Kätelhön, and André Bardow. Environmental potential of carbon dioxide utilization in the polyurethane supply chain. Faraday Discuss., 2015, 183, 291 https://pubs.rsc.org/en/content/articlelanding/2015/fd/c5fd00067j

[222] "thermPIR Insulation Panels." Carbon Footprint Decleration, 1 Mar. 2021, termpir.eu/files/upload/file/EN/Certyfikaty/Carbon-footprint-Declaration-No-179-2021.pdf.

[223] Danielle Densley Tingley, Abigail Hathway, Buick Davison, and Dan Allwood. The environmental impact of phenolic foam insulation boards, Proceedings of the Institution of Civil Engineers - Construction Materials 2017 170:2, 91-103. https://www.icevirtuallibrary.com/doi/10.1680/coma.14.00022

[224] Designing Buildings, www.designingbuildings.co.uk/wiki/Phenolic_foam_insulation. Accessed 6 Oct. 2022.

[225] "Kingspan Kooltherm Pipe Insulation | Kingspan Insulation | NBS Source." https://source.thenbs.com/product/kingspan-kooltherm-pipe-insulation/nfNUZJ1KgXq5Jhq1kdk815/ecGePxjGsKpt7384aajNcM

[226] 403 Forbidden. www.kingspan.com/gb/en/knowledge-articles/types-of-insulation-a-guide.https://www.kingspan.com/gb/en-gb/products/insulation-boards/insulation-technical-hub/articles-and-advice/types-of-insulation-a-beginners-guide.

[227] Gunathilaka L F D Z, and Gunawardana K D. Carbon Footprint Calculation from Cradle to Grave: A Case Study of Rubber Manufacturing Process in Sri Lanka. International Journal of Business and Social Science Vol. 6, No. 10; October 2015. http://www.ijbssnet.com/journals/Vol_6_No_10_October_2015/8.pdf

[228] PROMATECT®-250 | Promat UK | NBS Source. source.thenbs.com/product/promatect-250/jZnwT5ouTNNscF6M4YU494/wbGwK5PF3pjh4xQ2Macjtr. Accessed 6 Oct. 2022.

[229] Ebert, Hans-Peter, and Frank Hemberger. "Intercomparison of Thermal Conductivity Measurements on a Calcium Silicate Insulation Material." International Journal of Thermal Sciences, vol. 50, no. 10, 2011, pp. 1838–44, https://doi.org/10.1016/j.ijthermalsci.2011.05.007.

[230] "Industry-wide Type III EPD Conventional Loose-Fill Cellulose Insulation." Sustainable Minds, 2019, www.transparencycatalog.com/assets/uploads/pdf/CIMA_CIMAC_Conventional_Loose-Fill_Cellulose_Insulation_EPD_JAN20.pdf.

[231] Ostermeyer, Goto, Y., Wallbaum, H., Kono, J., & Frischknecht, R. (2016). Factors for Eco-Efficiency Improvement of Thermal Insulation Materials. Key Engineering Materials, 678, 1–13. https://doi.org/10.4028/www.scientific.net/KEM.678.1

[232] European Commission. https://ec.europa.eu/research/participants/documents/downloadPublic?documentIds=080166e5cca5f849&appId=PPGMS.

[233] Silvestre JD, Pargana N, de Brito J, Pinheiro MD, Durão V. Insulation Cork Boards-Environmental Life Cycle Assessment of an Organic Construction

Material. Materials (Basel). 2016 May 20;9(5):394. doi: 10.3390/ma9050394. PMID: 28773516; PMCID: PMC5503064.

[234] Thermal Conductivity. http://hyperphysics.phy-astr.gsu.edu/hbase/Tables/thrcn.html

[235] Meys, Raoul. "Towards Sustainable Elastomers From CO2: Life Cycle Assessment of Carbon Capture and Utilization for Rubbers." Green Chemistry (RSC Publishing), 17 June 2019, pubs.rsc.org/en/content/articlelanding/2019/gc/c9gc00267g/unauth.

[236] Yin, Qing. "Enhanced Mechanical, Dielectric, Electrical and Thermal Conductive Properties of HXNBR/HNBR Blends Filled With Ionic Liquid-modified Multiwalled Carbon Nanotubes." SpringerLink, 5 June 2017, link.springer.com/article/10.1007/s10853-017-1251-y?error=cookies_not_supported&code=896a341b-3729-4f64-9711-35078aec1683.

[237] Cabrales H, Arzola N, Araque O. The effects of moisture content, fiber length and compaction time on African oil palm empty fruit bunches briquette quality parameters. Heliyon. 2020 Dec 2;6(12):e05607. doi: 10.1016/j.heliyon.2020.e05607. PMID: 33305051; PMCID: PMC7718462.

[238] Zeghichi, N., et al. "Genetic Algorithm with Pareto Fronts for Multi-Criteria Optimization Case Study 'Milling Parameters Optimization.'" 2011 5th International Conference on Software, Knowledge Information, Industrial

Management and Applications (SKIMA) Proceedings, IEEE, 2011, pp. 1–5, https://doi.org/10.1109/SKIMA.2011.6089970.

Appendix A

Table of Thermal conductivity Results

Thermal conductivity of biomass reinforced composites with standard deviations

Sample	NEAT	OAK10%	OAK20%	BRY10%	BRY20%	BRY30%	STR10%	STR20%	JUT2.25%	JUT4.5%
Run#1	0.3102	0.2316	0.2278	0.1816	0.1654	0.2088	0.3053	0.2217	0.1905	0.1954
Run#2	0.2916	0.2195	0.2261	0.1811	0.1635	0.2122	0.3105	0.2185	0.1873	0.1957
Run#3	0.2928	0.2118	0.1961	0.18	0.1637	0.2065	0.3061	0.2191	0.194	0.1822
Run#4	0.2844	0.2121	0.227	0.1788	0.1619	0.2012	0.3057	0.2207	0.159	0.1831
Run#5	0.2772	0.2047	0.2367	0.1777	0.1604	0.1984	0.3033		0.1852	0.1789
Run#6	0.27	0.1997	0.24			0.2024	0.3212			0.197
Run#7	0.3224		0.1864				0.3184			0.1743
Run#8	0.2936		0.1616				0.3159			
Run#9	0.2958		0.1821				0.3126			
Run#10	0.2909		0.1882				0.3109			
Run#11	0.2936		0.2003				0.3119			
Run#12	0.293		0.2175				0.3083			
Run#13			0.2277				0.3079			
Run#14			0.2259				0.3051			
Run#15			0.2035				0.1279			
Run#16			0.2198				0.1295			
Run#17			0.2423				0.1284			

Run#18			0.2384				0.1165			
Run#19			0.2365				0.113			
Run#20			0.2344				0.1222			
Run#21			0.2332				0.1278			
Run#22							0.1233			
Number of runs	12	6	21	5	5	6	22	4	5	7
Average	0.292958	0.213233	0.216738	0.17984	0.16298	0.204917	0.24235	0.22	0.1832	0.186657
Standard deviation	0.013577	0.011278	0.022816	0.00161	0.001902	0.005162	0.092062	0.001465	0.013932	0.009225

Appendix B

MATLAB code

```
Main

%genetic optimization code

clear; clc; close all;

% Design Space 1 objective function

wiRange = [16, 22]./100; %insulation width (m)
hiRange = [48, 49.75]./100; %height of the insulation (m)
KiRange = [0.007, 0.1]; %thermal conductivity W/m*k
wsRange = [1, 4]./100; %insulation steel width (m)
hsRange = [0.5, 4]./100; %height of the steel (m)

objRange = [min(wiRange), max(wiRange);...
            min(hiRange), max(hiRange);...
            min(KiRange), max(KiRange);...
            min(wsRange), max(wsRange);...
            min(hsRange), max(hsRange)];

FitnessFunction = @objectiveFunction;
numberOfVariables = length(objRange);

opts = optimoptions(@ga,'PlotFcn',{@gaplotbestf,@gaplotstopping}, ...
    'HybridFcn', @fminunc,...
                    'SelectionFcn',@selectionstochunif, ...
                    'FitnessScalingFcn',@fitscalingprop, ...
                    'MutationFcn', @mutationadaptfeasible,...
                    'CrossoverFcn',@crossoverscattered, ...
                    'Display','final',...
                    'OutputFcn', @gaoutputfcn,...
                    'MaxGenerations',100);
opts.PopulationSize = 150;
opts.InitialPopulationRange = [min(wiRange), min(hiRange), min(KiRange),
min(wsRange), min(hsRange);...
                                max(wiRange), max(hiRange), max(KiRange),
max(wsRange), max(hsRange)];

lb = [objRange(:,1)]; %lower bounds
ub = [objRange(:,2)]; %upper bounds
intcon = 1;

rng default % For reproducibility
[x,Fval,exitFlag,Output,population,scores] = ...
    ga(FitnessFunction,numberOfVariables,[],[],[],[],lb,ub,[],opts);

wi = x(1);
hi = x(2);
```

```matlab
Ki = x(3);
ws = x(4);
hs = x(5);

fprintf('The number of generations is: %d\n', Output.generations);
fprintf('The number of function evaluations is: %d\n', Output.funccount);
fprintf('The best function value found is: %g\n', Fval);
fprintf('The best Steel width (ws): %g meters \n', ws);
fprintf('The best Insulation material width (wi): %f meters \n', wi);
fprintf('The best Steel height (hs): %f meters \n', hs);
fprintf('The best Insulation material height (hi): %f meters \n', hi);
fprintf('The bestThermal conductivity of the insulation material (Ki): %f
W/m.K \n', Ki);

% QbestFit = objectiveFunction(x);

for i = 1:100
    fitnessMeanObj(i) = mean(gafitnesshistory(:,i));
end

%Get min and max indexes
QminIdx = find(fitnessMeanObj == min(fitnessMeanObj));
QmaxIdx = find(fitnessMeanObj == max(fitnessMeanObj));

genTotal = 1:100;

%Plot
figure
plot(genTotal,fitnessMeanObj, 'b-', 'LineWidth', 1);
hold on
plot(genTotal(QminIdx), fitnessMeanObj(QminIdx), 'kx', 'MarkerSize', 10,
'LineWidth', 1)
plot(genTotal(QmaxIdx), fitnessMeanObj(QmaxIdx), 'rx', 'MarkerSize', 10,
'LineWidth', 1)
grid minor
xlabel('Generations')
ylabel('Heat Transfer Rate Q (W)')
legend('GA',sprintf('Min Q = %s W',  num2str(round(min(fitnessMeanObj), 4,
'significant')))),...
    sprintf('Max Q = %s W',  num2str(round(max(fitnessMeanObj), 5,
'significant'))))

%Calculate R
deltaT = 22;
R_fitness = deltaT./fitnessMeanObj;

%Get min and max indexes
RminIdx = find(R_fitness == min(R_fitness));
RmaxIdx = find(R_fitness == max(R_fitness));

figure
plot(genTotal,R_fitness, 'b-', 'LineWidth', 1);
hold on
```

```matlab
plot(genTotal(RminIdx), R_fitness(RminIdx), 'kx', 'MarkerSize', 10,
'LineWidth', 1)
plot(genTotal(RmaxIdx), R_fitness(RmaxIdx), 'rx', 'MarkerSize', 10,
'LineWidth', 1)
grid minor
xlabel('Generations')
ylabel('Fitness function R_{total} (C/W)')
legend('GA',sprintf('Min R = %s C/W',  num2str(round(min(R_fitness), 4,
'significant'))),...
    sprintf('Max R = %s C/W',  num2str(round(max(R_fitness), 5,
'significant'))))


function y = objectiveFunction(x)

wi = x(1);
hi = x(2);
Ki = x(3);
ws = x(4);
hs = x(5);

% Initial Conditions
t0 = 0; %initial temp C
t = 22; %final temp C
deltaT = t - t0; %TO DO TODO do we need to convert this to Kelvin?

Ks = 15.0;%[W / m.C]
wt = wi + ws + ws;
ht = hi + hi + hs;

% hs = hTotal - (2 * hi);
% ws = (wTotal - wi) / 2;

unitDepth = 1.0;

%Thermal Resistance
R1 = ws / (Ks * ht * unitDepth);
R2 = wi / (Ks * hs * unitDepth);
R3 = wi / (Ki * 2 * hi * unitDepth);
R4 = ws / (Ks * ht * unitDepth);

%R2 and R3 are in parallel
R23 = R2*R3/(R2+R3);

%Thermal Resistance
R_total = R1 + R23 + R4; %R equivalent

%objective function 1 Heat Transfer
y = deltaT/R_total;

end
```

```matlab
function y = objectiveFunctionMulti(x)

wi = x(1);
hi = x(2);
Ki = x(3);
ws = x(4);
hs = x(5);
co2 = x(6);

% Initial Conditions
deltaT = t - t0; %TO DO TODO do we need to convert this to Kelvin?

Ks = 15.0;%[W / m.C]
wt = wi + ws + ws;
ht = hi + hi + hs;

% hs = hTotal - (2 * hi);
% ws = (wTotal - wi) / 2;

unitDepth = 1.0;

%Thermal Resistance
R1 = ws / (Ks * ht * unitDepth);
R2 = wi / (Ks * hs * unitDepth);
R3 = wi / (Ki * 2 * hi * unitDepth);
R4 = ws / (Ks * ht * unitDepth);

%R2 and R3 are in parallel
R23 = R2*R3/(R2+R3);

%Thermal Resistance
R_total = R1 + R23 + R4; %R equivalent

%objective function 1 Heat Transfer
y(1) = deltaT/R_total;
y(2) = co2*exp(0.0001*Ki);
% y(2) = 0.0006*x(3)^4 + 0.0073*x(3)^3 - 0.0214*x(3)^2 + 0.0028*x(3) + 0.0898;


end



%% Genetic Algorithm with multiple objectives
clear; close all;

wiRange = [16, 22]./100; %insulation width (m)
hiRange = [48, 49.75]./100; %height of the insulation (m)
KiRange = [0.003, 0.1]; %thermal conductivity W/m*k
wsRange = [1, 4]./100; %insulation steel width (m)
hsRange = [0.5, 4]./100; %height of the steel (m)
co2range = [0.15 6.0];
```

```matlab
objRange = [min(wiRange), max(wiRange);...
            min(hiRange), max(hiRange);...
            min(KiRange), max(KiRange);...
            min(wsRange), max(wsRange);...
            min(hsRange), max(hsRange);
            min(co2range), max(co2range)];
genTotal = 200;
FitnessFunction = @objectiveFunctionMulti;
numberOfVariables = length(objRange);
% @gaplotstopping, @gaplotselection, @gaplotscores, @gaplotparetodistance
opts = optimoptions(@ga,'PlotFcn',{@gaplotpareto}, ...
                    'SelectionFcn',@selectiontournament, ...
                    'FitnessScalingFcn',@fitscalingprop, ...
                    'MutationFcn', @mutationadaptfeasible,...
                    'CrossoverFcn',@crossoverintermediate, ...
                    'OutputFcn', @gamultioutputfcn,...
                    'MaxGenerations',genTotal);
opts.PopulationSize = 150;
opts.InitialPopulationRange = [min(wiRange), min(hiRange), min(KiRange),
min(wsRange), min(hsRange), 6;...
                                    max(wiRange), max(hiRange), max(KiRange),
max(wsRange), max(hsRange), max(co2range)];

lb = [objRange(:,1)]; %lower bounds
ub = [objRange(:,2)]; %upper bounds

rng default % For reproducibility
[x,Fval,exitFlag,Output,population,scores] = ...
    gamultiobj(FitnessFunction,numberOfVariables,[],[],[],[],lb,ub,[],opts);

wi = x(1,1);
hi = x(1,2);
Ki = x(1,3);
ws = x(1,4);
hs = x(1,5);
co2 = x(end,6);

fprintf('The number of generations is: %d\n', Output.generations);
fprintf('The number of function evaluations is: %d\n', Output.funccount);
fprintf('The best function value found is: %g\n', Fval);
fprintf('The best Steel width (ws): %g meters \n', ws);
fprintf('The best Insulation material width (wi): %f meters \n', wi);
fprintf('The best Steel height (hs): %f meters \n', hs);
fprintf('The best Insulation material height (hi): %f meters \n', hi);
fprintf('The best Thermal conductivity of the insulation material (Ki): %f
W/m.K \n', Ki);
fprintf('The best CO2 footprint: %f \n', co2);


% QbestFit = objectiveFunction(x(end,:));

for i = 1:length(gafitnesshistory(1,1,:))
    fitnessMeanObj1(i) = mean(gafitnesshistory(:,1,i));
```

```matlab
        fitnessMeanObj2(i) = mean(gafitnesshistory(:,2,i));
end
co2Fitness = scores(:,2);
QFitness = scores(:,1);

%Calculate R
deltaT = 22;
R_fitness = deltaT./fitnessMeanObj1;

%Get min and max indexes
RminIdx = find(R_fitness == min(R_fitness));
RmaxIdx = find(R_fitness == max(R_fitness));

%Pareto Front Plot
figure
plot(min(co2Fitness),min(QFitness),'rx','MarkerSize', 4)
hold on; grid minor
plot(co2Fitness,QFitness, 'bx', 'MarkerSize', 4);
% h=text(0.1501,7.9,'\leftarrow Optimum location');
% set(h,'Rotation',45);
ylim([7.85,8.45])
xlim([0.1488, 0.165])
ylabel('Heat Transfer Rate (W)')
xlabel('Carbon Footprint value (kgCO2/kg)')
% title('Pareto Front -- GA Multi Object')
% legend('Optimal Value')

%Rfitntess plot
figure
plot(1:500,R_fitness, 'b-', 'LineWidth', 1);
hold on;grid minor;
plot(0, R_fitness(RminIdx), 'kx', 'MarkerSize', 10, 'LineWidth', 1)
plot(500, R_fitness(RmaxIdx), 'rx', 'MarkerSize', 10, 'LineWidth', 1)
xlabel('Generations')
ylabel('Fitness function R_{total} (C/W)')
% title('Pareto Front')
legend('GA',sprintf('Min R = %s C/W',  num2str(round(min(R_fitness), 4,
'significant'))),...
sprintf('Max R = %s C/W',  num2str(round(max(R_fitness), 5, 'significant'))))


function [state,options,optchanged] = gamultioutputfcn(options,state,flag)
persistent history fitnessHistory
optchanged = false;
switch flag
    case 'init'
        fitnessHistory(:,:,state.Generation+1) = state.Score;
        assignin('base','gafitnesshistory',fitnessHistory);
        history(:,:,state.Generation+1) = state.Population;
        assignin('base','gapopulationhistory',history);

    case 'iter'
        % Update the history every 1 generations
```

```matlab
        history(:,:, state.Generation+1) = state.Population;
        assignin('base','gapopulationhistory',history);
        fitnessHistory(:,:,state.Generation+1) = state.Score;
        assignin('base','gafitnesshistory',fitnessHistory);
        % Update the fraction of mutation and crossover after 25 generations.
        if state.Generation == 25
            options.CrossoverFraction = 0.8;
            optchanged = true;
        end
    case 'done'
        % Include the final population in the history.
        history(:,:,state.Generation) = state.Population;
        assignin('base','gapopulationhistory',history);
        fitnessHistory(:,:,state.Generation) = state.Score;
        assignin('base','gafitnesshistory',fitnessHistory);
end


function [state,options,optchanged] = gaoutputfcn(options,state,flag)
persistent history fitnessHistory
optchanged = false;
switch flag
    case 'init'
        fitnessHistory(:,state.Generation+1) = state.Score;
        assignin('base','gafitnesshistory',fitnessHistory);
        history(:,:,state.Generation+1) = state.Population;
        assignin('base','gapopulationhistory',history);

    case 'iter'
        % Update the history every 1 generations
        history(:,:,state.Generation+1) = state.Population;
        assignin('base','gapopulationhistory',history);
        fitnessHistory(:,state.Generation+1) = state.Score;
        assignin('base','gafitnesshistory',fitnessHistory);
        % Update the fraction of mutation and crossover after 25 generations.
        if state.Generation == 25
            options.CrossoverFraction = 0.8;
            optchanged = true;
        end
    case 'done'
        % Include the final population in the history.
        history(:,:,state.Generation) = state.Population;
        assignin('base','gapopulationhistory',history);
        fitnessHistory(:,state.Generation) = state.Score;
        assignin('base','gafitnesshistory',fitnessHistory);
end
```